Ultimate strength analysis of stiffened steel and aluminium panels using semi-analytical methods

A thesis submitted in partial fulfillment of the requirements for the degree of Doktor Ingeniør

by

Eirik Byklum

T rondheim,October 30, 2002

Department of Marine Technology
Faculty of Engineering Sciences and Technology
Norwegian University of Science and Technology

URN:NBN:no-3348

Abstract

Buckling and postbuckling of plates and stiffened panels are considered. Computational models for direct calculation of the response are developed using large deflection plate theory and energy principles. Deflections are represented by trigonometric functions. All combinations of biaxial in-plane compression or tension, shear, and lateral pressure are included in the formulations. The procedure is semi-analytical in the sense that the incremental equilibrium equations are derived analytically, while numerical method is used for solving the equation systems, and for incrementation of the solution.

Unstiffened plate models are developed both for the simply supported case and for the clamped case. For the simply supported case the material types considered are isotropic elastic, orthotropic elastic, and elastic-plastic. Two models are developed for analysis of local buckling of stiffened plates, one for open profiles and one for closed profiles. A global buckling model for stiffened panels is developed by considering the panel as a plate with general anisotropic stiffness. The stiffness coefficients are input from the local analysis. Two models are developed for combined local and global buckling, in order to account for interaction between local and global deflection. The first is for a single stiffened plate, and uses a column approach. The second is for a stiffened panel with several stiffeners.

Numerical results are calculated for a variety of plate and stiffener geometries for verification of the proposed model, and comparison is made with nonlinear finite element methods. Some examples are presented. For all models, the response in the elastic region is well predicted compared with the finite element method results. Also, the efficiency of the calculations is very high. Estimates of ultimate strength are found using first yield as a collapse criterion. In most cases, this leads to conservative results compared to predictions from finite element calculations.

URN:NBN:no-3348

Acknowledgments

This work has been carried out under the supervision of Professor Jørgen Amdahl at the Department of Marine Technology, Norwegian University of Science and Technology. I appreciate Professor Amdahl's guidance, and especially his positiv eattitude and his willingness to shear of his time.

Thanks to Dr. Eivind Steen at Det Norske Veritas for continuous support during the study. His understanding of the buckling phenomenon is exceptional, and I have been very fortunate to benefit from his experience. I also appreciate the numerous valuable discussions with the tw o other members of the PULS-team, Tom Østvold and Kjetil Vilming.

This study has been sponsored by the Research Council of Norway (NFR). I would also like to thank my excellent employer Det Norske Veritas for granting me leave to pursue a doctoral education and for giving me additional funding from the Educational Fund.

My love and gratitude goes to my wife, Marit, who has supported and encouraged me throughout the work with this thesis.

URN:NBN:no-3348

Contents

Nomenclature

General Rules

- Symbols are generally defined where they appear in the text for the first time
- The most used symbols are declared here
- Bold face is used to denote matrices, e.g. $\mathbf{K}$
- Overdots signify differentiation with respect to pseudo-time, e.g. $\dot{w}(x, y)$

Subscripts

$, ij$	differentiation with respect to i and j
b	bending
c	compression
lp	lateral pressure
m	membrane
τ	shear stress

Superscripts

c	cosine
f	flange
g	global
i	increment

p	plate
s	sine
s	stage
s	stiffener
w	web
D	part due to deflection
F	part due to external force

Roman Letters

a	Plate length
b	Plate width, stiffener spacing
b_f	Flange width
f_{mn}	Stress function coefficients
h	Web height
k	Spring stiffness
p	Lateral pressure
t	Plate thickness
t_f	Flange thickness
t_w	Web thic kness
$u(x, y)$	In-plane displacement in x-direction
$v(x, y)$	In-plane displacement in y-direction
$v(x, z)$	Stiffener sideways deflection
$w(x, y)$	Plate deflection
$w_0(x, y)$	Initial plate deflection
x	Longitudinal position
y	T ransv erse position
z	V ertical position
z_g	Distance to stiffener neutral axis
A_{mn}	Amplitude of deflection
A_T	Stiffened plate cross-sectional area
A_s	Stiffener cross-sectional area
B	P anel width
B_{mn}	Amplitude of initial deflection
C_{ijkl}	Material stiffness tensor
D	Isotropic bending stiffness
E	Y oung's modulus
F	Airy's stress function
G	Shear modulus
H	External work

H_p	Plastic modulus
I	Moment of inertia
I_f	Flange moment of inertia
J_f	Flange torsional moment of inertia
M_i	Bending moment
M_{ijkl}	Material flexibility tensor
P_{ij}	Internal in-plane force
P_{ij}	Applied in-plane force
S	Body surface
S_{ij}	Applied in-plane stress
T	Potential of external loads
U	Internal potential energy
V	Body volume
V_{1m}, V_{2m}	Amplitudes of stiffener deflection
W	Internal work
$\mathbf{x}$	Linear eigenmode
$\mathbf{G}$	Incremental load vector
$\mathbf{K}$	Incremental stiffness matrix
$\mathbf{K}_G$	Geometric stiffness matrix
$\mathbf{K}_M$	Material stiffness matrix

Greek Letters

α	Arc-length angle
β	Plate slenderness, $\beta = \frac{b}{t}\sqrt{\frac{\sigma_f}{E}}$
ε_{ij}	Membrane strain
η	Arc length
γ	Shear membrane strain
κ	Curvature due to global deflection
σ_{ij}	Membrane stress
σ_{eq}	von Mises equivalent stress
σ_f	Yield stress
ν	Poisson's ratio
τ	Membrane shear stress
θ	Transverse rotation
Π	Total potential energy
Λ	Load proportionality factor
Λ_E	Linear eigenvalue
Δu	Elongation in x-direction
Δv	Elongation in y-direction

Mathematical operators and other symbols

∇ Gradient operator
δ Variational operator
∂ Partial derivative

Abbreviations

FEM	Finite Element Methods
HAZ	Heat Affected Zone
NFEM	Nonlinear Finite Element Methods

Chapter 1

Introduction

1.1 Background and motivation

In design of ships and offshore structures, it is essential to ensure that the structure has sufficient strength to sustain an extreme loading situation. Marine structures are assembled of plates and stiffened panels, Fig. 1.1, and the strength of each panel is crucial for the overall structural capacity. Although a large degree of redundancy usually ensures that the structure has strength reserves after failure of individual panels, each panel should be designed so that its ultimate capacity is not exceeded.

A structural component may collapse due to excessive yielding, buckling, rupture or fatigue. Stiffened panels used in marine structures are especially vulnerable to buckling, since the plates are relatively thin and the loading predominantly in-plane. Determining the buckling characteristics of each panel is therefore a vital part of the structural strength assessment. Buckling does in itself not imply immediate collapse. Plates may have significant strength reserves in the postbuckling region, and it is important to account properly for this effect in order to achieve optimum design.

Traditionally the buckling strength of stiffened panels has been assessed using explicit design formulas, such as Det Norske Veritas Classification Note for Buckling Strength Analysis (Det Norske Veritas 1995). These kind of formulations are usually based on linear plate buckling theory, combined with empirical corrections to account for imperfections, residual stresses and plasticity. Combinations of loads are dealt with using various

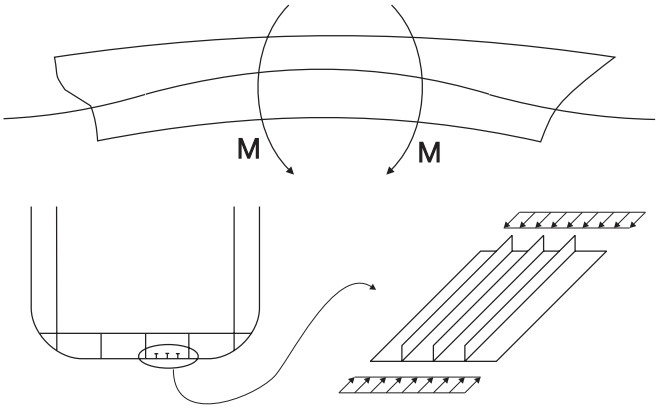

Figure 1.1: Ship hull girder

interaction formulas, while stiffener buckling is assessed using a column approach together with effective width correction.

Although having the advantage of being relatively simple and providing quick strength estimates, the use of explicit design formulas is not a satisfactory design approach. It is not possible to establish a set of formulas that are well suited for all geometries and load combinations, and inaccurate results may be obtained if the formulas are used on cases they were not originally intended for. They are not flexible with respect to various imperfection shapes and amplitudes, which may have a large influence on the response. Finally, they do not provide information on deflection modes and amplitudes.

Hand calculations using explicit design formulas have been important in the ship building industry, but computational tools are becoming more and more common. The need for explicit formulas is therefore decreasing. The most accurate alternative is the use of nonlinear finite element methods (NFEM). This is a useful tool for research and comparison purposes, but performing NFEM on stiffened panels is not practical for design. With the large amount of panels to be analysed in a ship structure, the cost of modelling and computing is too large for design purposes, even with the powerful computers of today.

The approach presented in this thesis is a compromise between explicit design formulas and nonlinear finite element methods. The motivation is to obtain a direct calculation tool which is more accurate than the simplified formulations used in existing design codes, and more efficient and simpler to use than NFEM. It should be fast and efficient to use, and give information regarding deformation modes and load-response characteristics. An analytical approach is combined with a numerical solution procedure, giving a semi-analytical method. The energy equations are integrated analytically, and stiffness coefficients are

obtained explicitly. A numerical method is used for solving the equation system and for incrementing the solution.

The emphasis is on analysis of an isolated stiffened panel. However, it is believed that the results presented can be useful for future development of an integrated hull girder design model. Such a model is required in order to take full account of the redistribution of forces between panels due to buckling, but is outside the scope of the current work.

1.2 Problem formulation

The stiffened panel is assumed to consist of a rectangular plate area with stiffeners running in the longitudinal direction. The panel is supported by heavy longitudinal and transverse girders, as shown in Fig. 1.2. This kind of arrangement is typical for the deck, side or bottom of a ship hull. It is assumed that the girders have sufficient strength to support the panel, so that the part relevant for analysis is the plating with stiffeners. The stiffeners may be open or closed profiles. Open types are flat bar, angle bar, tee bar or bulb bar, while the hat-profile is a typical example of a closed profile. The former types are typical for conventional ship structures, while the latter is used for lightweight applications such as high speed vessels and living quarters of offshore structures.

The loads acting on a stiffened panel in marine structures are in-plane compression or tension resulting from the overall hull girder bending moment, shear stress resulting from the hull girder shear force or torsion, and lateral pressure resulting from internal cargo or the external sea. In the current work, the shear force and lateral pressure are assumed to have constant values over the length and width of the plate, while the in-plane compression or tension is assumed to be linearly varying.

A stiffened panel is usually part of a larger structure, and it is therefore not obvious how to define the boundary conditions of an isolated panel. A common assumption is to consider the edges as simply supported, and free to move in-plane but forced to remain straight. This means that the neighboring panels are assumed to provide some in-plane constraint, but no rotational constraint.

The fabrication process will introduce imperfections in the structure. Plates have a certain initial out-of-plane deflection, stiffener webs have a sideways initial distortion, and the combined stiffened plate may have an initial lateral deflection in the global mode. Residual stress from the welding process will also be present. Due to the imperfections, the response is geometrically nonlinear from the start of the loading history. There is no well-defined buckling load, but a gradual transition from the prebuckling to the postbuckling region. At some point material yielding will occur, and finally the collapse load will be reached. The aim in this work is to trace the geometrically nonlinear load-deflection equilibrium curve

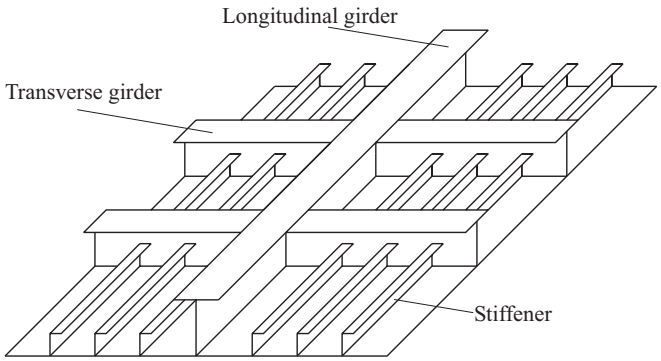

Figure 1.2: Stiffened panel

from the onset of loading until the maximum load is reached. Estimates of the ultimate load and deformation shall be provided.

Both steel and aluminium panels are considered. Steel panels are usually quite stocky, and local deformations dominate. Aluminium panels are usually slender and have much lower global buckling load. The coupling between local and global buckling is therefore much larger. Also, the material stiffness of aluminium is only one third of that of steel. Aluminium panels have the additional problem of heat affected zones (HAZ). This may be treated in the current computational model by reducing the yield stress in the HAZ-zones. More advanced treatment of HAZ-effects is not within the scope of the current work.

1.3 Previous work

The published literature on buckling of beams and plates is overwhelming, and only a few selected references can be mentioned here. A short historical review is given first, and some contributions from recent years are then presented.

The first work in the field of buckling theory was made by Euler (Euler 1759), who derived the linear elastic buckling value for an ideal, axially compressed column. It took almost a hundred years before Euler's theory became generally accepted, because experiments were only conducted on short columns that buckle inelastically. The Perry-Robertson approach, (Ayrton and Perry 1886) and (Robertson 1925), is based on the column model with an initial imperfection, and first yield in the extreme fiber is taken as the elastic limit load. This method has been widely used in design codes, such as (Det Norske Veritas 1995). Correction of the linear elastic value to account for plasticity can also be done using Johnson- Ostenfeldt correction.

Caldwell proposed the effective width method (Caldwell 1965) as a method for accounting for local plate deflection when using the column model on a stiffened plate. Following this, much work has been devoted to finding appropriate expressions for the effective width of plating, e.g. (Faulkner 1975), (Carlsen 1980), and (Valsgard 1980).

Navier derived the differential equation for bending of rectangular plates, and used trigonometric functions to obtain linear elastic buckling values for certain problems. Design formulas have been developed for unstiffened plates which implicitly account for imperfections and residual stress. Contributions in this field are numerous, e.g. (Soares 1988), (Ueda, Rashed, and Paik 1995), (Paik and Pedersen 1995), (Soares and Gordo 1996a), (Soares and Gordo 1996b), (Cui and Mansour 1998), (Fujikubo and Yao 1999), (Kristensen 2001), and (Paik and Kim 2002). Combined loads are handled using capacity interaction curves obtained from parametric studies.

Pioneering work on large deflection of plates was performed by Kirchoff (Kirchoff 1850), who discovered the importance of nonlinear terms for large deflections. The final form of the plate differential equation for large deformations was derived by von Karman, (von Karman 1910). The equations were extended to plates with initial curvature by Marguerre (Marguerre 1937).

The finite element method (FEM) was introduced about fifty years ago, (Turner, Clough, Martin, and Topp 1956), and it has become an increasingly more important tool with the continuous development of high-speed computers. Today the use of linear FEM during design of marine structures is standard, while the use of FEM for nonlinear problems such as buckling is mostly restricted to research, e.g. (Langseth and Hopperstad 1996), (Yao, Fujikubo, and Yanagihara 1997) and (Fujikubo, Yao, and Khedmati 2000).

The Idealized Structural Unit Method was developed in the 1970s, (Ueda and Rashed 1984). This is a method where a structure is divided into the biggest possible structural units, whose geometric and material nonlinear behaviorare idealized. The units are regarded as elements in a nonlinear analysis of the entire structure. Recent developments of the method are due to many researchers, e.g. (Paik 1987), (Ueda and Fujikubo 1992), (Ueda, Rashed, and Abdel-Nasser 1993) and (Fujikubo, Keading, and Yao 2000).

Recent work in the field of analytic or semi-analytic buckling formulations have been restricted mostly to linearized buckling predictions, neglecting non-linear geometrical effects in the large deflection region, such as (Hughes and Ma 1996), (Masaoka and Okada 1996), (Paik, Thayamballi, and Park 1998) and (Fujikubo and Yao 1999).

Some work has been performed on the large deflection response of unstiffened plates, e.g. (Levy 1942), (Ueda, Rashed, and Paik 1987), (Masaoka, Okada, and Ueda 1998) and (Paik, Thayamballi, Lee, and Kang 2001). In (Steen 1989) large deflection of a stiffened panel was analysed using a single degree of freedom model, but neglecting local buckling effects.

In recent years, the need for improved buckling formulations has been recognized by the ship classification society Det Norske Veritas (DNV). Until now, buckling assessment has been performed using explicit requirements such as those found in DNV Rules for Ships (Det Norske Veritas 2001) and DNV Classification Note for Buckling Strength Analysis (Det Norske Veritas 1995). Implementation of a new buckling code, Panel Ultimate Strength (PULS), is now being performed (Steen and Østvold 2000). This code is based on theoretical formulations and direct calculation procedures. Some of the buckling models developed in the current work have been implemented in PULS, (Det Norske Veritas 2002b). At the time of writing, the unstiffened plate model presented in chapter 3, and the local buckling model presented in chapter 4 have become part of PULS. Some examples of application using PULS will therefore be presented.

A summary of recent contributions in the field of ultimate strength of stiffened panels can also be found in reports from International Ship and Offshore Structures Congress, (ISSC 2000) and Society of Naval Architects and Marine Engineers, (Paik, Thayamballi, Wang, and Kim 2000).

1.4 Present work

In the present work, the aim has been to analyse the coupled behavior of a stiffened panel using large deflection theory for both the plate and the stiffeners in combination. For this purpose, the task is divided into several steps, where the first basic step is buckling analysis of a single unstiffened plate, and the last step is a complete model for combined buckling of a stiffened panel. Any combination of biaxial in-plane compression or tension, shear, and lateral pressure is included. Deflections are assumed in the form of trigonometric function series. The response history is traced using energy principles and perturbation theory. The formulations derived are implemented in a FORTRAN computer code for each model.

The theoretical basis for the computational models developed is presented in chapter 2. The use of energy principles is described, and a presentation of large deflection plate theory is given. Also, an overview of the material formulations and numerical procedures used is given.

A buckling model for an unstiffened elastic plate is derived in chapter 3, first for simply supported and then for clamped boundary conditions. A plate with orthotropic elastic stiffness coefficients is then studied, and finally a plate with elastic-plastic material properties is considered. This last model is the only one in the current work that accounts for material nonlinearities. It was found that satisfactory estimates of the ultimate strength can be obtained by using first yield due to membrane stress as a collapse criterion. This is also considered to be a sound design approach. Since the elastic-plastic model has poor computational efficiency compared to the elastic model, it was decided to focus on efficient

and accurate elastic solutions for the remaining models.

Local buckling of a stiffened plate is considered in chapter 4. In the local models, it is assumed that the plate and stiffener deflects locally, while lateral deflection of the stiffener in the global mode does not occur. A model is first derived for open profiles and then for a profile of the closed type.

A global buckling model using anisotropic stiffness coefficients is presented in chapter 5. Local deformations are accounted for by using reduced stiffness coefficients calculated from the local buckling model. The stiffness is reduced compared to the linear stiffness due to local buckling effects. However, the coupling between local and global deformation is not fully accounted for in this model, since the global deformation is assumed not to influence the local deformations.

A complete buckling model for a stiffened panel with open profile stiffeners, including coupling between local and global buckling modes, is presented in chapter 6. A single stiffened plate is assumed be representative for the local deformations of all the stiffeners in the panel, and global deformation is included as an additional degree of freedom.

Estimation of design collapse load using a first yield criterion is discussed in chapter 7. Some examples of application of the developed buckling models are presented using PULS. Comparisons with the nonlinear finite element code ABAQUS are given.

Finally, conclusions and recommendations are given in chapter 8.

Chapter 2

General theory

This chapter gives an overview of the general theory and methods used for development of the buckling models presented in the subsequent chapters. Some of the theory presented here is standard textbook material. More on variational principles and energy methods can be found in (Lanczos 1986), (Shames and Dym 1985), (Dym and Shames 1973), and (Washizu 1975). Recognized references on plate theory are for instance (Timoshenko and Gere 1959), (Bulson 1970), (Szilard 1974) and (Murray 1984). Buckling and stability theory is presented by (Bleich 1952), (Timoshenko and Gere 1961), (Gerard 1962), (Brush and Almroth 1975) and (Troitsky 1976). The theory on material behavior is mostly taken from (Chen and Han 1988), (Lemaitre and Chaboche 1994), and (Mazzolani 1995). Buckling problems related to ship structures are presented in (Hughes 1988).

Nonlinear plate deflection is a complex phenomenon, especially due to the development of second order strains. Even linear buckling problems may only for a few special cases be solved analytically. For more general problems, energy principles can provide approximate formulations. Variational methods is the basis for finite element methods used in structural analysis, but they may also be used for establishing analytical or semi-analytical solutions for a structural member as a whole.

In the current work, the principle of virtual work and the principle of minimum potential energy are used to study the response of plates and stiffened plates during buckling. The energy formulations are combined with the Rayleigh-Ritz method for obtaining a solution for the displacement. In contrast to the finite element method, where the displacement shape is taken as piecewise polynomial, the displacements are here assumed on global form,

and the energy of the whole system is considered. The number of unknowns in the problem is therefore only a small fraction of that necessary for a FEM-analysis. Different types of material behavior are studied; isotropic elastic, anisotropic elastic and elastic-plastic. An incremental solution procedure is applied. Solving for the rate of displacement at each increment, a response curve is produced by incrementation.

In the last section of this chapter, eigen valuecalculations are discussed. Although the emphasis in the presen t work is on nonlinear analysis, eigenvalue calculation has also been implemented in all models. The eigen valueis in itself not very informative, but the associated eigenmode gives an indication of the preferred deformation mode of the structure. The eigenmode may therefore be useful for choosing the initial imperfection mode. How ever, it will be shown that for some cases the eigenmode is different from the preferred postbuckling deformation mode.

2.1 Buckling and stability

The word buckling is used with different meanings in different con texts. Mathematically, it is connected to instability phenomena. Ph ysically we usually say that a plate is buckling when in-plane loads results in out-of-plane deflection. The term buckling load is usually used to denote the linear elastic buckling load. This is also referred to as the initial buckling value, or the eigen value. The eigen valueis calculated assuming that no out-of-plane deformation occur before the buc kling value is reac hed, and that the material behavior is linear elastic.

For a perfect plate, the poin tof instabilit yis referred to as the bifurcation load. For a plate with initial deflection, bifurcation will not occur and the buckling load is not a w ell-defined value. The plate will start to deform immediately when the load is applied, and the response is nonlinear from the start. If a maximum loadexists, it is called the limit load, Fig. 2.1. F rom a practical point of view, it is desirable to account for the effect of initial deflections, since all real plates have imperfections. It is also n umerically easier to include initial deflections, since bifurcation points do not have to be treated, and the response curve will be smooth.

F or some problems, the buckling response may be very unstable. This is often connected to mode-snapping. If the current deflection shape is not the preferred one, the plate may try to snap to a different shape. This may lead to quite dramatic response, including snap-through or snap-back response, Fig. 2.1. One reason could be that the initial deflection is in a different mode than the preferred deflection mode. Another reason could be that the preferred deflection shape in the large deflection region is different from the preferred shape in the pre-buckling region, or that the load condition is changed. Examples of this will be shown in the next chapter.

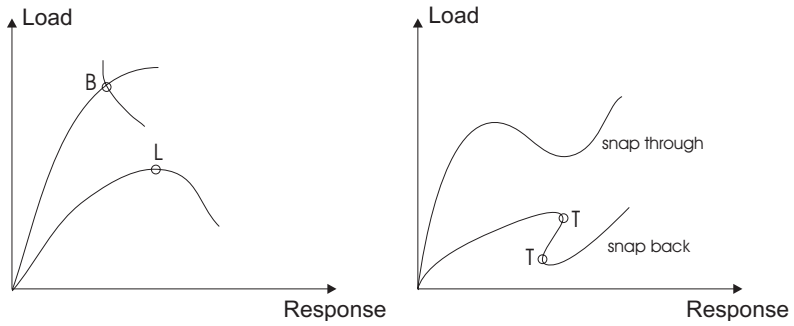

Figure 2.1: Equilibrium curves: (L)=Limit poin t, (B)=Bifurcation point, (T)=Turning point

2.2 Energy principles

2.2.1 The principle of virtual work

The principle of virtual work states that a system is in static equilibrium if the sum of virtual work for internal and external forces is zero for all virtual deformations and strains that are kinematically allow ed.

$$\delta W + \delta H = 0 \tag{2.1}$$

where δW is internal virtual work in the plate, δH is virtual work of external loads, and δ is the v ariational operator. The principle of virtual work is v ery general, and valid also for non-conservativ e systems. It is independent of any constitutive law, and it can therefore be applied for structures with inelastic material properties.

As mentioned, the solution to the nonlinear buckling problem is calculated using incrementation. Consequently, it is the rates that are solved for in each increment. Therefore, the principle of virtual work is used on the following rate form

$$\delta \dot{W} + \delta \dot{H} = 0 \tag{2.2}$$

where the dot signifies differentiation with respect to a rate parameter. The rate parameter is defined in a subsequent section.

2.2.2 The principle of minimum potential energy

The principle of minimum potential energy can be derived from the principle of virtual work for conservative systems. It states that of all the possible deflections satisfying kinematic compatibility, those which satisfy static equilibrium will give a stationary value of the potential energy of the body:

$$\delta\Pi = \delta U + \delta T = 0 \tag{2.3}$$

where Π is total potential energy , U is internal energy , and T is potential of external loads. The principle can only be established for conservative, or reversible, systems. That means that the material must be elastic, and the loads must be directionally constant. The material does not necessarily have to be linear elastic, however.

It can be shown that the stationary value of the total potential energy is a minimum value. If the deformed configuration can be described by the deflection w, we can write:

$$\frac{\partial \Pi}{\partial w} = 0 \tag{2.4}$$

The principle of minimum potential energy can also be used on rate-form:

$$(\frac{\partial \dot{\Pi}}{\partial w}) = 0 \tag{2.5}$$

2.3 The Rayleigh-Ritz method

In the Rayleigh-Ritz method, the continuous displacement of a body is represented by a set of assumed displacement functions. The problem is reduced to finding the unknown coefficients, or amplitudes, of these functions. It is required that the assumed functions satisfy the essential boundary conditions, but they do not need to satisfy the natural boundary conditions. For a plate, displacements and rotations along the edges are essential boundary conditions, while forces and moments along the edges are natural boundary conditions.

The Rayleigh-Ritz method is convenient to use in connection with the principle of minimum potential energy. The displacement is assumed to be written as

$$w(x, y) = \sum_m \sum_n A_{mn} g_m(x) g_n(y) \tag{2.6}$$

where g_m and g_n are shape functions, and A_{mn} are displacement amplitudes. The principle of minimum potential energy may then be rewritten as

$$\frac{\partial \Pi}{\partial A_{mn}} = 0 \tag{2.7}$$

The rate form of this equation is

$$(\frac{\partial \dot{\Pi}}{\partial A_{mn}}) = 0 \tag{2.8}$$

The problem is now to find a set of unknowns A_{mn} or $\dot{A}_{mn}$, rather than to find a continuous displacement $w(x, y)$.

2.4 Large deflection plate theory

Using the Love-Kirchoff assumption that lines normal to the undeformed middle surface remain normal to this surface, the strains in a material point can be taken as the sum of membrane and bending strain:

$$\varepsilon_{ij}^{tot} = \varepsilon_{ij} - z w_{,ij} \qquad i, j = x, y \tag{2.9}$$

where z is the vertical distance from the plate neutral axis to the material point in consideration, and ε_{ij} is the membrane strain. This is the two-dimensional extension of the Euler-Bernoulli hypothesis for bending of beams. According to Marguerre (Marguerre 1937), who extended the von Kármán nonlinear plate theory to plates with an initial curvature, the membrane strains can be written as:

$$\varepsilon_x = u_{,x} + \frac{1}{2} w_{,x}^2 + w_{0,x} w_{,x} \tag{2.10}$$

$$\varepsilon_y = v_{,y} + \frac{1}{2} w_{,y}^2 + w_{0,y} w_{,y} \tag{2.11}$$

$$\gamma_{xy} = u_{,y} + v_{,x} + w_{,x} w_{,y} + w_{0,x} w_{,y} + w_{,x} w_{0,y} \tag{2.12}$$

where w and w_0 are the additional and initial out-of-plane deflection of the plate, respectively, and u and v are displacement in x and y-direction, respectively. Static equilibrium is achieved through the plate differential equation. Using the Airy stress function F, defined

in terms of the membrane stress σ so that

$$\sigma_x = F_{,yy} \tag{2.13}$$
$$\sigma_y = F_{,xx} \tag{2.14}$$
$$\sigma_{xy} = -F_{,xy} \tag{2.15}$$

the differential equation for large deflections of an isotropic elastic plate can be written as

$$\nabla^4 w = \frac{t}{D}\left[\frac{p}{t} + F_{,yy}(w+w_0)_{,xx} + F_{,xx}(w+w_0)_{,yy} - 2F_{,xy}(w+w_0)_{,xy}\right] \tag{2.16}$$

Here, p is the lateral pressure, t is plate thickness, and D is the bending stiffness of the plate,

$$D = \frac{Et^3}{12(1-\nu^2)} \tag{2.17}$$

where E is elastic modulus, and ν is P oisson's ratio. The condition for strain compatibility can be derived from the membrane strain equations, Eq. (2.10) through (2.12). By differentiation and combination of the equations, the requirement for strain compatibility can be written:

$$\varepsilon_{x,yy} + \varepsilon_{y,xx} - \gamma_{xy,xy} = w_{,xy}^2 - w_{,xx}w_{,yy} + 2w_{0,xy}w_{,xy} - w_{0,xx}w_{,yy} - w_{0,yy}w_{,xx} \tag{2.18}$$

Using Hook's law, and introducing the stress function, the plate compatibility equation becomes:

$$\nabla^4 F = E(w_{,xy}^2 - w_{,xx}w_{,yy} + 2w_{0,xy}w_{,xy} - w_{0,xx}w_{,yy} - w_{0,yy}w_{,xx}) \tag{2.19}$$

T ogether, the tw o differential equations Eq. (2.16) and (2.19) are the von Karman plate equations modified for plates with imperfections. They are of the fourth order and coupled, and therefore in general not possible to solve exactly .In the current work, the continuous deflection w is replaced by a set of assumed displacement functions. Then, a stress function F that satisfies the compatibility equation must be found. When the principle of virtual w ork or minimum potential energy is used, the plate differential equation does not need to be solved.

2.5 Material law

The material law for elastic material is:

$$\sigma_{ij} = C_{ijkl}\varepsilon_{kl} \qquad i,j,k,l = x,y,z \tag{2.20}$$

where C_{ijkl} is the general linear elastic stiffness tensor. For thin plates it is usual to assume plane stress condition, so that $\sigma_z = \tau_{yz} = \tau_{zx} = 0$. For an isotropic material we then have Hook's law

$$\sigma_x = \frac{E}{(1+\nu^2)}(\varepsilon_x + \nu\varepsilon_y) \tag{2.21}$$

$$\sigma_y = \frac{E}{(1+\nu^2)}(\varepsilon_y + \nu\varepsilon_x) \tag{2.22}$$

$$\sigma_{xy} = 2G\varepsilon_{xy} \tag{2.23}$$

where $G = \frac{E}{2(1+\nu)}$ is the shear modulus. The inverse relation is

$$\varepsilon_x = \frac{1}{E}(\sigma_x - \nu\sigma_y) \tag{2.24}$$

$$\varepsilon_y = \frac{1}{E}(\sigma_y - \nu\sigma_x) \tag{2.25}$$

$$\varepsilon_{xy} = \frac{1}{2G}\sigma_{xy} \tag{2.26}$$

Yielding is assessed by the von Mises yield criterion:

$$\sigma_{eq} = \sqrt{\sigma_x^2 + \sigma_y^2 - \sigma_x\sigma_y + 3\sigma_{xy}^2} < \sigma_f \tag{2.27}$$

where σ_{eq} is the equivalent stress, and σ_f is the initial yield stress of the material.

For most of the buckling models developed in the current work, the onset of yielding due to membrane stress is taken as the criterion for the ultimate load of the structure, and material nonlinearities are not considered. For the unstiffened plate, a model that includes plasticity effects has been developed. For elastic-plastic materials, an incremental flow law must be applied, in order to allow for elastic unloading in the plastic range. A material law on total form cannot be used, since there is no unique relationship between stresses and strains.

The incremental material law is written as

$$\dot{\sigma}_{ij} = C^{ep}_{ijkl}\dot{\varepsilon}_{kl} \qquad i,j,k,l = x,y \tag{2.28}$$

or

$$\dot{\varepsilon}_{ij} = M^{ep}_{ijkl}\dot{\sigma}_{kl} \qquad i,j,k,l = x,y \tag{2.29}$$

where C^{ep}_{ijkl} is the elastic-plastic stiffness matrix, and M^{ep}_{ijkl} is the elastic-plastic flexibility matrix. The strain rate $\dot{\varepsilon}_{kl}$ is the total strain, i.e. the sum of elastic and plastic strain in each material point.

The elastic-plastic stiffness matrix for plane stress and isotropic hardening is:

$$[C^{ep}_{ijkl}] = \begin{bmatrix} \frac{E}{1-\nu^2} - \frac{s_1^2}{s} & & sym. \\ \frac{\nu E}{1-\nu^2} - \frac{s_1 s_2}{s} & \frac{E}{1-\nu^2} - \frac{s_2^2}{s} & \\ -\frac{s_1 s_6}{s} & -\frac{s_2 s_6}{s} & \frac{E}{2(1+\nu)} - \frac{s_6^2}{s} \end{bmatrix} \tag{2.30}$$

where

$$s_1 = \frac{E}{1-\nu^2}(s_x + \nu s_y) \tag{2.31}$$

$$s_2 = \frac{E}{1-\nu^2}(\nu s_x + s_y) \tag{2.32}$$

$$s_6 = \frac{E}{1+\nu} s_{xy} \tag{2.33}$$

$$s = \frac{4}{9}\sigma_e H_p + s_1 s_x + s_2 s_y + 2 s_6 s_{xy} \tag{2.34}$$

s_{ij} is the stress deviation tensor, which for plane stress is

$$s_x = \frac{2}{3}\sigma_x - \frac{1}{3}\sigma_y \tag{2.35}$$

$$s_y = \frac{2}{3}\sigma_y - \frac{1}{3}\sigma_x \tag{2.36}$$

$$s_{xy} = \sigma_{xy} \tag{2.37}$$

while σ_e is the von Mises equivalent stress, and H_p is the plastic modulus, i.e. the slope of the uniaxial stress-plastic strain curve at the current value of σ_e.

2.6 Staging and incrementation

A stiffened plate may be subjected to a combination of several loads simultaneously. They may be applied sequentially, proportionally or by some other scheme. In order to reduce the number of load parameters to one, a piecewise linear load path is prescribed. Each linear part of the load history is called a stage, and the process is therefore referred to as staging. Within each stage s, the load parameter is varied from 0 to 1. The external forces P_i can then be represented by the single load parameter Λ as:

$$P_i(\Lambda) = P_i^{(s-1)} + \Lambda \left[P_i^{(s)} - P_i^{(s-1)} \right] \tag{2.38}$$

Now only the load parameter Λ enters the equation system as an unknown, and all loads may be calculated from the load parameter after the solution has been obtained. Any desired load history may be approximated by defining a sufficiently large number of load stages.

As will be shown, the potential energy of a plate subjected to large deflections is of the fourth order in the deflection. The equations resulting when using the principle of minimum potential energy and the Rayleigh-Ritz method are therefore of the third order in the displacement amplitudes. An incremental solution procedure is applied in order to obtain a linear equation system, and to avoid solving a set of third order equations. Linear equation systems are easily solved, and have a unique solution in contrast to third order systems. Using perturbation theory, as done in (Steen 1998), a general rate parameter η is defined so that:

$$\dot{A}_{mn} = \frac{\partial A_{mn}}{\partial \eta} \tag{2.39}$$

$$\dot{\Lambda} = \frac{\partial \Lambda}{\partial \eta} \tag{2.40}$$

The rate parameter may be considered as a pseudo-time. Using this kind of parameter is a more general method than pure load control or pure displacement control methods, since any type of behavior can be handled, including passing limit points and turning points. This means that even unstable phenomenon such as snap-through and snap-back problems can be treated. The updated displacements and load parameter are calculated as a Taylor series:

$$A^i_{mn} = A^{i-1}_{mn} + \eta \dot{A}^{i-1}_{mn} + \frac{1}{2}\eta^2 \ddot{A}^{i-1}_{mn} + ... \tag{2.41}$$

$$\Lambda^i = \Lambda^{i-1} + \eta \dot{\Lambda}^{i-1} + \frac{1}{2}\eta^2 \ddot{\Lambda}^{i-1}_{mn} + ... \tag{2.42}$$

where i is the current increment. In principle, the perturbation theory can be applied up to any order. For the unstiffened plate, the energy formulations have been derived up to the second order. The second order terms can be considered as an alternative to using equilibrium iterations between the increments. They increase the accuracy and can be used to control the size of the increments in the analysis, since the second order rate represents the curvature of the equilibrium curve. It is found, however, that the first order approximation gives sufficient accuracy when small increments are used. This will be demonstrated by numerical examples, which are all based on first order incrementation. It can also be useful to have information about the response in many increments. For the subsequent derivations, only first order incrementation is therefore used.

The perturbation parameter can be defined in various ways. A convenient approach is to use arc-length incrementation. This is achieved by defining the perturbation parameter so that the increments are taken as specified steps along the equilibrium curve in the load-displacement space. The following relation must then be satisfied:

$$\Delta\Lambda^2 + \Delta q_{mn}^2 = \Delta\eta^2 \tag{2.43}$$

Summation over all mn is implied. q_{mn} are the displacement amplitudes made non-dimensional with respect to some geometry parameter, such as the plate thickness:

$$q_{mn} = \frac{A_{mn}}{t} \tag{2.44}$$

The scaling is necessary to make the equations dimensionally consistent. By letting the increments go towards zero, the following relation is found:

$$\dot{\Lambda}^2 + \dot{q}_{mn}^2 = 1 \tag{2.45}$$

2.7 Solving the first order equations

Applying the principle of minimum potential energy on rate form, and assuming a displacement shape with $(M \cdot N)$ terms, the problem is reduced to a system of $(M \cdot N)$ linear equations with $(M \cdot N + 1)$ unknowns. The unknowns are the $M \cdot N$ displacement rate amplitudes $\dot{A}_{mn}$ and the load rate parameter $\dot{\Lambda}$. The last equation necessary to solve the equation system is Eq. (2.45). This last equation is nonlinear in the unknown rate parameters, and can therefore not be included in the equation system directly. The solution procedure is explained in the following.

The rate of minimum potential energy may be written:

$$(\frac{\partial\dot{\Pi}}{\partial A_{fg}}) = \frac{\partial^2\Pi}{\partial A_{fg}\partial A_{mn}}\frac{\partial A_{mn}}{\partial\eta} + \frac{\partial^2\Pi}{\partial A_{fg}\partial\Lambda}\frac{\partial\Lambda}{\partial\eta} = 0 \tag{2.46}$$

Using matrix notation, this equation system can be written:

$$\mathbf{K}\dot{\mathbf{A}} + \mathbf{G}\dot{\mathbf{\Lambda}} = \mathbf{0} \tag{2.47}$$

where

$$\mathbf{K} = \frac{\partial^2\Pi}{\partial\mathbf{A}^2} \tag{2.48}$$

$$\mathbf{G} = \frac{\partial^2\Pi}{\partial\mathbf{A}\partial\Lambda} \tag{2.49}$$

The **K**-matrix may be interpreted as an incremental stiffness matrix, while the **G**-vector can be interpreted as an incremental load vector. The solution of this equation system is written:

$$\begin{aligned} \dot{\mathbf{A}} &= -\dot{\Lambda}\mathbf{K}^{-1}\mathbf{G} \\ &= -\dot{\Lambda}\mathbf{D} \end{aligned} \tag{2.50}$$

The matrix **D** is defined as $\mathbf{D} = \mathbf{K}^{-1}\mathbf{G}$ and has the elements d_{mn}. Substituting **D** into Eq. (2.45) gives:

$$\dot{\Lambda}^2(d_{11}^2 + d_{12}^2 + ... + d_{MN}^2 + t^2) = t^2 \tag{2.51}$$

$$\Rightarrow \dot{\Lambda} = \pm\frac{t}{\sqrt{d_{11}^2 + d_{12}^2 + ... + d_{MN}^2 + t^2}} \tag{2.52}$$

The displacement rate amplitudes are then found as

$$\dot{A}_{mn} = \dot{\Lambda} d_{mn} \tag{2.53}$$

The reason for the $\pm$ in Eq. (2.52) is that by specifying an arc length increment along the equilibrium curve there will always be two possible solutions, one in the direction of positive traversal and one in the direction of negative traversal.

In order to trace the complete response curve, the solution of positive traversal must be found. Two common criteria for choosing the correct solution are the work criterion and the angle criterion. The former is based on the requirement that the work performed by the external forces shall be increasing. This criterion works fine for most usual problems, but breaks down in case of snap-back problems, in which the work after the turning point is decreasing.

The angle criterion is applicable even for such problems, and is therefore used in the current work. It is based on the assumption that the equilibrium curve is smooth. Hence, the angle between the tangents to the curve in two consecutive increments should be a small number. More precisely, the angle between the tangent to the curve in increment (i) and the tangent to the curve in the next increment (i+1) in the direction of positive traversal, should always be smaller than the angle between the tangent to the curve in increment (i) and the tangent to the curve in the next increment (i-1) in the direction of negative traversal.

Numerically, this can be implemented by calculating the angles α_+ and α_- corresponding

to the + and - sign in Eq. (2.52) above:

$$\alpha_+ = \arccos\left[\dot{\Lambda}_+(\dot{\Lambda}_{i-1} + \frac{d_{mn}\dot{A}_{mn,i-1}}{t^2})\right] \tag{2.54}$$

$$\alpha_- = \arccos\left[\dot{\Lambda}_-(\dot{\Lambda}_{i-1} + \frac{d_{mn}\dot{A}_{mn,i-1}}{t^2})\right] \tag{2.55}$$

The correct sign of the load rate parameter is $\dot{\Lambda}_+$ if α_+ is the smaller angle, and $\dot{\Lambda}_-$ if α_- is the smaller angle.

2.8 Solving the second order equations

The second order rate of minimum potential energy may be written:

$$\begin{aligned}(\frac{\partial\ddot{\Pi}}{\partial A_{fg}}) &= \frac{\partial^3\Pi}{\partial A_{fg}^3}\dot{A}_{fg}^2 + 2\frac{\partial^3\Pi}{\partial A_{fg}^2\partial\Lambda}\dot{A}_{fg}\dot{\Lambda} + \frac{\partial^2\Pi}{\partial A_{fg}^2}\ddot{A}_{fg} + \frac{\partial^2\Pi}{\partial A_{fg}\partial\Lambda}\ddot{\Lambda} \\ &= \mathbf{K}\ddot{\mathbf{A}} + \mathbf{G}\ddot{\mathbf{\Lambda}} + \mathbf{F} = \mathbf{0}\end{aligned} \tag{2.56}$$

where

$$\mathbf{F} = \frac{\partial^3\Pi}{\partial A_{fg}^3}\dot{A}_{fg}^2 + 2\frac{\partial^3\Pi}{\partial A_{fg}^2\partial\Lambda}\dot{A}_{fg}\dot{\Lambda} \tag{2.57}$$

The last equation necessary in order to solve the above equation system is found by differentiation of Eq. (2.45):

$$\dot{\Lambda}\ddot{\Lambda} + \dot{q}_{mn}\ddot{q}_{mn} = 0 \tag{2.58}$$

Since this equation is linear in the second order rate parameters, it can be included in the equation system directly. The first order perturbation parameters are known from the solution of the first order equations. Hence, a new equation system is formed, and the second order rates can be calculated:

$$\mathbf{K_2}\ddot{\mathbf{A}}_\mathbf{2} + \mathbf{G_2} = \mathbf{0} \quad \Rightarrow \quad \ddot{\mathbf{A}} = -\mathbf{K_2^{-1}}\mathbf{G_2} \tag{2.59}$$

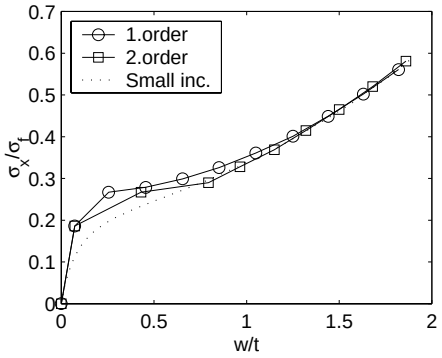

Figure 2.2: Deflection at midpoint under axial loading for 1.0x1.0x0.009m plate ($\beta = 3.7$)

where

$$\mathbf{K_2} = \begin{bmatrix} \mathbf{K} & \mathbf{G} \\ \dot{\mathbf{A}} & \dot{\Lambda} \end{bmatrix} \quad , \quad \mathbf{G_2} = \begin{bmatrix} \mathbf{F} \\ \mathbf{0} \end{bmatrix} \quad , \quad \ddot{\mathbf{A}}_\mathbf{2} = \begin{bmatrix} \ddot{\mathbf{A}} \\ \ddot{\Lambda} \end{bmatrix} \tag{2.60}$$

Comparisons are made between results obtained with first order incrementation and with second order incrementation in Fig. 2.2. The plot is for a 1.0x1.0x0.009m plate subjected to axial loading. The load is made non-dimensional with the yield stress $\sigma_f = 235MPa$. The plate slenderness is $\beta = \frac{b}{t}\sqrt{\frac{\sigma_f}{E}} = 3.7$. First order and second order approximations are plotted for an arc-length of $\eta = 0.2$, which is considered to be large. Some difference is seen, but not so much considering the large arc-length. When $\eta = 0.02$ is used (labelled 'Small inc.' in the figure), no difference is seen. With respect to computational efficiency, it is found that the cost of calculating the second order rates is of the same order as calculation of the first order rates. This indicates that computational gain is not likely to be achieved by including the second order terms. The rest of the models are therefore derived using only first order incrementation.

2.9 Calculation of linear eigenmode

The emphasis in the current work is calculation of nonlinear buckling response. The linear buckling eigenvalue is of less practical interest, because it does not give much information about the real strength of the structure. It can be useful, however, to calculate the linear eigenmode. Although the shape of the eigenmode is not necessarily the same as the post-buckling deflection shape, it is useful for setting the initial deflection. All structures have

imperfections, but the actual shape is usually not known. The most conservative approach is then usually to use the eigenmode as the imperfection shape.

The condition for structural instability is that the incremental stiffness matrix $\mathbf{K}$ is singular. The eigenproblem is therefore defined so that:

$$\mathbf{K}\mathbf{x} = \mathbf{0} \tag{2.61}$$

where $\mathbf{x} \neq \mathbf{0}$ is the eigenvector.

In a linear eigenvalue calculation, the change in geometry prior to buckling is neglected. The stiffness matrix is then decomposed as a sum of material and geometric stiffness:

$$\mathbf{K} = \mathbf{K}_M + \mathbf{K}_G \tag{2.62}$$

The material stiffness is the stiffness evaluated at the reference configuration. Usually the reference configuration is the initial configuration, so that the material stiffness is evaluated with $\mathbf{A} = \mathbf{0}$ and $\Lambda = 0$. For the specific cases considered here, the material stiffness equals the stiffness due to bending potential energy:

$$\mathbf{K}_M = \mathbf{K}_B \tag{2.63}$$

The geometrical stiffness is linearly dependent on the load factor Λ:

$$\mathbf{K}_G = \Lambda \mathbf{K}_1 \tag{2.64}$$

The matrix $\mathbf{K}_1$ is the stiffness matrix due to external potential energy ,evaluated with $\mathbf{A} = \mathbf{0}$ and $\Lambda = 1$.

$$\mathbf{K}_1 = \mathbf{K}_{ext}(\Lambda = 1) \tag{2.65}$$

The eigenproblem is now written:

$$(\mathbf{K}_0 + \Lambda_E \mathbf{K}_1)\mathbf{x} = \mathbf{0} \tag{2.66}$$

or equivalently

$$\mathbf{K}_0\mathbf{x} = -\Lambda_E \mathbf{K}_1\mathbf{x} \tag{2.67}$$

This is a generalized symmetric algebraic eigenproblem

$$\mathbf{M}_1\mathbf{x} = \Lambda_E \mathbf{M}_2\mathbf{x} \tag{2.68}$$

where Λ_E is the eigenvalue corresponding to the eigenvector $\mathbf{x}$. For the cases considered here, both $\mathbf{M}_1 = \mathbf{K}_0$ and $\mathbf{M}_2 = -\mathbf{K}_1$ are real symmetric. In addition, $\mathbf{M}_1$ is positive definit.

The mathematical solution can be obtained using standard algebraic routines. Efficient solution may be obtained for the case where $\mathbf{M}_1$ and $\mathbf{M}_2$ are symmetric, and $\mathbf{M}_2$ is positive definit. In order to achieve this, the equation is rewritten as:

$$-\mathbf{K}_1\mathbf{x} = \Lambda_E^{'}\mathbf{K}_0\mathbf{x} \tag{2.69}$$

so that $\mathbf{M}_1 = -\mathbf{K}_1$, $\mathbf{M}_2 = \mathbf{K}_0$, and $\Lambda_E^{'} = 1/\Lambda_E$.

Chapter 3

Buckling of unstiffened plates

Buckling of unstiffened plates is now considered. This is a first step towards a buckling model for an integrated stiffened panel. The formulations derived here are developed further in subsequent chapters. The unstiffened plate is also of interest in itself. An example is applications where the serviceability limit state is important. A simplified deflection analysis may then be performed by taking the plate between stiffeners as simply supported, neglecting the rotational restraint from the stiffeners. Another example is a stiffened panel with weak stiffeners, where deflection in the global mode is dominant. Such a panel may be analysed as an orthotropic plate, by including the effect of the stiffeners as orthotropic stiffness coefficients in the model.

An isotropic elastic, simply supported plate is considered in section 3.1, while a plate with clamped edges is discussed in section 3.2. These models are used as part of the local model presented in chapter 4. An orthotropic elastic plate is studied in section 3.3. This model is developed further in chapter 5 to a global buckling model for stiffened panels. Finally, a plate with elastic-plastic material properties is analysed in section 3.4. Plasticity is not considered further in this work, so the derivations for the elastic-plastic unstiffened plate is presented as an independent study.

For all models, examples of application are given, and comparisons are made with nonlinear finite element calculations using ABAQUS. A large number of cases have been studied in order to test the developed models, and only a few may be included here.

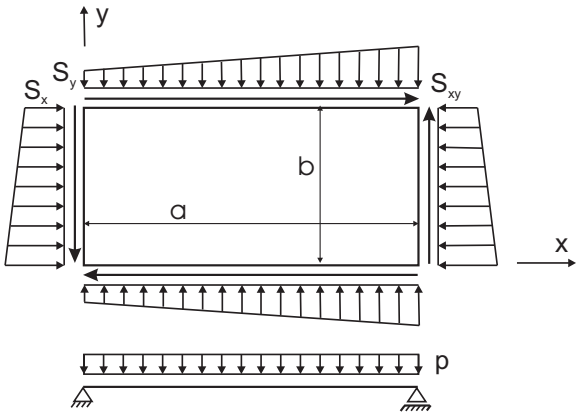

Figure 3.1: Unstiffened simply supported plate

3.1 Simply supported plate

An unstiffened, rectangular plate is studied, Fig. 3.1. The length is a, the breadth is b, and the thickness is t. The material is assumed to be isotropic and linear elastic, and is characterized by the elastic modulus E and Poison's ratio ν.

The external loads are in-plane compression, shear force and lateral pressure. The external in-plane stress S_x, S_y and forces P_x, P_y are defined as positive in compression, since it is mainly compression that is of interest for study of the buckling phenomenon. However, the internal stress σ_x and σ_y is defined as positive in tension as usual.

3.1.1 Assumptions

The edges of the plate are assumed to be free to move in-plane, but forced to remain straight. According to Marguerre's plate theory ,Eq. (2.10) and Eq. (2.11), this means that

$$\int_0^a (\varepsilon_x - \frac{1}{2}w_{,x}^2 - w_{,x}w_{0,x})dx = \Delta u \ \ \forall \ \ y \tag{3.1}$$

$$\int_0^b (\varepsilon_y - \frac{1}{2}w_{,y}^2 - w_{,y}w_{0,y})dy = \Delta v \ \ \forall \ \ x \tag{3.2}$$

This restriction represents the effect of the neighboring plates that will support the plate

in a larger structure. The conditions for simply supported edges are:

$$\begin{array}{ll} w = 0 & \text{at all edges} \\ w_{,yy} + \nu w_{,xx} = 0 & \text{at } y = 0, b \\ w_{,xx} + \nu w_{,yy} = 0 & \text{at } x = 0, a \end{array} \tag{3.3}$$

These conditions are satisfied by taking the additional and initial deflections as double Fourier series, as first suggested by Navier:

$$w^s = \sum_{m=1}^{M_s} \sum_{n=1}^{N_s} A^s_{mn} \sin(\frac{m\pi x}{a}) \sin(\frac{n\pi y}{b}) \tag{3.4}$$

$$w^s_0 = \sum_{m=1}^{M_s} \sum_{n=1}^{N_s} B^s_{mn} \sin(\frac{m\pi x}{a}) \sin(\frac{n\pi y}{b}) \tag{3.5}$$

where the superscript s is used to indicate sine-mode, in contrast to the cosine-mode which is used in the next section for the clamped plate. Initial deflection is included in order to avoid bifurcation problems, and because all plates in the real world have a certain degree of out-of-plane imperfection resulting from the fabrication process. The most common approach is to set the imperfection shape equal to the eigenmode of the plate. Alternatively, the measured imperfection w_i in a plate may be represented by w^s_0 by calculating the Fourier coefficients:

$$B^s_{mn} = \frac{4}{ab} \int_a \int_b w_i(x, y) \sin(\frac{m\pi x}{a}) \sin(\frac{n\pi y}{b}) dy dx \tag{3.6}$$

Perfect plates can be analysed as a limiting case by specifying a very small initial deflection.

In order to satisfy strain compatibility, a stress function F must be found using the assumed displacements, so that the plate compatibility equation is satisfied. The approach followed is the same as that of Levy (Levy 1942), but in addition geometrical imperfections are accounted for using Marguerre's plate theory. Shear force is also included as an additional load case. The stress function is assumed to have the following form:

$$F^s = -\frac{S_x y^2}{2} - \frac{S_y x^2}{2} - S_{xy} xy + \sum_{0}^{2M_s} \sum_{0}^{2N_s} f^s_{mn} \cos(\frac{m\pi x}{a}) \cos(\frac{n\pi y}{b}) \tag{3.7}$$

The first three terms results from constant external stress, while the summation term represents the membrane stress developing due to deflection. The stress function coefficients f^s_{mn} satisfying compatibility are found by substitution of the above equations into the compatibility equation, Eq. (2.19), as shown in appendix A. The coefficients derived in the

current work are not equal to the ones presented in the work b y Levy This could be due to some different definitions. The result obtained here is:

$$f^s_{mn} = \frac{E}{4(m^2\frac{b}{a} + n^2\frac{a}{b})^2} \sum_{rspq} b^s_{rspq}(A^s_{rs}A^s_{pq} + A^s_{rs}B^s_{pq} + A^s_{pq}B^s_{rs}) \tag{3.8}$$

where $f^s_{0,0}$ is defined as zero, and the coefficients b^s_{rspq} are in teger n umbers given as

$$b^s_{rspq} = rspq + r^2q^2 \quad \text{if} \quad \begin{cases} \pm(r-p) = m, s+q = n \\ r+p = m, \pm(s-q) = n \end{cases} \tag{3.9}$$

$$b^s_{rspq} = rspq - r^2q^2 \quad \text{if} \quad \begin{cases} r+p = m, s+q = n \\ \pm(r-p) = m, \pm(s-q) = n \end{cases} \tag{3.10}$$

It can be sho wn that the stress function F as defined abo ve satisfies not only the compatibilit y equation, but also the boundary conditions for the plate. The integrated stress resultan t in an y cross-section equals the external load, while the integrated elongation is constant o ver the edges. F rom the stress function, the membrane stress components $\sigma_x = F^s_{,yy}$, $\sigma_y = F^s_{,xx}$, and $\sigma_{xy} = -F^s_{,xy}$ are found by differentiation. Knowing the stresses, the in ternal poten tial energy can be calculated as outlined in the following.

3.1.2 Internal potential energy

In general, the internal potential energy is

$$U = \frac{1}{2}\int_V \sigma_i\varepsilon_i dV \tag{3.11}$$

where V is the body volume. Summation is implied. The internal energy can be divided into a part due to membrane stretching of the middle plane of the plate, and a part due to bending about the middle plane. F or this purpose, the Lo ve-Kirchhoff assumption is applied. The stress and strain is written as the sum of a membrane part which is constant o ver the thic kness, and a bending part whic h is linearly varying. We can then write:

$$U = \frac{1}{2}\int_V (\sigma_m + \sigma_b)(\varepsilon_m + \varepsilon_b)dV \tag{3.12}$$

$$= \frac{1}{2}\int_V (\sigma_m\varepsilon_m + \sigma_b\varepsilon_b)dV \tag{3.13}$$

$$= U_m + U_b \tag{3.14}$$

The coupling terms disappear when integrating over the thickness, since the bending is acting about the plate middle plane. The potential energy due to bending and membrane stretching can therefore be calculated separately.

Using Hook's law, and then substituting the stress function for the membrane stress, the membrane energy can be expressed as:

$$U_m = \frac{t}{2E}\int_0^a\int_0^b \left[(\sigma_{xx}+\sigma_{yy})^2 - 2(1+\nu)(\sigma_{xx}\sigma_{yy}-\sigma_{xy}^2)\right] dydx \tag{3.15}$$

$$= \frac{t}{2E}\int_0^a\int_0^b \left[(F^s_{,xx}+F^s_{,yy})^2 - 2(1+\nu)(F^s_{,xx}F^s_{,yy}-(F^s_{,xy})^2)\right] dydx \tag{3.16}$$

Introducing the assumed form of the stress function, integration over the plate area can be carried out analytically, and a closed form expression is obtained. The result is given in appendix A. It can be seen that the membrane energy is proportional to the displacement amplitudes A^s_{mn} to the fourth order, since f^s_{mn} is quadratic in A^s_{mn}. The minimum membrane energy and rate of minimum membrane energy is calculated by differentiation, and is of third and second order in A^s_{mn}, respectively. Hence, the membrane energy gives a second order contribution to the incremental stiffness matrix.

By substituting the Love-Kirchhoff assumption for the bending strain, using Hook's law, and integrating over the thickness, the following expression for the potential energy due to bending is derived:

$$U_b = \frac{D}{2}\int_0^a\int_0^b \left[(w^s_{,xx}+w^s_{,yy})^2 - 2(1-\nu)(w^s_{,xx}w^s_{,yy}-(w^s_{,xy})^2)\right] dydx \tag{3.17}$$

Integration over the plate area is carried out analytically by introducing the assumed form of the displacements. The result is differentiated twice to find the minimum potential energy and the rate of minimum potentialenergy . The resulting expressions are given in appendix A. The bending energy is proportional to the square of the displacement amplitudes, and gives a constant contribution to the incremental plate stiffness. The incremental bending stiffness therefore only needs to be calculated once, in contrast to the incremental membrane stiffness which must be calculated for each new increment.

3.1.3 Potential of external loads

In general, the external potential energy is calculated as:

$$T = \int_S t_i u_i dS \tag{3.18}$$

where S is body surface, t_i is external surface load in direction i, and u_i is surface displacement in direction i.

Constant edge-loads are considered first. The poten tial ofin-plane compressive forces is calculated as external force multiplied with displacement:

$$T_c = S_x bt\Delta u + S_y at\Delta v \tag{3.19}$$

where Δu and Δv are the elongations of the plate in the x- and y-direction, respectively. These are calculated according to Eq. (3.1) and Eq. (3.2). For compression loads, the elongations will be negative. Carrying out the integration, as shown in appendix A, it is found that the potential of external loads consists of tw o parts. One part contributes to the incremental load vector $\mathbf{G}$, and is proportional to the displacement amplitudes A_{mn}. The other part contributes to the incremental stiffness matrix $\mathbf{K}$, and is proportional to the external load parameter Λ, defined in Eq. (2.38).

If the in-plane loads vary linearly, the external stress is written:

$$S_x(y) = S_x^1 + (S_x^2 - S_x^1)\frac{y}{b} \tag{3.20}$$

$$S_y(x) = S_y^1 + (S_y^2 - S_y^1)\frac{x}{a} \tag{3.21}$$

where S_x^1 and S_x^2 are the magnitudes of the external axial stress at $y = 0$ and $y = b$, respectiv ely.Similarly, S_y^1 and S_y^2 are the external transverse stress at $x = 0$ and $x = a$, respectiv ely.The stress function is then modified as:

$$\begin{aligned} F^s = & - S_x^1\frac{y^2}{2} - (S_x^2 - S_x^1)\frac{y^3}{6b} - S_y^1\frac{x^2}{2} - (S_y^2 - S_y^1)\frac{x^3}{6a} - S_{xy}xy \\ & + \sum_0^{2M_s}\sum_0^{2N_s} f_{mn}^s \cos(\frac{m\pi x}{a})\cos(\frac{n\pi y}{b}) \end{aligned} \tag{3.22}$$

The external energy is calculated as:

$$\begin{aligned} T_c &= t\int_0^a\int_0^b (S_x(y)u_{,x} + S_y(x)v_{,y})dxdy \\ &= t\int_0^a\int_0^b \left(S_x(y)(\varepsilon_x - \frac{1}{2}(w_{,x}^s)^2 - w_{,x}^s w_{0,x}^s) + S_y(x)(\varepsilon_y - \frac{1}{2}(w_{,y}^s)^2 - w_{,y}^s w_{0,y}^s)\right)dxdy \end{aligned} \tag{3.23}$$

The membrane strain terms ε_x and ε_y are troublesome. For the case with constant edge load, the integrated membrane terms must be zero if static equilibrium of the plate is to be fulfilled. For non-constant loads, this is not necessarily the case. Until now, it has been assumed that the external stress is transferred directly into the plate. For a plate with constant edge-loads and straight edges, this is also the case in practice. For a plate with non-constant edge-loads, however, this is not exactly correct. For the limiting case of a plate in pure in-plane bending, the assumed stress distribution is actually equal to that of a plate with edges free to deform in-plane. For a plate with straight edges in pure in-plane bending, the stresses will be transferred into the plate in a more complex pattern. This can be seen by performing nonlinear finite element analysis on a flat plate subjected to pure in-plane bending.

The external energy is here calculated by neglecting the membrane terms. The calculated response will therefore be somewhere in between the solution for straigh t edges and the solution for free edges. Since it is more conservative to assume that the edges are free to bend in-plane than to assume straight edges, this solution method is considered acceptable. If the load gradient is moderate, the resulting response will be very close to the case with straigh t edges, but with increasing gradient the solution will always be on the safe side. It is also worth noticing that the linear elastic buckling value for plates in pure in-plane bending is very high. The analytical k-factor for this load condition is close to 24, compared with 4 for constant load. This means that the linear buckling stress for practical applications will be well above yield stress, so that the postbukling stiffness is of less practical importance.

From the arguments above, the external potential energy due to linearly varying edge loads can be calculated using Eq. (3.23), with $\varepsilon_x = 0$ and $\varepsilon_y = 0$. The details are given in appendix A.

The potential energy due to external shear stress S_{xy} is

$$T_\tau = S_{xy} t \int_0^a \int_0^b (u_{,y} + v_{,x}) dy dx \tag{3.24}$$

Rearranging the shear strain expression in Marguerre's equation, Eq. (2.12), we get

$$T_\tau = S_{xy} t \int_0^a \int_0^b (\gamma_{xy} - w^s_{,x} w^s_{,y} - w^s_{0,x} w^s_{,y} - w^s_{,x} w^s_{0,y}) dy dx \tag{3.25}$$

where the contribution from the γ_{xy}-term must be zero due to static equilibrium. The expressions resulting from integration over the plate area and differentiation with respect to the displacement are given in appendix A.

The contribution to the potential of external energy from lateral pressure is:

$$T_{lp} = -\int_0^a \int_0^b p w^s dy dx \tag{3.26}$$

The result is given in appendix A. The lateral pressure gives a constant contribution to the incremental load vector, but no contribution to the incremental stiffness matrix.

3.1.4 Implementation

The total rate of minimum potential energy is found by adding the contributions from internal and external energy:

$$\left(\frac{\partial \dot{\Pi}}{\partial A_{fg}}\right) = \left(\frac{\partial \dot{U}_m}{\partial A_{fg}}\right) + \left(\frac{\partial \dot{U}_b}{\partial A_{fg}}\right) + \left(\frac{\partial \dot{T}_c}{\partial A_{fg}}\right) + \left(\frac{\partial \dot{T}_\tau}{\partial A_{fg}}\right) + \left(\frac{\partial \dot{T}_{lp}}{\partial A_{fg}}\right) \tag{3.27}$$

The result is a linear equation system, on the form of Eq. (2.47). Solving this equation system, a set of displacement rate amplitudes $\dot{A}_{mn}$ is found, which are used to calculate the next increment in the analysis.

The computational model is implemented using the programming language Fortran 90. Since all expressions have been integrated analytically, the elements of the stiffness matrix $\mathbf{K}$ and $\mathbf{G}$ are exactly calculated based on the explicit expressions derived. The equation system are solved by matrix inversion for each increment. The solution procedure may hence be classified as semi-analytical.

3.1.5 Results

Some numerical examples using the presented model are given. The results are compared with analyses performed with the nonlinear FEM program ABAQUS (Hibbitt, Karlsson, and Sorensen 1994). Isotropic, elastic material is assumed. For all calculations, an elastic modulus of E=208000MPa is used. The plates are modelled using 4 node double curved general-purpose shell elements, S4R. The sources of inaccuracy in the computational model developed are drift from the correct equilibrium curve due to the incrementation, and difference between correct and assumed displacement shape. The former is controlled by specifying sufficiently small values of the perturbation parameter. The latter is controlled by specifying sufficiently large number of terms in the assumed displacement functions. This depends on the geometry and load condition, as will be shown in the following. The initial deflections are set to a small value in all the examples.

To the left in Fig. 3.2, the load-deflection response of a quadratic plate subjected to biaxial loading is shown. The load is made non-dimensional with the yield stress σ_f=313.6MPa. Proportional loading is used, and the magnitude of the load is the same in both directions. The number of terms in the deflection function is 3x3, and it is seen that the correspondence with ABAQUS results is good. The right plot shows the load-average strain response of

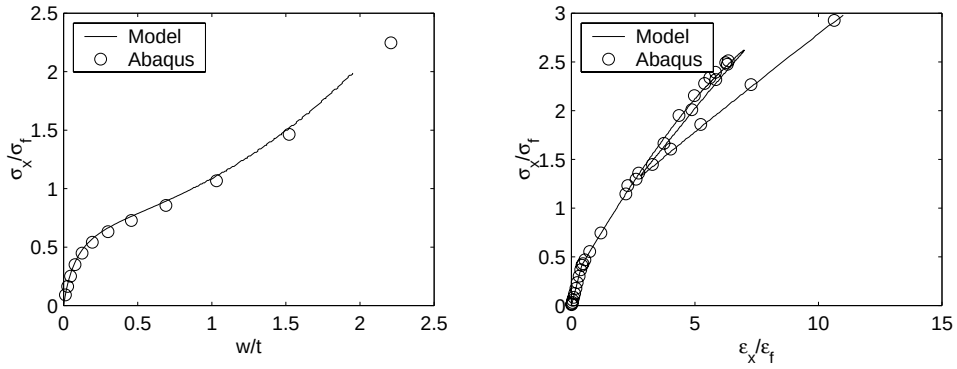

Figure 3.2: Left: Deflection at midpoint under biaxial loading for axbxt=1.0x1.0x0.026m plate ($\beta = 1.5$). Right: Snap-back under axial loading for axbxt=1.68x0.98x0.011m plate ($\beta = 3.0$)

a rectangular plate subjected to axial loading. The load is made non-dimensional with the yield stress σ_f=235MPa, and the average strain is made non-dimensional with the corresponding yield strain. Here, 8x8 deflection terms have been used in the calculation model. The snap-back in the postbuckling region is provoked by specifying an initial deflection mode which is different from the preferred one, leading to violent mode snapping. It should be noted that the snap-back occurs very late in the postbuckling region, and is therefore of more academic than practical interest. The intention is to demonstrate that such complex responses is well treated with the perturbation method used, even if only first order terms are included in the formulations.

In Fig. 3.3, the load-deflection response for a quadratic plate subjected to lateral pressure (left) and shear loading (right) is shown. The shear load is made non-dimensional with the yield stress σ_f=235MPa. The number of terms used is 3x3 for both cases. The accuracy of the calculations is good, and the computational efficiency is very high.

3.2 Clamped plate

The edges of a plate can be considered as clamped if the surrounding structure is strong enough to prevent rotation of the edges. Clamped-like conditions may also occur due to the applied loads. Lateral pressure may cause a plate to deflect symmetrically about a stiffener, and thereby causing a clamped deflection mode, as seen in Fig. 3.4.

Here, it is assumed that the longitudinal edges of the plate are clamped, while the transverse

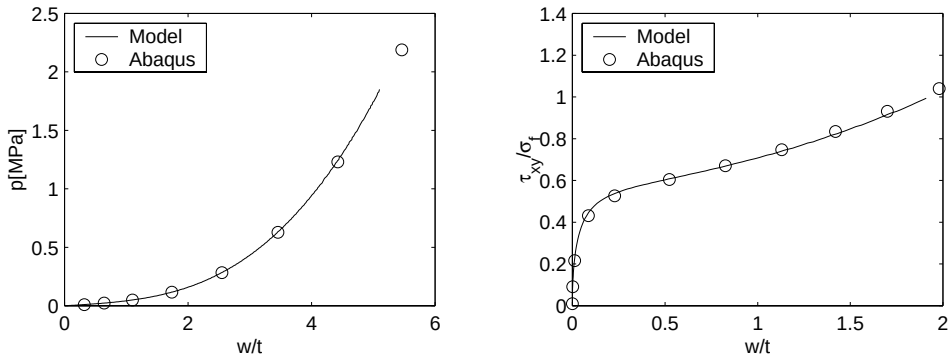

Figure 3.3: Deflection at midpoint under lateral pressure (left) and shear loading (right) for 1.0x1.0x0.009m plate ($\beta = 3.7$)

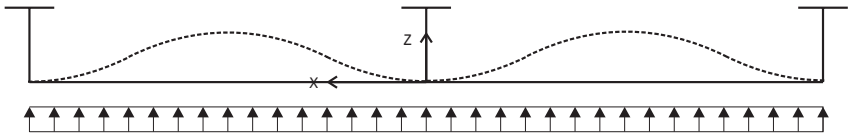

Figure 3.4: Clamped-like conditions due to lateral pressure

edges are taken as simply supported, Fig. 3.5. The number of half waves will usually be greater than one in the longitudinal direction, due to the effect of axial compression and the plate aspect ratio, and the effect of the lateral pressure on the deflection shape is therefore less significant.

3.2.1 Assumptions

As for the simply supported plate, the edges are assumed to be free to move in-plane, but forced to remain straight. The conditions for clamped longitudinal edges are expressed as:

$$\begin{array}{ll} w = 0 & \text{at all edges} \\ w_{,y} = 0 & \text{at } y = 0, b \\ w_{,xx} + \nu w_{,yy} = 0 & \text{at } x = 0, a \end{array} \tag{3.28}$$

One way to handle clamped edges is to use the same displacement functions as for the simply supported plate, and to add a rotational spring along the clamped edges. The essential boundary conditions are then satisfied, and the clamped condition can be analysed by ap-

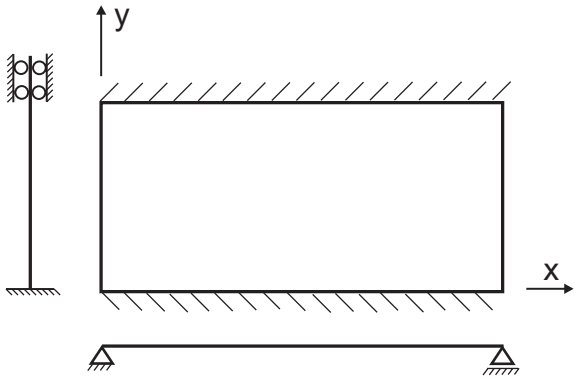

Figure 3.5: Boundary conditions for clamped plate model

plying a very stiff spring. Good results was obtained using this approach, but the number of terms required in the displacement function was found to be large. The displacement shape is estimated reasonably well with less terms, but the bending moment distribution requires more terms. This is because the bending moment resulting from a sine-series is zero along the edges, while the bending moment for a clamped plate attains its maximum value at the edges.

Better results were achieved using cosine-terms. The following displacement shape is then used:

$$w^c = \sum_{m=1}^{M_c}\sum_{n=1}^{N_c} \frac{A^c_{mn}}{2} \sin(\frac{m\pi x}{a})[1-\cos(\frac{2n\pi y}{b})] \tag{3.29}$$

$$w^c_0 = \sum_{m=1}^{M_c}\sum_{n=1}^{N_c} \frac{B^c_{mn}}{2} \sin(\frac{m\pi x}{a})[1-\cos(\frac{2n\pi y}{b})] \tag{3.30}$$

The above expressions represent a far better approximation to the clamped condition than the sine-terms, and good results may be obtained with only a few degrees of freedom, e.g. 2 or 3. Similarly, a plate with all edges clamped may be analysed using cosine-terms in both directions:

$$w^c = \sum_{m=1}^{M_c}\sum_{n=1}^{N_c} \frac{A^c_{mn}}{4} [1-\cos(\frac{2m\pi x}{a})][1-\cos(\frac{2n\pi y}{b})] \tag{3.31}$$

$$w^c_0 = \sum_{m=1}^{M_c}\sum_{n=1}^{N_c} \frac{B^c_{mn}}{4} [1-\cos(\frac{2m\pi x}{a})][1-\cos(\frac{2n\pi y}{b})] \tag{3.32}$$

The former case is considered to be of more practical interest. This is because plates between stiffeners are usually quite long, and the boundary conditions on the transverse edges are therefore less important. The latter case is not further described here. In the following, a stress function corresponding to the chosen displacements is presented, and potential energy-expressions are derived.

3.2.2 Stress function

The approach used for establishing the stress function for the clamped plate is the same as for the simply-supported plate, and the derivation is therefore omitted. The result is:

$$F^c = -\frac{S_x y^2}{2} - \frac{S_y x^2}{2} - S_{xy} xy + \sum_{0}^{2M_c} \sum_{0}^{2N_c} f^c_{mn} \cos(\frac{m\pi x}{a}) \cos(\frac{2n\pi y}{b}) \tag{3.33}$$

The coefficients f^c_{mn} are

$$f^c_{mn} = \frac{E}{4(m^2 \frac{b}{a} + 4n^2 \frac{a}{b})^2} \sum_{rspq} b^c_{rspq} (A^c_{rs} A^c_{pq} + A^c_{rs} B^c_{pq} + A^c_{pq} B^c_{rs}) \tag{3.34}$$

where $f^c_{0,0}$ is defined as zero, and the coefficients b^c_{rspq} are

$$b^c_{rspq} = \begin{cases} 2r^2q^2 & \text{if} \quad \pm(r-p) = m, q = n \\ -2r^2q^2 & \text{if} \quad r+p = m, q = n \\ -rspq - r^2q^2 & \text{if} \quad \pm(r-p) = m, s+q = n \\ rspq + r^2q^2 & \text{if} \quad r+p = m, \pm(s-q) = n \\ -rspq + r^2q^2 & \text{if} \quad r+p = m, s+q = n \\ rspq - r^2q^2 & \text{if} \quad \pm(r-p) = m, \pm(s-q) = n \end{cases} \tag{3.35}$$

3.2.3 Potential energy

The potential energy is calculated in the same way as for the simply supported plate. By substitution of the new displacement function and stress function, analytical integration can be carried out. The resulting expressions for all contributions are given in appendix A.

However, for the shear force, substituting the assumed displacements into the energy expression used for the unstiffened plate gives:

$$T_\tau = S_{xy} t \int_0^a \int_0^b (\gamma_{xy} - w^c_{,x} w^c_{,y} - w^c_{0,x} w^c_{,y} - w^c_{,x} w^c_{0,y}) dy dx \tag{3.36}$$

$$= 0 \tag{3.37}$$

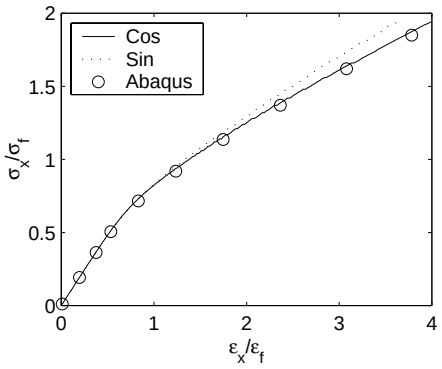

Figure 3.6: Load-average strain for 1.0x1.0x0.013m clamped plate ($\beta = 2.6$) under axial loading calculated using 2x3 cosine-terms (Cos) and 2x11 sine-terms (Sin)

The reason for this result is that the cosine-terms are alw ayssymmetric, and they are therefore not able to describe shear deformation. F or shear force analysis, it is necessary to include sine-terms in the deflection shape. A possible approach is the method described previously, where a pure sine-series is used together with a very stiff spring. An even better strategy is to use cosine-terms and sine-terms in combination. This is done for the combined plate/stiffener-model presented later, and it is therefore not further described here.

3.2.4 Results

In Fig. 3.6, the non-dimensional load-a veragestrain response for a plate with clamped longitudinal edges subjected to axial loading is shown. The load is made non-dimensional using the yield stress σ_f=235MPa. The initial deflection is set to a small value. Calculations using sine-terms as well as cosine-terms are shown. It is seen that good accuracy is obtained with only 2x3 cosine-terms, while the analysis with 2x11 sine-terms is less accurate.

3.3 Orthotropic elastic plate

Orthotropy is a special form of anisotropy, in which the material of the plate has three planes of symmetry with respect to its elastic properties. The orthotropy may be due to material properties, but for applications in steel and aluminium marine structures,

structural orthotropy is more relevant. The plates are stiffened in such a way that the panel may be considered as an orthotropic plate in terms of its overall stiffness coefficient.

In this section, a plate with orthotropic material properties is discussed. It is assumed to be homogeneous in the thickness direction, and is therefore not directly suitable for structural orthotropic problems. However, the model is developed further in chapter 5 to include general anisotropy and bending stiffness independent of in-plane stiffness. The derivations are performed for a simply supported plate. The procedure for a clamped plate would be similar.

3.3.1 Orthotropic elastic material law

The material law for an orthotropic plate is generally:

$$\sigma_{ij} = C_{ijkl}\varepsilon_{kl} \qquad i,j,k,l = 1,2,3 \tag{3.38}$$

or

$$\varepsilon_{ij} = M_{ijkl}\sigma_{kl} \qquad i,j,k,l = 1,2,3 \tag{3.39}$$

where C_{ijkl} are stiffness coefficients, and M_{ijkl} are flexibility coefficients. The nine independent and non-zero stiffness coefficients are C_{1111}, C_{1122}, C_{1133}, C_{2222}, C_{2233}, C_{3333}, C_{1212}, C_{1313}, and C_{2323}. These can be related to the three moduli of extension E_1, E_2, E_3, in the directions of orthotropy, three shear moduli G_{12}, G_{23}, G_{31}, and three coefficients of contraction, ν_{12}, ν_{23}, ν_{31}. For plane stress the six independent material coefficients may be calculated directly from the three-dimensional coefficients, or they may be defined through the two moduli of extension E_1, E_2, three shear moduli G_{12}, G_{23}, G_{31}, and the coefficient of contraction ν_{31}.

3.3.2 Orthotropic stress function

The compatibility equation for an orthotropic plate is:

$$\begin{aligned} & M_{1111}F_{,yyyy} + M_{2222}F_{,xxxx} + 2(M_{1122} + 2M_{1212})F_{,xxyy} \\ = \;& w_{,xy}^2 + 2w_{0,xy}w_{,xy} - w_{,xx}w_{,yy} - w_{0,yy}w_{,xx} - w_{,yy}w_{0,xx} \end{aligned} \tag{3.40}$$

The solution can be written on the same form as for the isotropic, simply supported plate:

$$F = -\frac{S_x y^2}{2} - \frac{S_y x^2}{2} - S_{xy}xy + \sum_0^{2M}\sum_0^{2N} f_{mn}\cos(\frac{m\pi x}{a})\cos(\frac{n\pi y}{b}) \tag{3.41}$$

The coefficients f_{mn} for the orthotropic case become:

$$\begin{aligned} f_{mn} &= \frac{1}{4a^2b^2}\left(\frac{m^4}{a^4}M_{2222} + 2\frac{m^2n^2}{a^2b^2}(M_{1122} + 2M_{1212}) + \frac{n^4}{b^4}M_{1111}\right)^{-1} \\ &\cdot \sum_{rspq} b_{rspq}(A_{rs}A_{pq} + A_{rs}B_{pq} + A_{pq}B_{rs}) \end{aligned} \tag{3.42}$$

where $f_{0,0}$ is defined as zero, and the coefficients b_{rspq} are the same integer numbers as for the isotropic, simply supported plate, Eq. (3.9).

3.3.3 Internal potential energy

The potential of in ternal energy is divided into a bending part and a membrane part, as before.

The plate membrane energy is:

$$U_m = \frac{1}{2}\int_V \sigma^m \varepsilon^m dV \tag{3.43}$$

$$= \frac{t}{2}\int_A (\sigma^m_{11}\varepsilon^m_{11} + \sigma^m_{22}\varepsilon^m_{22} + 2\sigma^m_{12}\varepsilon^m_{12})dV \tag{3.44}$$

$$= \frac{t}{2}\int_A \left(M_{1111}F^2_{,yy} + 2M_{1122}F_{,xx}F_{,yy} + M_{2222}F^2_{,xx} + 4M_{1212}F^2_{,xy}\right) \tag{3.45}$$

By substitution of the material parameters for an isotropic plate, the usual plate membrane energy equation is obtained, Eq. (3.15). Expressions resulting from integration over the plate area are found in appendix A.

The bending energy is

$$U_b = \frac{1}{2}\int_V \sigma^b \varepsilon^b dV \tag{3.46}$$

$$= \frac{1}{2}\int_V (\sigma^b_{11}\varepsilon^b_{11} + \sigma^b_{22}\varepsilon^b_{22} + 2\sigma^b_{12}\varepsilon^b_{12})dV \tag{3.47}$$

Introducing the orthotropic material law, and substituting $\varepsilon^b_{ij} = -zw_{,ij}$ for the bending

strain, we can write

$$\begin{aligned} U_b &= \frac{1}{2}\int_V \left[\varepsilon^b_{11}(C_{1111}\varepsilon^b_{11} + C_{1122}\varepsilon^b_{22}) + \varepsilon^b_{22}(C_{2211}\varepsilon^b_{11} + C_{2222}\varepsilon^b_{22}) + 4\varepsilon^b_{12}C_{1212}\varepsilon^b_{12}\right] dV \quad (3.48)\\ &= \frac{1}{2}\int_V \frac{z^2}{2}\left[w_{,11}(C_{1111}w_{,11} + C_{1122}w_{,22}) + w_{,22}(C_{2211}w_{,11} + C_{2222}w_{,22}) + 4C_{1212}w^2_{,12}\right] dV \end{aligned}$$

Using the stiffness matrix symmetry, $C_{2211} = C_{1122}$, and performing the integration over the thic kness, we get:

$$U^b = \frac{t^3}{24}\int_A \left(C_{1111}w^2_{,11} + 2C_{1122}w_{,11}w_{,22} + C_{2222}w^2_{,22} + 4C_{1212}w^2_{,12}\right) dA \quad (3.49)$$

Again, it can be shown that substitution of the isotropic stiffness coefficients reduces this equation to the usual plate bending energy equation, Eq. (3.17). The final expressions resulting from integration are given in appendix A.

3.3.4 Potential of external loads

The elongation is partly due to the membrane effect of the external force, (superscript F), and partly due to the plate deflection, (superscript D):

$$\begin{aligned} \Delta u &= \Delta u^F + \Delta u^D \quad (3.50)\\ \Delta v &= \Delta v^F + \Delta v^D \quad (3.51)\\ \gamma &= \gamma^F + \gamma^D \quad (3.52) \end{aligned}$$

The displacements due to the external force is:

$$\begin{aligned} \Delta u^F &= a(S_x M_{1111} + S_y M_{1122}) \quad (3.53)\\ \Delta v^F &= b(S_x M_{2211} + S_y M_{2222}) \quad (3.54)\\ \gamma^F &= S_{xy} M_{1212} \quad (3.55) \end{aligned}$$

This part is irrelevan t with respect to the potential energy since it disappears when differentiating with respect to the deflection.

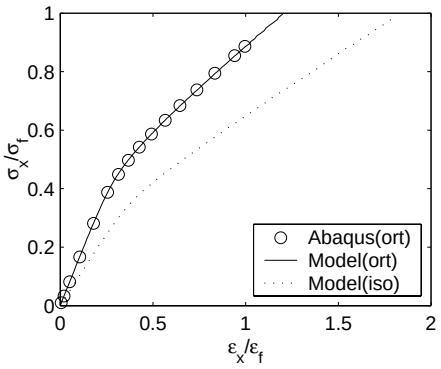

Figure 3.7: Load-average strain for 1.68x0.98x0.011m ($\beta = 3.0$) orthotropic (ort) and isotropic (iso) plate under axial loading using 5x3 terms

The part due to the deflection is independent of the material properties, and is therefore the same as for the isotropic plate. Hence, all external energy expressions derived for the isotropic plate are valid also for the orthotropic plate.

3.3.5 Results

In ABAQUS, elastic orthotropy may be specified either by the material type orthotropic or by the material type lamina. The former is valid for a general stress state, and 3D-material properties are automatically reduced to 2D-parameters for a plane stress condition. The lamina-type is only applicable for plane stress.

An example is shown in Fig. 3.7, where results from the orthotropic plate model using 5x3 displacement shape terms is compared with results from ABAQUS using the lamina material type. The orthotropic stiffness coefficients C^o_{ijkl} are chosen arbitrarily as $C^o_{1111} = 1.5C^i_{1111}$, $C^o_{2222} = 0.7C^i_{2222}$, and $C^o_{1212} = 1.3C^i_{1212}$, where C^i_{ijkl} are the isotropic stiffness coefficients corresponding to E=208000MPa. The loading is axial, the plate geometry is 1.68x0.98x11m, and the results are made non-dimensional with the yield stress σ_f=235MPa. The initial deflection is set to a small value. It is seen that the agreement is very good. The results using isotropic coefficients are also included for comparison.

3.4 Elastic-plastic plate

A plate with elastic-plastic material properties is now studied. The derivations presented here are for a simply supported plate, but the procedure would be similar for a clamped plate. Only in-plane compression and tension have been considered for this case.

In the present context, the major difference between elastic and elastic-plastic material is that plasticity makes the plate non-homogeneous. First of all, this means that analytic integration is not possible, and much of the computational efficiency that was achieved for the elastic plate is lost. Second, some approximations must be introduced in the formulations, giving larger inaccuracy than for the elastic case. Bearing this in mind, it is clear that the elastic-plastic model will not perform as well as the elastic one.

The material is assumed to be isotropic and elastic-plastic. It is characterized by the elastic modulus E and Poison's ratio ν in the elastic range, and by an incremental flow law in the plastic range. Plasticity problems are non-conservative, which means that the principle of minimum potential energy is not valid. The more general principle of virtual work is therefore applied, as presented in chapter 2. Since an incremental material law is applied, all expressions must in the following be written on incremental form.

3.4.1 Assumptions

The additional and initial deflections are again taken as double Fourier series, Eq. (3.4). The rates of deflection are

$$\dot{w} = \sum_{m=1}^{M}\sum_{n=1}^{N} \dot{A}_{mn} \sin(\frac{m\pi x}{a}) \sin(\frac{n\pi y}{b}) \tag{3.56}$$

$$\dot{w}_0 = 0 \tag{3.57}$$

the virtual deflections

$$\delta w = \sum_{m=1}^{M}\sum_{n=1}^{N} \delta A_{mn} \sin(\frac{m\pi x}{a}) \sin(\frac{n\pi y}{b}) \tag{3.58}$$

$$\delta w_0 = 0 \tag{3.59}$$

while the rates of virtual deflection are

$$\delta\dot{w} = 0 \tag{3.60}$$
$$\delta\dot{w}_0 = 0 \tag{3.61}$$

The deflection shape should automatically adjust itself so as to minimize the virtual work, pro vided that a sufficient number of terms are included in the displacement function. For the elastic plate, this was demonstrated for a plate where mode snapping occurred during the analysis. When plasticity is included, change of shape due to localization of plasticity is an important effect. It will be shown that the presented model is able to account for the effect of plastic localization.

3.4.2 Plate theory

Using Marguerre's plate theory, the membrane strain rates are

$$\dot{\varepsilon}_x = \dot{u}_{,x} + \dot{w}_{,x}(w_{,x} + w_{0,x}) \tag{3.62}$$
$$\dot{\varepsilon}_y = \dot{v}_{,y} + \dot{w}_{,y}(w_{,y} + w_{0,y}) \tag{3.63}$$
$$\dot{\gamma}_{xy} = \dot{u}_{,y} + \dot{v}_{,x} + \dot{w}_{,x}(w_{,y} + w_{0,y}) + \dot{w}_{,y}(w_{,x} + w_{0,x}) \tag{3.64}$$

The virtual membrane strains are

$$\delta\varepsilon_x = \delta u_{,x} + \delta w_{,x}(w_{,x} + w_{0,x}) \tag{3.65}$$
$$\delta\varepsilon_y = \delta v_{,y} + \delta w_{,y}(w_{,y} + w_{0,y}) \tag{3.66}$$
$$\delta\gamma_{xy} = \delta u_{,y} + \delta v_{,x} + \delta w_{,x}(w_{,y} + w_{0,y}) + \delta w_{,y}(w_{,x} + w_{0,x}) \tag{3.67}$$

The virtual membrane strain rates are

$$\delta\dot{\varepsilon}_x = \delta\dot{u}_{,x} + \delta w_{,x}\dot{w}_{,x} \tag{3.68}$$
$$\delta\dot{\varepsilon}_y = \delta\dot{v}_{,y} + \delta w_{,y}\dot{w}_{,y} \tag{3.69}$$
$$\delta\dot{\gamma}_{xy} = \delta\dot{u}_{,y} + \delta\dot{v}_{,x} + \delta w_{,x}\dot{w}_{,y} + \delta w_{,y}\dot{w}_{,x} \tag{3.70}$$

By differentiation and combining equations Eq. (3.62) through Eq. (3.64), the requirement

for strain compatibility of the plate on rate form is

$$\begin{aligned} & \dot{\varepsilon}_{x,yy} + \dot{\varepsilon}_{y,xx} - \dot{\gamma}_{xy,xy} \\ = \;& 2w_{,xy}\dot{w}_{,xy} + 2w_{0,xy}\dot{w}_{,xy} - \dot{w}_{,xx}w_{,yy}\dot{w}_{,yy}w_{,xx} - \dot{w}_{,yy}w_{0,xx} - \dot{w}_{,xx}w_{0,yy} \end{aligned} \tag{3.71}$$

Using the incremental elastic-plastic material law gives

$$\dot{\varepsilon}_{x,yy} = M_{1111}\dot{\sigma}_{x,yy} + M_{1122}\dot{\sigma}_{y,yy} + (M_{1112} + M_{1121})\dot{\sigma}_{xy,yy} \tag{3.72}$$

$$\dot{\varepsilon}_{y,xx} = M_{2211}\dot{\sigma}_{x,xx} + M_{1122}\dot{\sigma}_{y,xx} + (M_{1112} + M_{1121})\dot{\sigma}_{xy,xx} \tag{3.73}$$

$$\dot{\varepsilon}_{xy,xy} = M_{1211}\dot{\sigma}_{x,xy} + M_{1222}\dot{\sigma}_{y,xy} + (M_{1212} + M_{1221})\dot{\sigma}_{xy,xy} \tag{3.74}$$

Now, introducing the stress rate function $\dot{F}$ so that

$$\dot{F}_{,xx} = \dot{\sigma}_y \tag{3.75}$$

$$\dot{F}_{,yy} = \dot{\sigma}_x \tag{3.76}$$

$$\dot{F}_{,xy} = -\dot{\sigma}_{xy} \tag{3.77}$$

the compatibility equation for the plate can be written as

$$\begin{aligned} & M_{1111}\dot{F}_{,yyyy} + M_{2222}\dot{F}_{,xxxx} + (M_{1122} + M_{2211} + 2M_{1212} + 2M_{1221})\dot{F}_{,xxyy} \\ & -(M_{1112} + M_{1121} + 2M_{1211})\dot{F}_{,xyyy} - (M_{2212} + M_{2221} + 2M_{1222})\dot{F}_{,yxxx} \\ = \;& 2w_{,xy}\dot{w}_{,xy} + 2w_{0,xy}\dot{w}_{,xy} - \dot{w}_{,xx}w_{,yy} - \dot{w}_{,yy}w_{,xx} - \dot{w}_{,yy}w_{0,xx} - \dot{w}_{,xx}w_{0,yy} \end{aligned} \tag{3.78}$$

Due to plasticity, the material parameters M_{ijkl} are functions of position (x, y) in the plate, and this makes it less attractive to solve the compatibility equation Eq. (3.78) directly. An alternative approach is suggested in the following.

In the elastic region, Eq. (3.7) is the solution of the stress function satisfying both strain compatibility and plate boundary conditions. More specifically, it ensures that the internal stresses integrated over any plate section are in equilibrium with the external forces, and that the integrated membrane strains are such that the plate edges remain straight. Now the membrane strain is divided into two parts. The first part, ε^D, is the membrane strain resulting from the deflection of the plate. The second part, ε^F, is the membrane strain necessary to ensure equilibrium between external forces and internal stresses. Hence, the total strain rate in any point is written as

$$\dot{\varepsilon}_{ij} = \dot{\varepsilon}^D_{ij} + \dot{\varepsilon}^F_{ij} - z\dot{w}_{,ij} \qquad i, j = x, y \tag{3.79}$$

The virtual strain is

$$\delta\varepsilon_{ij} = \delta\varepsilon^D_{ij} + \delta\varepsilon^F_{ij} - z\delta w_{,ij} \qquad i,j = x,y \tag{3.80}$$

The virtual strain rate is

$$\delta\dot{\varepsilon}_{ij} = \delta\dot{\varepsilon}^D_{ij} + \delta\dot{\varepsilon}^F_{ij} \qquad i,j = x,y \tag{3.81}$$

From the strain compatibility requirement, Eq. (3.71), it is seen that the membrane strain rates are geometry dependent only, that is they can be determined from the deflection and the deflection rates. Therefore, the strain rate due to the deflection of the plate can be determined from a strain function G:

$$\dot{G}^D = \sum_0^{2M}\sum_0^{2N} \dot{g}_{mn}\cos(\frac{m\pi x}{a})\cos(\frac{n\pi y}{b}) \tag{3.82}$$

where

$$\dot{g}_{mn} = \frac{1}{4(m^2\frac{b}{a} + n^2\frac{a}{b})^2}\sum_{kl}(b_{mnkl} + b_{klmn})(A_{kl} + B_{kl})\dot{A}_{kl} \tag{3.83}$$

and the coefficients b_{mnkl} and b_{klmn} are integer numbers determined as for the elastic plate, Eq. (3.9). The membrane strain rates are then

$$\dot{\varepsilon}^D_x = \dot{G}^D_{,yy} \tag{3.84}$$
$$\dot{\varepsilon}^D_y = \dot{G}^D_{,xx} \tag{3.85}$$
$$\dot{\varepsilon}^D_{xy} = -\dot{G}^D_{,xy} \tag{3.86}$$

The boundary conditions and stress equilibrium are not automatically satisfied by the above membrane strain rate in the plastic range, as it is in the elastic range. The strain rate $\dot{\varepsilon}^F_{ij}$ must be determined so that these requirements are fulfilled. In the elastic range, it means that the strain rate must be chosen so that it balances the external force increment.

In the plastic range, the stress rate distribution over one section resulting from the strain rate $\dot{\varepsilon}^D_{ij}$ will give a stress rate resultant over the section which is different from zero. Similarly, the stress rate distribution over the thickness due to the bending strain $-z\dot{w}_{,ij}$ will also give a stress rate resultant over the thickness which is different from zero after yielding has started at the top or bottom of the section. Thus, the strain rate $\dot{\varepsilon}^F_{ij}$ must also be such that these stress rate resultants are balanced.

In addition, $\dot{\varepsilon}_{ij}^F$ must be so that the compatibility requirement, Eq. (3.71), is not violated. Therefore, the following is chosen:

$$\dot{\varepsilon}_{x,y}^F = 0 \tag{3.87}$$
$$\dot{\varepsilon}_{y,x}^F = 0 \tag{3.88}$$

That is, the strain rate $\dot{\varepsilon}_x^F$ in x-direction is constant in the y-direction, while it can vary in the x-direction. The strain rate $\dot{\varepsilon}_y^F$ in y-direction is constant in the x-direction, while it can v ary in the$y$-direction. With this choice, $\dot{\varepsilon}_{ij}^F$ automatically satisfies the compatibility requirement and the boundary condition.

In order to ensure force equilibrium, the displacement rate $\dot{w}$ must be so that the following conditions are fulfilled:

$$\int_0^b \int_0^t \dot{\sigma}_x dz dy = -\dot{P}_x \quad \forall \quad x \tag{3.89}$$
$$\int_0^a \int_0^t \dot{\sigma}_y dz dy = -\dot{P}_y \quad \forall \quad y \tag{3.90}$$

The minus-sign in front of the external force rates are due to the definition of force. External forces are taken as positive in compression, while stresses are taken as positive in tension. By fulfilling these requirements, strain compatibility is ensured in every point, while stress equilibrium is ensured when integrating over an y plate section.

By variation of Eq. (3.89) and Eq. (3.90), we have:

$$\int_0^b \int_0^t \delta\dot{\sigma}_x dz dy = 0 \quad \forall \quad x \tag{3.91}$$
$$\int_0^a \int_0^t \delta\dot{\sigma}_y dz dy = 0 \quad \forall \quad y \tag{3.92}$$

The stress rates and virtual stress rates can be expressed using strain rates and virtual strain rates and the incremental material law. T aking the total strain rate in a material

point as the sum in Eq. (3.79), the requirements Eq. (3.89) and Eq. (3.90) becomes

$$\int_0^b \int_0^t \left[C_{1111}(\dot{\varepsilon}_x^D + \dot{\varepsilon}_x^F - z\dot{w}_{,xx}) + C_{1122}(\dot{\varepsilon}_y^D + \dot{\varepsilon}_y^F - z\dot{w}_{,yy}) + (C_{1112} + C_{1121})(\dot{\varepsilon}_{xy}^D - z\dot{w}_{,xy})\right] dzdy = -\dot{P}_x \quad \forall \quad x \tag{3.93}$$

$$\int_0^a \int_0^t \left[C_{2211}(\dot{\varepsilon}_x^D + \dot{\varepsilon}_x^F - z\dot{w}_{,xx}) + C_{2222}(\dot{\varepsilon}_y^D + \dot{\varepsilon}_y^F - z\dot{w}_{,yy}) + (C_{2212} + C_{2221})(\dot{\varepsilon}_{xy}^D - z\dot{w}_{,xy})\right] dzdx = -\dot{P}_y \quad \forall \quad x \tag{3.94}$$

In the first equation, $\dot{\varepsilon}_x^F$ is constant and can be taken outside the integral sign. In the second equation, $\dot{\varepsilon}_y^F$ is constant and can be taken outside the integral sign. We can then write

$$\begin{aligned} \dot{\varepsilon}_x^F &= \frac{-\dot{P}_x - \int_0^b \int_0^t \left[C_{1111}(\dot{\varepsilon}_x^D - z\dot{w}_{,xx}) + C_{1122}(\dot{\varepsilon}_y^D + \dot{\varepsilon}_y^F - z\dot{w}_{,yy})\right] dzdy}{\int_0^b \int_0^t C_{1111} dzdy} \\ &- \frac{\int_0^b \int_0^t \left[(C_{1112} + C_{1121})(\dot{\varepsilon}_{xy}^D - z\dot{w}_{,xy})\right] dzdy}{\int_0^b \int_0^t C_{1111} dzdy} \end{aligned} \tag{3.95}$$

$$\begin{aligned} \dot{\varepsilon}_y^F &= \frac{-\dot{P}_y - \int_0^a \int_0^t \left[C_{2211}(\dot{\varepsilon}_x^D + \dot{\varepsilon}_x^F - z\dot{w}_{,xx}) + C_{2222}(\dot{\varepsilon}_y^D - z\dot{w}_{,yy})\right] dzdx}{\int_0^a \int_0^t C_{2222} dzdx} \\ &- \frac{\int_0^a \int_0^t \left[(C_{2212} + C_{1121})(\dot{\varepsilon}_{xy}^D - z\dot{w}_{,xy})\right] dzdx}{\int_0^a \int_0^t C_{2222} dzdx} \end{aligned} \tag{3.96}$$

It appears that the strain rates can not be written out explicitly, since $\dot{\varepsilon}_x^F(x)$ in the first equation depends on the integral of $\dot{\varepsilon}_y^F(y)$ over bt, while $\dot{\varepsilon}_y^F(y)$ in the second equation depends on the integral of $\dot{\varepsilon}_x^F(x)$ over at. Therefore, an iterative procedure is applied. First, $\dot{\varepsilon}_x^F$ is calculated from Eq. (3.95) assuming $\dot{\varepsilon}_y^F$ to be zero. Then this value is used to calculate $\dot{\varepsilon}_y^F$ from Eq. (3.96). This value is then again used in the first equation to find a new and better estimate of $\dot{\varepsilon}_x^F$. This iteration proceeds until the relative difference between two consecutive calculated values are smaller than a certain error tolerance.

F or the virtual strain rates, similar expressions result,

$$\int_0^b \int_0^t \left[C_{1111}(\delta\dot{\varepsilon}_x^D + \delta\dot{\varepsilon}_x^F) + C_{1122}(\delta\dot{\varepsilon}_y^D + \delta\dot{\varepsilon}_y^F) + (C_{1112} + C_{1121})\delta\dot{\varepsilon}_{xy}^D\right] dzdy = 0 \quad \forall \quad x \tag{3.97}$$

$$\int_0^a \int_0^t \left[C_{2211}(\delta\dot{\varepsilon}_x^D + \delta\dot{\varepsilon}_x^F) + C_{2222}(\delta\dot{\varepsilon}_y^D + \delta\dot{\varepsilon}_y^F) + (C_{2212} + C_{2221})\delta\dot{\varepsilon}_{xy}^D\right] dzdx = 0 \quad \forall \quad y \tag{3.98}$$

and

$$\delta\dot{\varepsilon}_x^F = -\frac{\int_0^b \int_0^t \left[C_{1111}\delta\dot{\varepsilon}_x^D + C_{1122}(\delta\dot{\varepsilon}_y^D + \delta\dot{\varepsilon}_y^F) + (C_{1112} + C_{1121})\delta\dot{\varepsilon}_{xy}^D\right] dzdy}{\int_0^b \int_0^t C_{1111} dzdy} \tag{3.99}$$

$$\delta\dot{\varepsilon}_y^F = -\frac{\int_0^a \int_0^t \left[C_{2211}(\delta\dot{\varepsilon}_x^D + \delta\dot{\varepsilon}_x^F) + C_{2222}\delta\dot{\varepsilon}_y^D + (C_{2212} + C_{1121})\delta\dot{\varepsilon}_{xy}^D\right] dzdx}{\int_0^a \int_0^t C_{2222} dzdx} \tag{3.100}$$

and a similar iterative procedure is applied for solving these equations.

The virtual strains $\delta\varepsilon_x^F$ and $\delta\varepsilon_y^F$ are accumulated values, and must be calculated by incrementation when $\delta\dot{\varepsilon}_x^F$ and $\delta\dot{\varepsilon}_y^F$ have been found:

$$\delta\varepsilon_x^{F,s} = \delta\varepsilon_x^{F,s-1} + \eta\delta\dot{\varepsilon}_x^{F,s-1} \tag{3.101}$$

$$\delta\varepsilon_y^{F,s} = \delta\varepsilon_y^{F,s-1} + \eta\delta\dot{\varepsilon}_y^{F,s-1} \tag{3.102}$$

Similarly for the total strains:

$$\varepsilon_x^{F,s} = \varepsilon_x^{F,s-1} + \eta\dot{\varepsilon}_x^{F,s-1} \tag{3.103}$$

$$\varepsilon_y^{F,s} = \varepsilon_y^{F,s-1} + \eta\dot{\varepsilon}_y^{F,s-1} \tag{3.104}$$

3.4.3 Internal virtual work

The internal virtual work is

$$\delta W = \int_V \sigma_{ij}\delta\varepsilon_{ij} dV \qquad i,j = x,y \tag{3.105}$$

where the integration is carried out over the whole plate volume V. The rate of internal virtual work is then

$$\delta\dot{W} = \int_V (\dot{\sigma}_{ij}\delta\varepsilon_{ij} + \sigma_{ij}\delta\dot{\varepsilon}_{ij})dV \tag{3.106}$$

Using the expression for the total strain in a material poin t, Eq. (3.79), the follo wing expression for the rate of internal work is obtained:

$$\begin{aligned}\delta\dot{W} &= \int_V \left[\dot{\sigma}_{ij}(\delta\varepsilon^D_{ij} + \delta\varepsilon^F_{ij} - z\delta w_{,ij}) + \sigma_{ij}(\delta\dot{\varepsilon}^D_{ij} + \delta\dot{\varepsilon}^F_{ij})\right] dV \\ &= \int_A \left[(\delta\varepsilon^D_{ij} + \delta\varepsilon^F_{ij})\int_t \dot{\sigma}_{ij}dz + (\delta\dot{\varepsilon}^D_{ij} + \delta\dot{\varepsilon}^F_{ij})\int_t \sigma_{ij}dz - \delta w_{,ij}\int_t z\dot{\sigma}_{ij}dz\right] dA\end{aligned} \tag{3.107}$$

Written out, this becomes:

$$\begin{aligned}\delta\dot{W} = \int_A \Bigg[&(\delta\varepsilon^D_x + \delta\varepsilon^F_x)\int_t \dot{\sigma}_x dz + (\delta\varepsilon^D_y + \delta\varepsilon^F_y)\int_t \dot{\sigma}_y dz + 2\delta\varepsilon^D_{xy}\int_t \dot{\sigma}_{xy}dz \\ &+(\delta\dot{\varepsilon}^D_x + \delta\dot{\varepsilon}^F_x)\int_t \sigma_x dz + (\delta\dot{\varepsilon}^D_y + \delta\dot{\varepsilon}^F_y)\int_t \sigma_y dz + 2\delta\dot{\varepsilon}^D_{xy}\int_t \sigma_{xy}dz \\ &-\delta w_{,xx}\int_t z\dot{\sigma}_x dz - \delta w_{,yy}\int_t z\dot{\sigma}_y dz - 2\delta w_{,xy}\int_t z\dot{\sigma}_{xy}dz\Bigg] dA\end{aligned} \tag{3.108}$$

The integration is carried out numerically over the plate volume.

3.4.4 Virtual work of external loads

The virtual w orkof external in-plane loads is calculated as external force times virtual displacement:

$$\delta T = P_x\delta\Delta u + P_y\delta\Delta v \tag{3.109}$$

where $\delta\Delta u$ and $\delta\Delta v$ are the virtual elongations of the plate in the x- and y-direction, respectiv ely.The rate of virtual external work is

$$\delta\dot{T} = P_x\delta\Delta\dot{u} + \dot{P}_x\delta\Delta u + P_y\delta\Delta\dot{v} + \dot{P}_y\delta\Delta v \tag{3.110}$$

where $\dot{P}_x$ and $\dot{P}_y$ are load rates, and $\delta\Delta\dot{u}$ and $\delta\Delta\dot{u}$ are virtual elongation rates.

The elongation of the plate is

$$\Delta u = \int_0^a u_{,x} dx \tag{3.111}$$

$$\Delta v = \int_0^b v_{,y} dy \tag{3.112}$$

The virtual elongation is then

$$\delta\Delta u = \int_0^a \delta u_{,x} dx \tag{3.113}$$

$$\delta\Delta v = \int_0^b \delta v_{,y} dy \tag{3.114}$$

and the virtual elongation rates are

$$\delta\Delta \dot{u} = \int_0^a \delta \dot{u}_{,x} dx \tag{3.115}$$

$$\delta\Delta \dot{v} = \int_0^b \delta \dot{v}_{,y} dy \tag{3.116}$$

Using strain rate and virtual strain rate expressions Eq. (3.65) and Eq. (3.68), the rate of virtual external work can be written:

$$\begin{aligned} \delta\dot{H} &= \dot{P}_x \int_0^a \left[\delta\varepsilon_x^D + \delta\varepsilon_x^F - \delta w_{,x}(w_{,x} + w_{0,x})\right] dx \\ &+ P_x \int_0^a \left[\delta\dot{\varepsilon}_x^D + \delta\dot{\varepsilon}_x^F - \delta w_{,x}\dot{w}_{,x}\right] dx \\ &+ \dot{P}_y \int_0^b \left[\delta\varepsilon_y^D + \delta\varepsilon_y^F - \delta w_{,y}(w_{,y} + w_{0,y})\right] dy \\ &+ P_y \int_0^b \left[\delta\dot{\varepsilon}_y^D + \delta\dot{\varepsilon}_y^F - \delta w_{,y}\dot{w}_{,y}\right] dy \end{aligned} \tag{3.117}$$

The terms involving w and w_0 can be calculated and integrated analytically using the assumed displacement functions. Carrying out this integration, the expression for the rate

of virtual external work becomes:

$$\begin{aligned}\delta\dot{H} = & - \sum_{m=1}^{M}\sum_{n=1}^{N}(\frac{m^2}{4a}\dot{P}_x + \frac{n^2}{4b}\dot{P}_y)\pi^2(A_{mn}+B_{mn})\delta A_{mn} \\ & - \sum_{m=1}^{M}\sum_{n=1}^{N}(\frac{m^2}{4a}P_x + \frac{n^2}{4b}P_y)\pi^2\dot{A}_{mn}\delta A_{mn} \\ & + \frac{\dot{P}_x}{b}\int_A(\delta\varepsilon_x^D + \delta\varepsilon_x^F)dA + \frac{P_x}{b}\int_A(\delta\dot{\varepsilon}_x^D + \delta\dot{\varepsilon}_x^F)dA \\ & + \frac{\dot{P}_y}{a}\int_A(\delta\varepsilon_y^D + \delta\varepsilon_y^F)dA + \frac{P_y}{a}\int_A(\delta\dot{\varepsilon}_y^D + \delta\dot{\varepsilon}_y^F)dA\end{aligned} \tag{3.118}$$

The integration is carried out numerically over the plate area.

3.4.5 Implementation

In contrast to the elastic case, evaluation of the elastic-plastic formulations requires numerical integration. In addition, all variables must be calculated by incrementation, since only rates can be calculated at each increment. Consequently, stress and strain values for each integration point must be remembered from one increment to the next.

Using the principle of virtual work, an equation system is derived in the same form as for the elastic plate using the principle of minimum potential energy. The solution procedure is the same as before.

3.4.6 Results

Some calculations performed using the plate model is presented, and comparisons with ABAQUS are presented. An elastic modulus of E=208000MPa is used, and no hardening in the plastic region is assumed. The initial deflections are set to a small value in all the examples. The results from the model are obtained using 7x5 terms in the displacement function.

In Fig. 3.8, the load-deflection response of a 1.0x1.0m plate subjected to axial loading is shown. The load and average strain is made non-dimensional with the yield stress σ_f=313.6MPa. The example to the left is a plate with thickness t=13.0mm, which means a slenderness $\beta = \frac{b}{t}\sqrt{\frac{\sigma_f}{E}} = 3.0$. The example to the right is for t=26.0mm, meaning

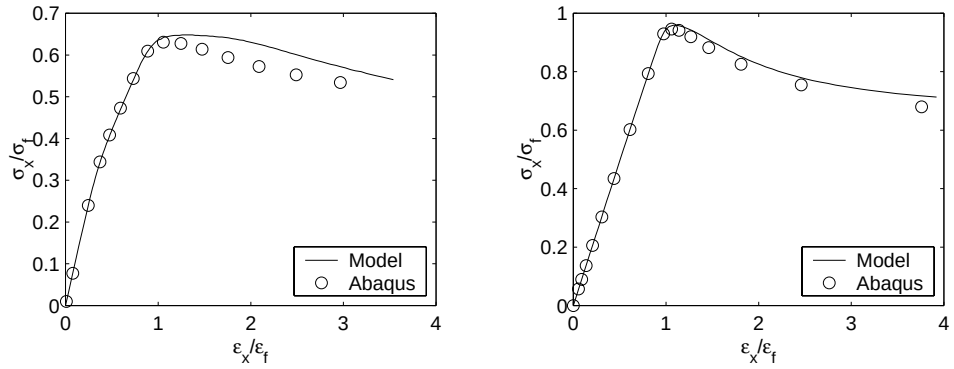

Figure 3.8: Non-dimensional load-average strain under axial loading for 1.0x1.0x0.013m plate, $\beta = 3.0$ (left) and 1.0x1.0x0.026m plate, $\beta = 1.5$ (righ t)

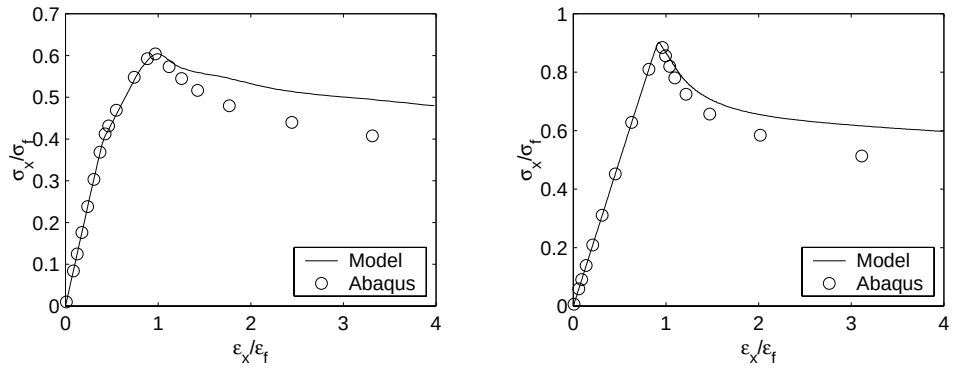

Figure 3.9: Non-dimensional load-average strain under axial loading for 1.68x0.98x0.011m plate, $\beta = 3.0$ (left) and 1.68x0.98x0.017m plate, $\beta = 1.93$ (righ t)

$\beta = 1.5$. It is seen that the agreement is best for the thicker plate, while the response is too stiff in the postcritical region for the thinner plate.

In Fig. 3.9, the response of a 1.68x0.98m plate subjected to axial loading is shown. The load and average strain is made non-dimensional with the yield stress σ_f=235MPa. The left plot is for a plate with t=11.0mm, i.e. $\beta = 3.0$, and the right plot is for t=17.0mm, i.e. $\beta = 1.93$. Also here the response is too stiff in the postcritical region.

Much of the stiffness reduction in the postcritical region is believed to be due to plastic localization. It is therefore essen tial that this effect is accounted for in the model. The

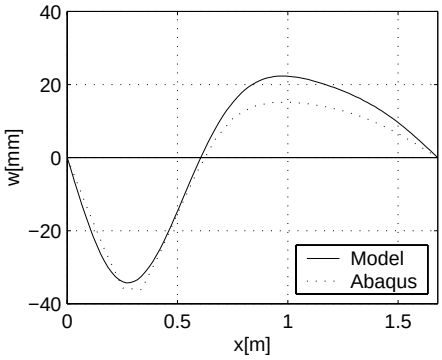

Figure 3.10: Longitudinal deflection shape under axial loading for 1.68x0.98x0.011m plate, $\beta = 3.0$

longitudinal deflection shape at half-width was therefore plotted for the 1.68x0.98x0.011m plate for comparison, Fig. 3.10. It is seen that plastic localization does take place also in the model, but the deflection shape is not exactly equal to the one calculated by ABAQUS. The deviation between the FEM-results and the model does probably indicate that the assumed strain distribution is not entirely correct in the plastic region. However, the results are quite good up until the ultimate limit state, and the ULS-loads predicted are quite close to that of ABAQUS. The problem is that the calculated response is non-conservative in the postcritical region. A simple way to reduce the stiffness is to set the membrane stiffness equal to zero after the onset of membrane yielding. Results for the 1.68x0.98m plate using this approach is shown in Fig. 3.11. It is seen that the results are now on the safe side, and not too far from the FEM-predictions.

Testing was also performed for transverse load, and for other geometries, with similar agreement in the results. The tests performed with the elastic-plastic plate model indicated that reasonable results could be obtained even in the plastic region, although the accuracy is not so good as in the elastic region. However, the computational efficiency of this model is drastically reduced compared to the elastic one. There are two reasons for this. The first one is that numerical integration must be used, which increases the effort necessary to calculate the membrane stiffness across the plate. The second is that a larger number of displacement shape terms are necessary in order to describe the non-regular displacement shape due to plastic localization.

The most important aim for a design model is to provide efficient and accurate calculation of the response in the elastic region, combined with safe predictions of ultimate strength. Both of these requirements can be met with an elastic model, using a first membrane yield criterion for estimation of design collapse load. It was therefore decided not to put further

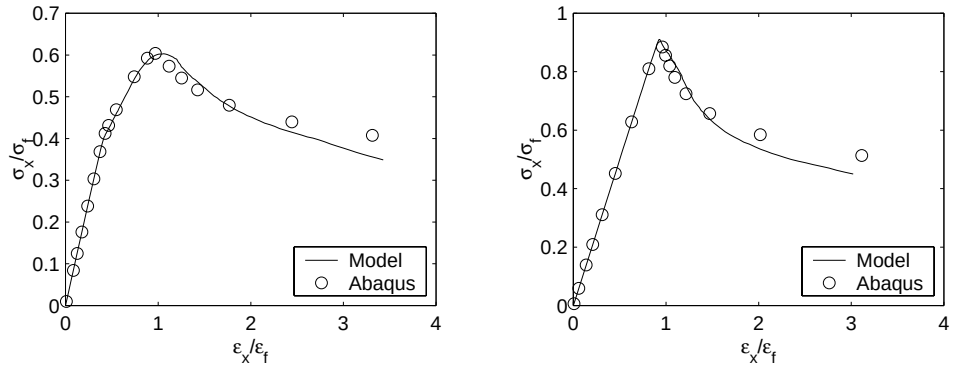

Figure 3.11: Non-dimensional load-average strain under axial loading for 1.68x0.98x0.011m plate, $\beta = 3.0$ (left) and 1.68x0.98x0.017m plate, $\beta = 1.93$ (righ t) using modified stiffness

effort into dev elopmen t or testing of the elastic-plastic plate model, and it is not developed further in subsequent chapters. Estimation of ultimate limit state using membrane yield criterion is further discussed in chapter 7.

Chapter 4

Local buckling of stiffened plates

Local buckling of a plate with an attached stiffener is considered. By local buckling, it is understood that the plate, the web and the flange may deform locally, but the entire stiffened plate shall not deflect laterally. In other words, the connection between the plate and the stiffener is fixed in the vertical direction. Lateral support is also provided by transverse girders.

The motivation for developing a local buckling model is that most stiffened panels in marine structures are built up of relatively thin plates, in the sense that the stiffener spacing and the web height are large compared to the plate and web thickness. Hence, the local buckling load for the plate and the web is much lower than the global buckling load of the combined stiffened plate. Panels with global buckling load close to the local buckling load may experience very unstable response in the postbuckling region, and it is therefore good design practice to ensure that the global buckling load is well above the local buckling load. In design codes, it is usual to accept that local buckling of plate members take place, but overall stiffener or grillage buckling should not occur.

The column approach is often used for buckling assessment in design codes, such as the DNV Classification Note for Buckling Strength Analysis (Det Norske Veritas 1995). These formulations have the advantage of being relatively simple, and provide quick strength estimates. However, looking at the deflection modes of actual stiffened panels, it is clear that a column model does not provide the best representation of the real structural response. Usually, local deformations dominate, while lateral deflection in the global mode is less significant.

Figure 4.1: Open profiles: Flat bar, angle bar, tee bar and bulb

For most of the panels used in traditional ships the global buckling load is well above the squash load of the panel, and is therefore of little importance. In such cases, the local buckling models presented in the following are sufficient for providing a reasonable strength estimate of the panel. For some cases, however, local bukling may interact with global buckling. The local models presented here may then be combined with a global buckling model. Global buckling is discussed in chapter 5 and combined local and global buckling in chapter 6.

4.1 Open profiles

A stiffener of the open profile type is considered first. It may be a flat bar, angle bar, tee-bar, or bulb profile, Fig. 4.1. These are the stiffener types which are most frequently used in conventional steel ships. The computational model developed for open profiles was also presented in (Byklum and Amdahl 2002b).

4.1.1 Plate deflection

The stiffener acts as a rotational line spring on the plate. As a result, the boundary condition for a plate between two stiffeners is somewhere in between simply supported and clamped. For most stiffened plates the web is quite slender compared to the plate itself, so that the situation is quite close to that of simply support. The clamped mode becomes more important for stronger webs and under influence of lateral pressure. In order to include the possibility of all types of plate deflection in the range from simply supported to fully clamped, it is necessary to assume the deflection shape as a combination of sine-terms and cosine-terms. Hence, the assumed displacement patterns for additional and initial deflection are, Fig. 4.2:

$$w = w^s + w^c \tag{4.1}$$

$$w_0 = w_0^s + w_0^c \tag{4.2}$$

where s and c denotes sine and cosine mode deflection, respectively. Both w^s and w^c are

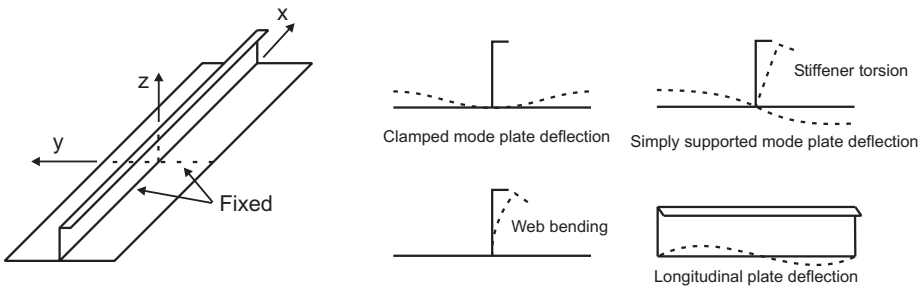

Figure 4.2: Local model with assumed plate and stiffener deflection modes

as giv en in c hapter 3 for the unstiffened plate.

Combining the sine-deflection and the cosine-deflection affects the strain compatibility. Due to coupling terms in the strain compatibility equation, a new stress function must be derived. The total stress function is now written as:

$$F = F^0 + F^s + F^c + F^{sc} \tag{4.3}$$

where F^s and F^c satisfy the compatibility equation for the simply supported and the clamped displacement terms, respectiv ely,as presented in c hapter3. F^0 is the external force part, while F^{sc} satisfy the coupling terms in the compatibility equation:

$$\begin{aligned} \nabla^4 F^{sc} &= E(2w^s_{,xy}w^c_{,xy} - w^s_{,xx}w^c_{,yy} - w^c_{,xx}w^s_{,yy} + 2w^s_{0,xy}w^c_{,xy} \\ &+ 2w^c_{0,xy}w^s_{,xy} - w^s_{0,xx}w^c_{,yy} - w^c_{0,xx}w^s_{,yy} - w^s_{0,yy}w^c_{,xx} - w^c_{0,yy}w^s_{,xx}) \end{aligned} \tag{4.4}$$

The stress function contributions are:

$$F^0 = -\frac{S_x y^2}{2} - \frac{S_y x^2}{2} - S_{xy}xy \tag{4.5}$$

$$F^s = \sum_0^{2M_s}\sum_0^{2N_s} f^s_{mn}\cos(\frac{m\pi x}{a})\cos(\frac{n\pi y}{b}) \tag{4.6}$$

$$F^c = \sum_0^{2M_c}\sum_0^{2N_c} f^c_{mn}\cos(\frac{m\pi x}{a})\cos(\frac{2n\pi y}{b}) \tag{4.7}$$

$$F^{sc} = \sum_0^{M_s+M_c}\sum_0^{N_s+2N_c} f^{sc}_{mn}\cos(\frac{m\pi x}{a})\sin(\frac{n\pi y}{b}) \tag{4.8}$$

The coefficients f^s_{mn} and f^c_{mn} are as given before for the simply supported and clamped plate, while f^{sc}_{mn} are:

$$f^{sc}_{mn} = \frac{E}{4(m^2\frac{b}{a} + n^2\frac{a}{b})^2} \sum_{rspq} b^{sc}_{rspq}(A^s_{rs}A^c_{pq} + A^s_{rs}B^c_{pq} + A^c_{pq}B^s_{rs}) \tag{4.9}$$

where $f^{sc}_{0,0}$ is defined as zero, and the coefficients b^{sc}_{rspq} are:

$$b^{sc}_{rspq} = \begin{cases} 2rspq + 2r^2q^2 + \frac{1}{2}s^2p^2 & \text{if} \quad \begin{cases} p + r = m, 2q - s = n \\ \pm(p - r) = m, s + 2q = n \end{cases} \\ 2rspq - 2r^2q^2 - \frac{1}{2}s^2p^2 & \text{if} \quad \begin{cases} p + r = m, 2q + s = n \\ \pm(p - r) = m, 2q - s = n \end{cases} \\ -2rspq + 2r^2q^2 + \frac{1}{2}s^2p^2 & \text{if} \quad \pm(p - r) = m, s - 2q = n \\ -2rspq - 2r^2q^2 - \frac{1}{2}s^2p^2 & \text{if} \quad p + r = m, s - 2q = n \\ s^2p^2 & \text{if} \quad p + r = m, s = n \\ -s^2p^2 & \text{if} \quad \pm(p - r) = m, s = n \end{cases} \tag{4.10}$$

The derivation is similar as for the simply supported plate and is therefore omitted.

4.1.2 Stiffener deflection

The displacement shapes chosen for the stiffener deflection v and initial deflection v_0 are:

$$v = v_1 + v_2 \tag{4.11}$$
$$v_0 = v_{01} + v_{02} \tag{4.12}$$

where

$$v_1 = \frac{z}{h} \sum_{m=1}^{M_w} V_{1m} \sin\left(\frac{m\pi x}{a}\right) \tag{4.13}$$
$$v_{01} = \frac{z}{h} \sum_{m=1}^{M_w} V_{01m} \sin\left(\frac{m\pi x}{a}\right) \tag{4.14}$$
$$v_2 = \left(1 - \cos\left(\frac{\pi z}{2h}\right)\right) \sum_{m=1}^{M_w} V_{2m} \sin\left(\frac{m\pi x}{a}\right) \tag{4.15}$$
$$v_{02} = \left(1 - \cos\left(\frac{\pi z}{2h}\right)\right) \sum_{m=1}^{M_w} V_{02m} \sin\left(\frac{m\pi x}{a}\right) \tag{4.16}$$

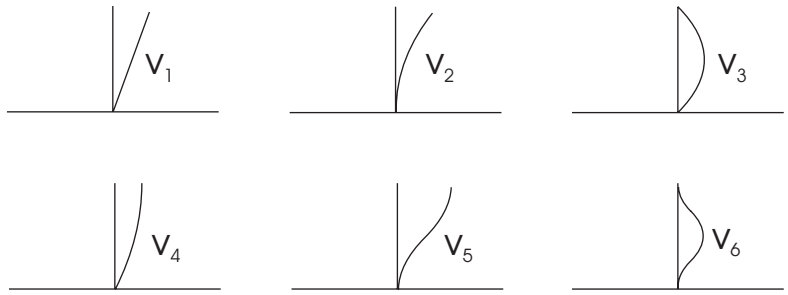

Figure 4.3: Possible displacement shapes for stiffener

M_w is the number of terms included in the longitudinal direction. The first term, v_1, represents torsion of the stiffener as a rigid body, while the second term, v_2 represents bending of the web, see Fig. 4.2. Both terms involve torsion and bending of the flange.

There are other displacement functions that also could be used to represent the stiffener deflection, and increasingly better results would be obtained if more terms were included. For stiffeners with very heavy flanges, for instance, buckling may occur in the web without much distortion of the flange. In such cases, it may be beneficial to use a deflection pattern which allows for web deflection that is clamped-like towards the flange. Other possible deflection shapes for the stiffener are, Fig. 4.3:

$$v_3 = \sin(\frac{\pi z}{h}) \sum_m V_{3m} \sin(\frac{m\pi x}{a}) \tag{4.17}$$

$$v_4 = \sin(\frac{\pi z}{2h}) \sum_m V_{4m} \sin(\frac{m\pi x}{a}) \tag{4.18}$$

$$v_5 = (1 - \cos(\frac{\pi z}{h})) \sum_m \frac{V_{5m}}{2} \sin(\frac{m\pi x}{a}) \tag{4.19}$$

$$v_6 = (1 - \cos(\frac{2\pi z}{h})) \sum_m \frac{V_{6m}}{2} \sin(\frac{m\pi x}{a}) \tag{4.20}$$

Deflection shape number three includes rotation of the flange, but no bending. Number four and five includes bending but no rotation of the flange, while number five is also without rotation at the plate. Number six represents web deflection without neither rotation nor bending of the flange or the plate.

Eigenvalue analyses including several possible deflection shapes showed that the two mode shapes v_1 and v_2 are the most important for practical cases. Though linear eigenvalue calculation does not tell the truth about the nonlinear response, they give an indication

to which deflection shape is most probable. In order to limit the number of degrees of freedom in the model, and hence maximize computational efficiency, it was decided to include only the deflection shapes V_1 and V_2 in the model. This choice was also supported by nonlinear FEM calculations with ABAQUS. Requiring rotation continuity at the plate-stiffener connection, as discussed in the next section, eliminates the variables V_{1m}, and leaves the additional variables V_{2m}. The total number of degrees of freedom is therefore $(M_s N_s + M_c N_c + M_w)$.

4.1.3 Transverse continuity

The requirement for rotational continuity at the plate-stiffener connection is:

$$\left.\frac{\partial v}{\partial z}\right|_{z=0} = -\left.\frac{\partial w}{\partial y}\right|_{y=0} \tag{4.21}$$

The minus-sign is due to the definition of the right-handed coordinate system. For the plate a positive deflection gives a positive rotation, while for the stiffener a positive deflection gives a negative rotation. Substituting the deflection shapes for the plate and the stiffener we find that:

$$V_{1m} = -h \sum_n \frac{n\pi}{b} A^s_{mn} \tag{4.22}$$

The deflection modes V_{2m} has no rotation at the plate-stiffener connection, and does therefore not enter the continuity equations. This is also the case for the cosine-deflection modes A^c_{mn} of the plate.

4.1.4 Longitudinal continuity

When considering the plate and the stiffener as one member, longitudinal continuity also has to be fulfilled. The transverse members, i.e. girders or bulkheads, are assumed to enforce the same displacement in the longitudinal direction for the stiffener as for the plate. If the displacement is constant over the heigh tof the stiffened plate, while the stiffness is not, it follows that the applied external stress must be unevenly distributed between the two members. Since the stiffness of each member is changing during buckling, the ratio of external load carried by each is initially unknown, and the force distribution needs to be included in the energy formulations.

For the unstiffened plate, the external stress was assumed to be directly transferred into the plate, and did not enter the equilibrium equations. Turning to the stiffened plate, the

membrane stress is divided into a part due to deflection, σ^D, and a part due to the external force, σ^F:

$$\sigma^p = \sigma^{p,D} + \sigma^{p,F} \tag{4.23}$$
$$\sigma^s = \sigma^{s,D} + \sigma^{s,F} \tag{4.24}$$

where p denotes plate, and s stiffener. Both the deflection part and the force part are now unknowns. It is still assumed that the membrane stress due to the external force is constant over each member, but in general unevenly distributed between the two.

Expressions for the membrane strains due to external force may be derived using two requirements. The first is that the elongation takes a constant value over the cross section, so that the plate displacement equals the stiffener displacement, and the second is that the internal stress resultant equals the external force:

$$\Delta u^p = \Delta u^s \tag{4.25}$$
$$N_x^p + N_x^s = -P_x \tag{4.26}$$

where P_x is the total external force acting on the stiffened plate, and N is internal stress resultant in the plate and the stiffener.The minus-sign is because the external force P_x is defined as positive in compression, in contrast to the internal forces. The elongations in the plate may be written

$$\Delta u^p = \int_a (\varepsilon_x^{p,F} + \varepsilon_x^{p,D} - \frac{1}{2} w_{,x}^2 - w_{0,x} w_{,x}) dx \tag{4.27}$$
$$= a\varepsilon_x^{p,F} + \Delta u^{p,D} \tag{4.28}$$
$$\Delta v^p = \int_b (\varepsilon_y^{p,F} + \varepsilon_y^{p,D} - \frac{1}{2} w_{,y}^2 - w_{0,y} w_{,y}) dy \tag{4.29}$$
$$= b\varepsilon_y^{p,F} + \Delta v^{p,D} \tag{4.30}$$

while the internal stress resultants are

$$N_x^p = \int_b \int_t (\sigma_x^{p,F} + \sigma_x^{p,D}) dz dy \tag{4.31}$$
$$= bt\sigma_x^{p,F} \tag{4.32}$$
$$N_y^p = \int_a \int_t (\sigma_y^{p,F} + \sigma_y^{p,D}) dz dx \tag{4.33}$$
$$= at\sigma_y^{p,F} \tag{4.34}$$

The integrated effect of the deflection membrane stress must be zero due to static equilibrium, and does therefore fall out of the equations. In the transverse direction, we have

$$N_y^p = at\sigma_y^{p,F} \tag{4.35}$$

$$= at(\varepsilon_y^{p,F} + \nu\varepsilon_x^{p,F})\frac{E}{1-\nu^2} \tag{4.36}$$

which gives

$$\varepsilon_y^{p,F} = -(1-\nu^2)\frac{P_y}{atE} - \nu\varepsilon_x^{p,F} \tag{4.37}$$

We then have:

$$N_x^p = Ebt(\varepsilon_x^{p,F} - \frac{\nu P_y}{atE}) \tag{4.38}$$

A fundamental assumption introduced for the stiffener is that the longitudinal displacement is constant over the height of the stiffener, so that

$$u_{,x}^s = \varepsilon_x^{s,F} + \varepsilon_x^{s,D} - \frac{1}{2}v_{,x}^2 = \text{constant} \tag{4.39}$$

This assumption is based on the fact that the length of the stiffener is usually much larger than the height, and it has been verified by non-linear FEM-analysis for some practical cases. The reason for using a different method for calculating the strain distribution for the stiffener than for the plate, is the presence of a free upper edge of the stiffener. A stress function of the type that was used for the plate cannot be used for the stiffener, and the simplification given in Eq. (4.39) is therefore introduced.

Since $\varepsilon_x^{s,F}$ is also assumed to be constant, we can simply choose

$$\varepsilon_x^{s,F} = u_{,x}^s \tag{4.40}$$

$$\varepsilon_x^{s,D} = \frac{1}{2}v_{,x}^2 \tag{4.41}$$

In reality each of these membrane strain components will be functions of x. For simplicity, however, it is decided to use average values in the x-direction for calculation of potential

energy . This is conserv ative, since using mean values giv e smaller internal energy than using the actual values. The deflection membrane strain is then:

$$\varepsilon_x^{s,D}(z) = \frac{1}{2a}\int_a v_{,x}^2 dx \tag{4.42}$$

The elongation becomes

$$\begin{aligned} \Delta u^s &= \int_0^a u_{,x} dx & (4.43)\\ &= a\varepsilon_x^{s,F} & (4.44) \end{aligned}$$

and the stiffener stress resultant

$$\begin{aligned} N_x^s &= \frac{1}{a}\int_{V_s} (\sigma_x^{s,F} + \sigma_x^{s,D}) dV_s & (4.45)\\ &= A_s E\varepsilon_x^{s,F} + \frac{E}{a}\int_{V_s} \varepsilon_x^{s,D} dV_s & (4.46) \end{aligned}$$

where V_s and A_s are stiffener volume and cross-sectional area, respectiv ely. In the last relation, the one-dimensional Hooke's law, $\sigma_x = E\varepsilon_x$, is used. It is thus assumed that no membrane stress develops in the stiffener in the vertical direction. Using the continuit y condition $\Delta u^p = \Delta u^s$ it is found that:

$$\varepsilon_x^{s,F} = \varepsilon_x^{p,F} + \frac{\Delta u^{p,D}}{a} \tag{4.47}$$

Now considering force equilibrium in the longitudinal direction, we write:

$$\begin{aligned} -P_x &= N_x^s + N_x^p & (4.48)\\ &= A_s E(\varepsilon_x^{p,F} + \frac{\Delta u^{p,D}}{a}) + \frac{E}{2a}\int_{V_s} v_{,x}^2 dV_s + Ebt(\varepsilon_x^{p,F} - \frac{\nu P_y}{atE}) & (4.49) \end{aligned}$$

Rearranging, an expression for the plate membrane strain due to the external force is found:

$$\varepsilon_x^{p,F} = \frac{-P_x a + \nu P_y b - \Delta u^{p,D} E A_s - \frac{E}{2}\int_{V_s} v_{,x}^2 dV_s}{aE(bt + A_s)} \tag{4.50}$$

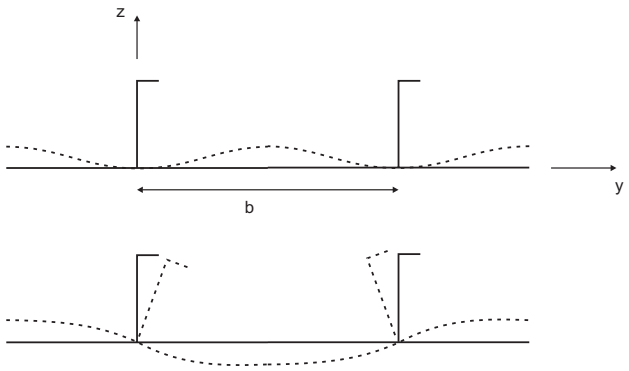

Figure 4.4: Integration area for local model: Clamped mode deflection above, and simply supported mode below

The strain $\varepsilon_x^{p,F}$ is here expressed by the load variables P_x and P_y, and by the displacement variables A^s_{mn}, A^c_{mn}, and V_{2m} through $\Delta u^{p,D}$ and $v_{,x}$. The strain will therefore come out as part of the solution to the whole problem.

4.1.5 Internal potential energy

For the unstiffened plate, the area between two stiffeners, (0 to a), and two transverse girders, (0 to b), was considered. For a stiffened plate it is more common to consider the stiffener/girder-connection to be in center, and include half a stiffener length and half a plate breadth on each side, i.e. to look at the region (-a/2 to a/2), (-b/2 to b/2).

Looking at the chosen displacement functions, however, it is seen that the cosine-part is periodic within one plate breadth, while the sine-part is periodic within two plate widths and two plate lengths. In order to take proper account of the continuity of the plating, it is necessary to perform the integration over two widths and lengths. Hence, the area of integration is taken as (-a/2 to 3a/2) and (-b/2 to 3b/2), Fig. 4.4. From the derivations shown in appendix B, it can be seen that integrating the potential energy to 3a/2 and 3b/2 instead of a/2 and b/2 eliminates the coupling terms between odd and even half wave numbers. That means that no assumptions have to be made beforehand regarding symmetry or antisymmetry of the deflection mode. The deflection shape will automatically adjust itself to the one which is the most beneficial with respect to the plate geometry and loading. In FEM-analyses the continuity of plating must be accounted for by prescribing symmetry or anti-symmetry conditions at the edges, depending on the anticipated deflection mode.

The chosen area of plate integration is so that two stiffeners must be included, one at $y = 0$

and one at $y = b$. It is assumed that both make the same contribution to the potential energy of the system, so the energy for the stiffener at $y = 0$ is multiplied with tw o.

Calculation of each con tribution to the poten tial energy is outlined in the following. Further details can be found in appendix B. The plate bending energy is due to the combined effect of the sine-deflection and the cosine-deflection. It is expressed by:

$$U_b^p = \frac{D}{2}\int_{-a/2}^{3a/2}\int_{-b/2}^{3b/2}\left[(w_{,xx}+w_{,yy})^2 - 2(1-\nu)(w_{,xx}w_{,yy}-w_{,xy}^2)\right]dydx \tag{4.51}$$

The web bending energy is:

$$U_b^w = \frac{D_w}{2}\int_{-a/2}^{3a/2}\int_{0}^{h}\left[(v_{,xx}+v_{,zz})^2 - 2(1-\nu)(v_{,xx}v_{,zz}-v_{,xz}^2)\right]dzdx \tag{4.52}$$

It is calculated by inserting the expression for V_{1m} found from the con tinuity condition, integrating over the area, and differentiating with respect to the rate and displacement amplitudes.

The flange bending energy is:

$$U_b^f = \frac{EI_f}{2}\int_{-a/2}^{3a/2}(v_{,xx}|_{z=h})^2dx + \frac{GJ_f}{2}\int_{-a/2}^{3a/2}(v_{,xz}|_{z=h})^2dx \tag{4.53}$$

where the first part is due to in-plane bending of the flange, and the second is due to torsion of the flange. EI_f is the bending stiffness and GJ_f the torsional stiffness of the flange. As for the web, the bending stiffness is found by inserting the expression for V_{1m} and differentiating with respect to the rate and displacement amplitudes.

The plate membrane energy is

$$\begin{aligned} U_m^p &= \frac{E}{2(1-\nu^2)}\int_{V_p}\left[(\varepsilon_x^{p,F})^2+(\varepsilon_y^{p,F})^2+2\nu(\varepsilon_x^{p,F})(\varepsilon_y^{p,F})\right]dV_p \qquad (4.54)\\ &+ \frac{E}{2(1-\nu^2)}\int_{V_p}\left[(\varepsilon_x^{p,D})^2+(\varepsilon_y^{p,D})^2+2\nu(\varepsilon_x^{p,D})(\varepsilon_y^{p,D})+\frac{1-\nu}{2}\gamma_{xy}^2\right]dV_p \\ &= U_m^{p,F}+U_m^{p,D} \qquad (4.55)\end{aligned}$$

The coupling betw een$\varepsilon^{p,D}$ and $\varepsilon^{p,F}$ is zero, since $\varepsilon^{p,F}$ is constant and the integral of $\varepsilon^{p,D}$ over the plate area is zero. The deflection part $U_m^{p,D}$ of the membrane energy for the plate

may be written

$$U_m^{p,D} = U_m^{p,s} + U_m^{p,c} + U_m^{p,sc} \tag{4.56}$$

where $U_m^{p,s}$ is the membrane energy due to sine-deflection, $U_m^{p,c}$ is that due to cosine-deflection, and $U_m^{p,sc}$ is due to coupling terms. More details are given in appendix B.

The external force part, $U_m^{p,F}$, can be found by taking the constant membrane strain outside the in tegration, and substituting the expression for$\varepsilon_y^{p,F}$:

$$\begin{aligned} U_m^{p,F} &= \frac{abtE}{2(1-\nu^2)}\left[(\varepsilon_x^{p,F})^2 + (\varepsilon_y^{p,F})^2 + 2\nu(\varepsilon_x^{p,F})(\varepsilon_y^{p,F})\right] && (4.57)\\ &= \frac{1}{2}abtE(\varepsilon_x^{p,F})^2 && (4.58)\end{aligned}$$

It is seen that the contribution from $\varepsilon_y^{p,F}$ cancels out of the equations. The final result is obtained by substitution of the expression derived for $\varepsilon_x^{p,F}$.

The stiffener membrane energy is

$$\begin{aligned} U_m^s &= \frac{E}{2}\int_{V_s}(\varepsilon_x^{s,F} + \varepsilon_x^{s,D})^2 dV_s && (4.59)\\ &= \frac{EV_s}{2}(\varepsilon_x^{s,F})^2 + \frac{E}{2}\int_{V_s}(\varepsilon_x^{s,D})^2 dV_s + E\varepsilon_x^{s,F}\int_{V_s}\varepsilon_x^{s,D} dV_s && (4.60)\end{aligned}$$

By substitution of the expressions for $\varepsilon_x^{s,F}$ and $\varepsilon_x^{s,D}$, integration can be carried out. U_m^s is then found as a function of the unknown load parameter and displacement amplitudes. Since the energy expressions are of the fourth order the resulting expressions are lengthy. They are therefore not presented explicitly.

4.1.6 Potential of external loads

Using the displacements calculated for the plate and stiffener in combination, the external energy due to in-plane compression can be calculated directly:

$$\begin{aligned} T_c &= P_x\Delta u + P_y\Delta v && (4.61)\\ &= P_x(2a\varepsilon_x^{p,F} + \Delta u^{p,D}) + P_y(2b\varepsilon_y^{p,F} + \Delta v^{p,D}) && (4.62)\end{aligned}$$

where expressions for $\varepsilon_x^{p,F}$, $\varepsilon_y^{p,F}$, $\Delta u^{p,D}$ and $\Delta v^{p,D}$ are given previously

The external energy due to shear force and lateral pressure needs some special consideration. The sine-terms in the deflection shape are anti-symmetric about $x = 0$ and $y = 0$. This means that integrating the external shear energy directly gives zero contribution, since only sine-terms are included in the longitudinal direction. The chosen deflection shape is therefore not able to describe the continuous deflection of two neighboring plates under the action of shear loading correctly. An approximate solution may be obtained by neglecting the interaction between the plates, and looking at each plate individually. This means that the plate energy is integrated between $(0 - a), (0 - b)$ and then multiplied with a factor 4. Only the sine-terms will then contribute to the potential energy. This is a conservative approach, since the restraining effect of the two plates on each other is neglected. However, FEM-analyses have shown that the restraining effect under pure shear loading is quite small. Hence, the shear energy is calculated as:

$$T_\tau = -4P_{xy} \int_0^a \int_0^b (w^s_{,x} w^s_{,y} + w^s_{0,x} w^s_{,y} + w^s_{,x} w^s_{0,y}) dy dx \tag{4.63}$$

A similar consideration has to be made regarding calculation of external energy due to lateral pressure. When integrating the sine-terms in the longitudinal direction, the $(-a/2$ to $0)$ part will always cancel the $(0$ to $a/2)$ part. As for the shear-force, the integration is therefore taken between $(0$ to $a)$, and multiplied by two. Physically, this means that the plate continuity at the transverse member is not fulfilled, which makes the model less stiff than the real structure. However, the lateral pressure is believed to have the largest influence on the deflection shape in the transverse direction. The cosine-terms included are capable of describing the transverse deflection shape due to the pressure, and the integration can therefore be taken directly between $(-b/2$ to $3b/2)$. The potential of external energy due to lateral pressure is therefore taken as:

$$T_{lp} = -2 \int_0^a \int_{-b/2}^{3b/2} p w_c dy dx \tag{4.64}$$

4.1.7 Results

Computations have been performed on a variety of stiffener geometries for verification of the proposed model. Results are presented for a flat bar, an angle bar and a tee bar stiffener, with dimensions given in Table 4.1. The flat bar is from a tanker deck panel, the angle bar is from a bulk carrier bottom panel, and the tee bar is from a tanker bottom panel. The elastic modulus is 206000MPa for all cases. Results for axial and transverse compression are shown for each stiffener in Fig. 4.5 through Fig. 4.7. The initial deflection for each stiffener

Table 4.1: Dimensions for stiffened steel plates

Stiffener	a[m]	b[m]	t[m]	h[m]	t_w[m]	b_f[m]	t_f[m]	σ_f[MPa]
Flat bar	4.75	0.91	0.018	0.325	0.020			355
Angle bar	2.73	0.85	0.0165	0.350	0.012	0.100	0.017	355
Tee bar	4.335	0.814	0.020	0.475	0.012	0.200	0.025	325

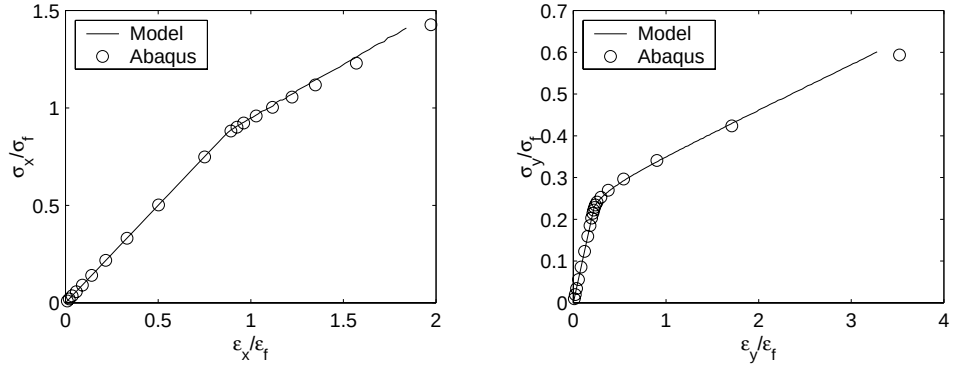

Figure 4.5: Steel flat bar under axial loading using 5x1 terms (left) and transverse loading using 7x3 terms (right)

is taken as the eigenmode, with an amplitude of 1.0mm. The real imperfections present in actual stiffened plates are usually larger and more complex, but such considerations are not a main issue in the current work. The results are compared with FEM-calculations, and the accuracy is good. Increasingly better results are obtained with more terms included in the deflection function and smaller increments. For the geometries and load conditions presented, deflection in the cosine-mode is small, and good results are obtained with sine-terms included only.

It is seen that the load-average strain responses compare well for these cases. A deformation plot is made for the angle-bar in order to compare the model deflection shape with the ABAQUS deflection shape, Fig. 4.8. The deflection shapes resulting from ABAQUS and the developed model are both plotted using the ABAQUS postprocessor. It is seen that deflection shape is well predicted by the model, although only six degrees of freedom is applied to represent the deformation in this case.

In order to investigate the effect of the rotational restraint on the plate from the stiffener, analyses are performed on the angle bar stiffener with the stiffener removed. Results with and without stiffener, both calculated using the presented model, are shown in Fig. 4.9. It

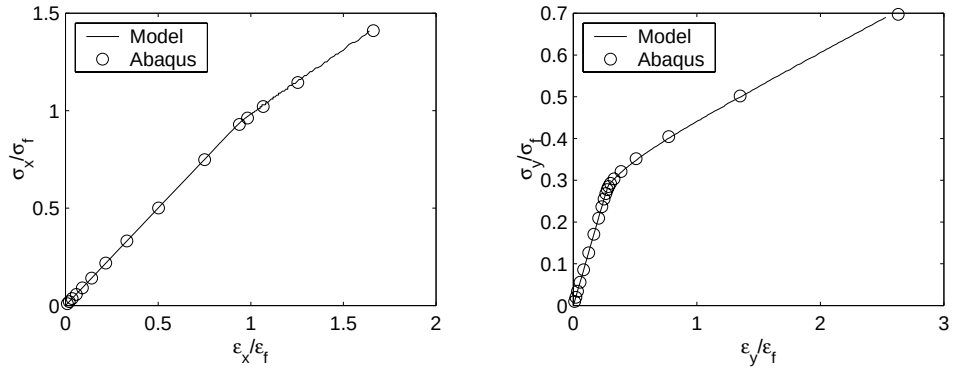

Figure 4.6: Steel angle bar under axial loading using 3x1 terms (left) and transverse loading using 5x3 terms (right)

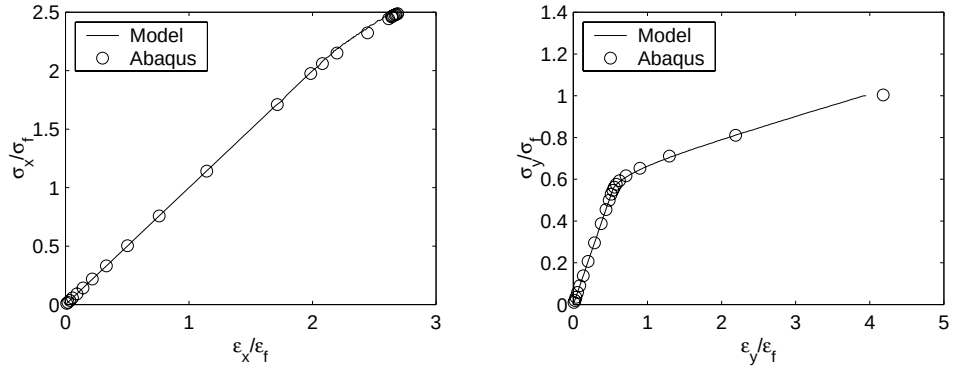

Figure 4.7: Steel tee bar under axial loading using 5x1 terms (left) and transverse loading using 7x3 terms (right)

is seen that for axial load, the stiffness reduction after buckling is larger for the unstiffened plate than for the stiffened plate. For transverse load the stiffness reduction is almost the same for the two cases, but the buckling load is lower for the unstiffened plate. It should be noted however, that this figure only shows the local effect of the stiffener. The main purpose of the stiffener is to prevent global buckling of the stiffened panel.

An example is also shown for an aluminium profile, Table 4.2. This is an extruded tee-profile used for high speed passenger ships. The dimensions are quite different from the more conventional steel stiffeners discussed above, and it is therefore an interesting test

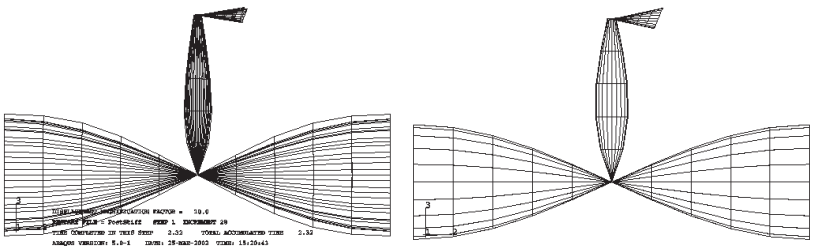

Figure 4.8: Deflection shape for steel angle bar under axial load resulting from ABAQUS analysis (left) and Model calculations (right)

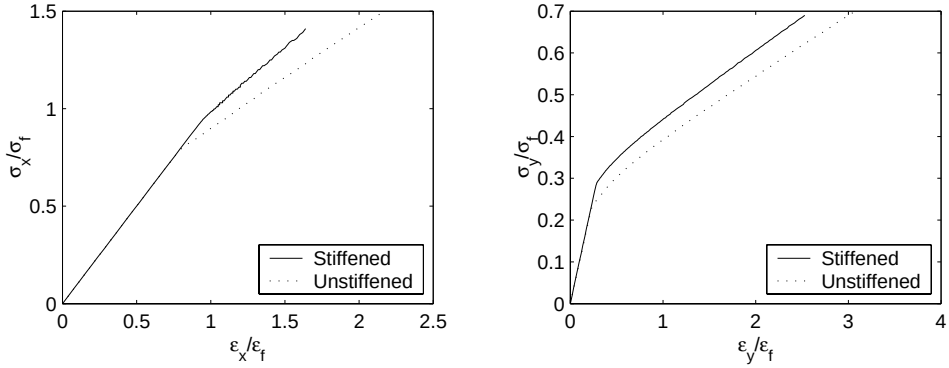

Figure 4.9: Steel angle bar under axial loading using 3x1 terms (left) and transverse loading using 5x3 terms (right): Comparison betw een stiffened plate and unstiffened plate

case. The elastic modulus is taken as 70000MPa. The imperfection is 1.0mm in the elastic eigenmode. Results for axial and transverse compression are shown in Fig. 4.10.

It is seen that the agreement is good also for this geometry and material. The computational efficiency is high, since only a few degrees of freedom are necessary for most of the cases. In the next chapter, it will be shown how stiffness coefficients may be derived using

T able 4.2: Dimensions for stiffened aluminium plate

Stiffener	a[m]	b[m]	t[m]	h[m]	t_w[m]	b_f[m]	t_f[m]	σ_f[MPa]
T ee bar	2.4	0.32	0.005	0.075	0.005	0.040	0.005	240

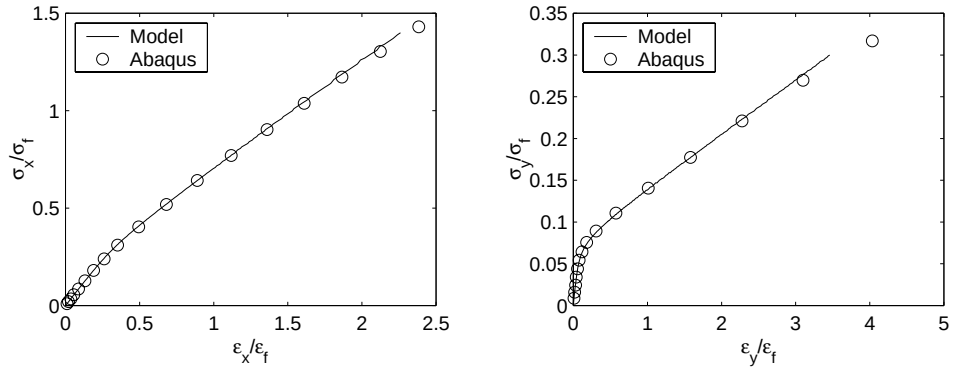

Figure 4.10: Aluminium tee bar under axial loading using 9x1 terms (left) and transverse loading using 15x1 terms (right)

the local model, and how these may be used for global buckling assessment. But first a local model will be presented for a closed profile.

4.2 Closed profiles

Local buckling of a plate with an attached stiffener of the closed type, more specifically a hat-profile, is now considered. Closed profiles are relevant for certain types of aluminum structures, for instance in high speed vessels and in living quarters on offshore structures. Since they may be produced by extrusion, they come in a variety of shapes and sizes. The hat-profile, Fig. 4.11, is just one of the possible profile types. The objective in this section is to show the difference between open and closed profiles, and to demonstrate the applicability of the proposed method for analysis of both types.

4.2.1 Deflection shapes

The main difference between a profile of the open type and a closed type, is that a closed profile has a very large torsional stiffness. Torsional buckling of the stiffener as a whole is not very relevant, and it is necessary instead to look at local buckling of the individual plate members of the stiffener. It is an important property of the hat-profiles that all angles between the plates building the profile is larger than 90 degrees. This is because larger angles leads to larger in-plane support between the plates, and therefore a stiffer profile.

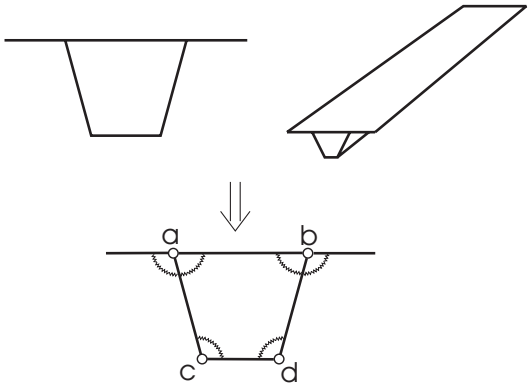

Figure 4.11: Closed profile of the hat-type

Here, the whole profile is considered as an assembly of individual plates. Each plate is treated in the same way as the unstiffened plate considered in chapter 3. In addition, the transverse and longitudinal continuity of the plates must be taken care of.

During deformation, the individual plates in the profile interact and provide rotational stiffness to each other. The plates will have boundary conditions somewhere between simply supported and fully clamped, as was the case for the main plate of the open stiffener profile. The degree of fixation for each plate depends on the stiffness of the neighboring plates. In principle, the best would be to assume that all the plates deflect in a combination of sine-shape and cosine-shape. Requiring continuity of rotation at the edges, the sine-displacements would be coupled for all the plates. The cosine-deflection, giving no rotation at the edges, would be independent.

It is decided to simplify somewhat, and try to solve the problem using only sine-deflection. The approach used is to let all plates deflect independently first, and then apply springs at the corners in order to account for the continuity. By specifying a large spring stiffness, each plate should then take on a displacement shape that is compatible with the other plates.

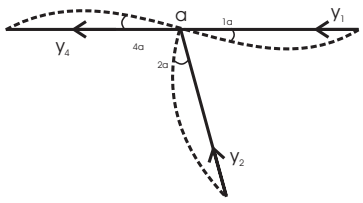

Figure 4.12: Rotation of plate members 1, 2, and 4 at node a

The assumed displacement pattern for each plate is:

$$w^1 = \sum_{m=1}^{M_s} \sum_{n=1}^{N_s} A^1_{mn} \sin(\frac{m\pi x}{a}) \sin(\frac{n\pi y}{b_1}) \tag{4.65}$$

$$w^2 = \sum_{m=1}^{M_s} \sum_{n=1}^{N_s} A^2_{mn} \sin(\frac{m\pi x}{a}) \sin(\frac{n\pi y}{b_2}) \tag{4.66}$$

$$w^3 = \sum_{m=1}^{M_s} \sum_{n=1}^{N_s} A^3_{mn} \sin(\frac{m\pi x}{a}) \sin(\frac{n\pi y}{b_3}) \tag{4.67}$$

$$w^4 = \sum_{m=1}^{M_s} \sum_{n=1}^{N_s} A^4_{mn} \sin(\frac{m\pi x}{a}) \sin(\frac{n\pi y}{b_4}) \tag{4.68}$$

and similarly for the initial displacements. The superscripts $1, 2, 3, 4$ refer to the individual plates, as indicated in Fig. 4.11. It is assumed that one of the two vertical plates can be taken as representative for both, so that only four different displacements are included. The number of degrees of freedom is now $4(M_s \mathrm{x} N_s)$.

4.2.2 Transverse continuity

The requirement for rotational continuity at the edges is

$$\left.\frac{\partial w^i}{\partial y}\right|_{y=y_i} = \left.\frac{\partial w^j}{\partial y}\right|_{y=y_j} \tag{4.69}$$

for an edge between plate i and plate j, where y_i is 0 or b_i in the local coordinate system of plate i. The intersection between the plates a, b and d is shown in Fig. 4.12.

As explained, the requirement for transverse continuity is not initially fulfilled. Instead, it is accounted for using line springs at the corners. For each plate, the rotation at each

edge is calculated. The difference betw een the rotation of two neighboring plates gives a discontinuity, and this will give additional energy to the system. If the spring stiffness is set sufficiently large, the system will try to keep the difference betw een the plate rotations at zero.

The difference in rotation at the corner node a in Fig. 4.12 is:

$$\Delta\theta_{12} = \theta_{1a} - \theta_{2a} \tag{4.70}$$
$$\Delta\theta_{14} = \theta_{1a} - \theta_{4a} \tag{4.71}$$
$$\Delta\theta_{24} = \theta_{2a} - \theta_{4a} \tag{4.72}$$

The rotations are calculated using a local coordinate system for each plate, and become:

$$\theta_1 = \left.\frac{\partial w^1}{\partial y}\right|_{y=b_1} = \frac{\pi}{b_1}\sum_m\sum_n nA^1_{mn}\sin(\frac{m\pi x}{a})\cos(n\pi) \tag{4.73}$$
$$\theta_2 = \left.\frac{\partial w^2}{\partial y}\right|_{y=b_2} = \frac{\pi}{b_2}\sum_m\sum_n nA^2_{mn}\sin(\frac{m\pi x}{a})\cos(n\pi) \tag{4.74}$$
$$\theta_4 = \left.\frac{\partial w^4}{\partial y}\right|_{y=0} = \frac{\pi}{b_4}\sum_m\sum_n nA^4_{mn}\sin(\frac{m\pi x}{a}) \tag{4.75}$$

The potential energy due to rotation is:

$$U_\theta = \frac{1}{2}k_\theta\sum_i\int_a(\Delta\theta)^2_i dx \tag{4.76}$$

where the summation is over all plate intersections in the profile, and k_θ is the line spring stiffness. In order to prevent discontinuity, it should be set to a large value. It may for instance be given suc h that the rotational stiffness is ten times the plate bending stiffness.

By substitution of the displacement functions, the rotational potential energy is found as a second order function of the displacements. Applying the principle of minimum potential energy on rate form, a constant stiffness contribution is obtained. The stiffness matrix con tains coupling terms whih ensures that the deflection of each plate is compatible with the other deflections. More details are found in appendix B.

4.2.3 Longitudinal continuity

As for the open profile considered previously, longitudinal contin uit y of the plate members has to be fulfilled. Girders or bulkheads are assumed to enforce equal displacement in the

longitudinal direction for all the plates in the cross-section. The stiffness of the plates will be different after buckling, and this is therefore not automatically satisfied. The approach used here is the same as that applied for the open profile. The applied external stress must be unevenly distributed betw een the plate members, and the ratio of external load carried by each member is initially unknown. It needs to be included in the energy-formulations, and will be a part of the solution for each increment.

For each plate, the membrane stress is divided into a part due to deflection, σ^D, and a part due to the external force, σ^F:

$$\sigma^i = \sigma^{i,D} + \sigma^{i,F} \tag{4.77}$$

where i denotes plate number i. Both the deflection part and the force part are now unknowns. It is assumed that the membrane stress due to the external force is constant over each member, however different for each one. Alternatively, we may write for the membrane strains:

$$\varepsilon^i = \varepsilon^{i,D} + \varepsilon^{i,F} \tag{4.78}$$

Expressions for the membrane strains due to external force may be derived using two requirements. The first requirement is that the elongations takes a constant value over the cross section, so that the displacement is equal for all plates:

$$\Delta u^i = \Delta u = \text{constant} \tag{4.79}$$

The second requirement is that the internal stress resultant equals the external force:

$$\sum_{i=1}^{4} N_x^i = -P_x \tag{4.80}$$

The displacement requirement is considered first. The longitudinal elongations, equal for all plates, may be written

$$\Delta u^i = \int_0^a (\varepsilon_x^{i,F} + \varepsilon_x^{i,D} - \frac{1}{2}(w_{,x}^i)^2 - w_{0,x}^i w_{,x}^i) dx \tag{4.81}$$

$$= a\varepsilon_x^{i,F} + \Delta u^{i,D} \tag{4.82}$$

which means that the unknown membrane strains due to the external force is

$$\varepsilon_x^{i,F} = \frac{\Delta u - \Delta u^{i,D}}{a} \tag{4.83}$$

The transverse elongation is the sum of the elongations for plate 1 and 4:

$$\begin{aligned}\Delta v &= \int_0^{b_1}(\varepsilon_y^{1,F}+\varepsilon_y^{1,D}-\frac{1}{2}(w_{,y}^1)^2-w_{0,y}^1 w_{,y}^1)dy && (4.84)\\ &+ \int_0^{b_4}(\varepsilon_y^{4,F}+\varepsilon_y^{4,D}-\frac{1}{2}(w_{,y}^4)^2-w_{0,y}^4 w_{,y}^4)dy && (4.85)\\ &= b_1\varepsilon_y^{1,F}+b_4\varepsilon_y^{4,F}+\Delta v^{1,D}+\Delta v^{4,D} && (4.86)\end{aligned}$$

The internal stress resultants for eac h plate are

$$\begin{aligned}N_x^i &= \int_0^{b_i}\int_0^{t_i}(\sigma_x^{i,F}+\sigma_x^{i,D})dzdy = b_i t_i \sigma_x^{i,F} && (4.87)\\ N_y^i &= \int_0^{a}\int_0^{t_i}(\sigma_y^{i,F}+\sigma_y^{i,D})dzdx = a t_i \sigma_y^{i,F} && (4.88)\end{aligned}$$

The integrated effect of the deflection membrane stress is zero, as before.

In the transverse direction, the internal force in plate 1 and plate 4 must both equal the external load:

$$\begin{aligned}-P_y &= N_y^1 = a t_1 \sigma_y^{1,F} && (4.89)\\ -P_y &= N_y^4 = a t_4 \sigma_y^{4,F} && (4.90)\end{aligned}$$

Introducing Hooke's law, we may write

$$\begin{aligned}-P_y &= a t_1(\varepsilon_y^{1,F}+\nu\varepsilon_x^{1,F})\frac{E}{1-\nu^2} && (4.91)\\ &= a t_4(\varepsilon_y^{4,F}+\nu\varepsilon_x^{4,F})\frac{E}{1-\nu^2} && (4.92)\end{aligned}$$

which means that

$$\begin{aligned}\varepsilon_y^{1,F} &= -(1-\nu^2)\frac{P_y}{a t_1 E}-\nu\varepsilon_x^{1,F} && (4.93)\\ \varepsilon_y^{4,F} &= -(1-\nu^2)\frac{P_y}{a t_4 E}-\nu\varepsilon_x^{4,F} && (4.94)\end{aligned}$$

Using this, the longitudinal stress due to external load in plate 1 and 4 becomes

$$\sigma_x^{1,F} = (\varepsilon_x^{1,F} - \frac{\nu P_y}{at_1E})E \tag{4.95}$$
$$\sigma_x^{4,F} = (\varepsilon_x^{4,F} - \frac{\nu P_y}{at_4E})E \tag{4.96}$$

For practical applications, the thickness of plate 1 and 4 will usually be equal, $t_1 = t_4$. For plates 2 and 3 there is no transverse force, which means that $\sigma_y^F = 0$ and

$$\sigma_y^{2,F} = E\varepsilon_y^{2,F} \tag{4.97}$$
$$\sigma_y^{3,F} = E\varepsilon_y^{3,F} \tag{4.98}$$

Now these relations may be used to establish the condition for equilibrium in the longitudinal direction:

$$\begin{aligned} -P_x &= b_1t_1\sigma_x^{1,F} + b_2t_2\sigma_x^{2,F} + 2b_3t_3\sigma_x^{3,F} + b_4t_4\sigma_x^{4,F} && (4.99)\\ &= (\varepsilon_x^{1,F} - \frac{\nu P_y}{at_1E})Eb_1t_1 + (\varepsilon_x^{4,F} - \frac{\nu P_y}{at_4E})Eb_4t_4 && (4.100)\\ &+ \varepsilon_y^{2,F}Eb_2t_2 + 2\varepsilon_y^{3,F}Eb_3t_3 && (4.101)\end{aligned}$$

Introducing the strain-elongation relation we get

$$\begin{aligned} -P_x &= \Delta u(b_1t_1 + b_2t_2 + 2b_3t_3 + b_4t_4) - \Delta u^{2,D}Et_2\frac{b_2}{a} - 2\Delta u^{3,D}Et_3\frac{b_3}{a}\\ &- (\Delta u^{1,D} + \frac{\nu P_y}{t_1E})Et_1\frac{b_1}{a} - (\Delta u^{4,D} + \frac{\nu P_y}{t_4E})Et_4\frac{b_4}{a} \end{aligned} \tag{4.102}$$

which means that the longitudinal elongation can be written

$$\Delta u = \frac{-P_xa + \nu P_y(b_1 + b_4) + (\Delta u^{1,D}t_1b_1 + \Delta u^{2,D}t_2b_2 + 2\Delta u^{3,D}t_3b_3 + \Delta u^{4,D}t_4b_4)E}{(b_1t_1 + b_2t_2 + 2b_3t_3 + b_4t_4)E} \tag{4.103}$$

Using this expression for the combined elongation, the membrane strain in each plate is calculated from Eq. (4.83).

4.2.4 Potential energy

The bending energy for each plate is calculated as for the unstiffened plate presented in chapter 3.

The membrane energy for each plate is

$$U_m^i = U_m^{i,F} + U_m^{i,D} \tag{4.104}$$

The coupling between $\varepsilon^{i,D}$ and $\varepsilon^{i,F}$ is zero, since $\varepsilon^{i,F}$ is constant and the integral of $\varepsilon^{i,D}$ over the plate area is zero.

The deflection part, $U_m^{i,D}$, is calculated as for the unstiffened plate in chapter 3. The external force part, $U_m^{i,F}$, is:

$$U_m^{i,F} = \frac{1}{2} a b_i t_i E (\varepsilon_x^{i,F})^2 \tag{4.105}$$

By substitution of all parameters, U_m^i can be found as functions of the unknown load parameter and displacement amplitudes.

Using the common displacements calculated for the plates in combination, the external energy due to in-plane compression or tension is calculated as:

$$T_c = P_x \Delta u + P_y \Delta v \tag{4.106}$$

where expressions for Δu and Δv are given previously Shear force and lateral pressure will only affect plates 1 and 4, and is calculated as for the unstiffened plate.

4.2.5 Results

Results for axial and transverse compression are shown for a hat profile in Fig. 4.13. The stiffener length is 1.0m, the cross-section widths are $b_a = b_d$ =0.14m, b_b =0.12m, b_c=0.08m, and the thicknesses $t_a = t_d$ =5mm, $t_b = t_c$=3mm. The elastic modulus is E=70000MPa, and the yield stress σ_f=240MPa. The initial deflection is taken as the eigenmode, with an amplitude of 0.1mm.

The agreement is good for the load range presented, but due to convergence problems in the FEM-calculations, the analyses were terminated at a lower load level than intended.

Deformation-shape plots are also included in order to evaluate the goodness of the model. Deformation shape resulting from ABAQUS is shown in Fig. 4.14 and deformation shape

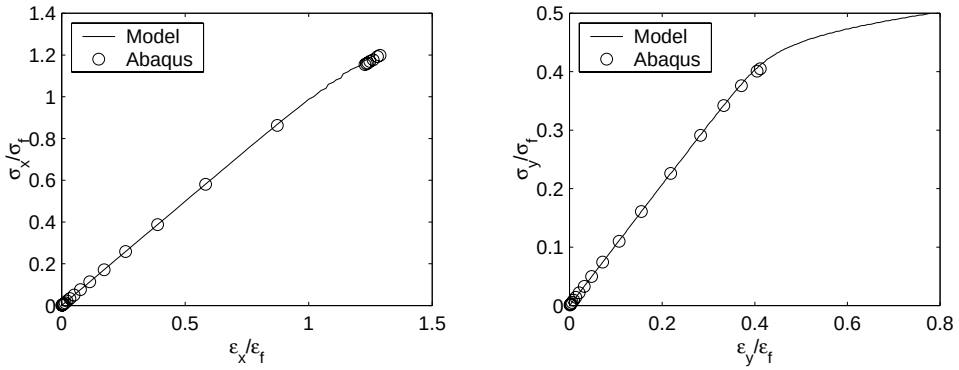

Figure 4.13: Aluminium hat profile under axial loading (left) and transverse loading (right) using 10x3 terms)

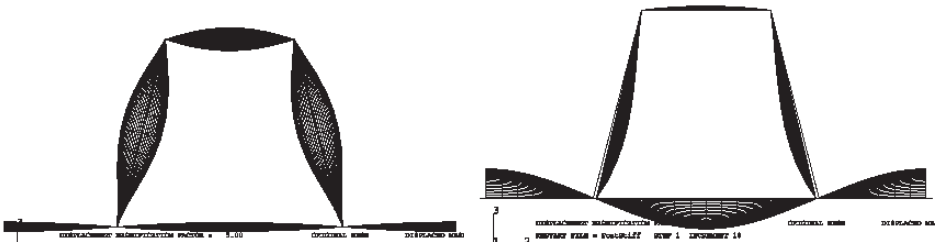

Figure 4.14: 3-dimensional deflection shape for aluminium hat profile under axial load (left) and transverse load (right) resulting from ABAQUS analysis

from the developed model is shown in Fig. 4.15. It should be noted that the former is a 3-dimensional plot, while the latter is a 2-dimensional plot of the cross-sectional displacement. It is seen thatthe deformation shapes from the model qualitatively agrees well with the deformation shapes from ABAQUS. The method of using rotational springs to ensure the continuity between the plate members seems to work well. It is especially interesting to look at the deflection of the vertical plates, where the deflection is clearly non-symmetric. For axial load the deformation mode is close to clamped at the lower end, and close to simply supported at the upper end. Only three terms was necessary in the transverse direction to produce this shape.

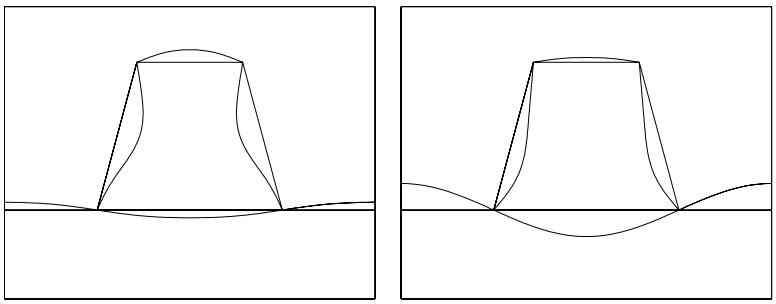

Figure 4.15: 2-dimensional deflection shape for aluminium hat profile under axial load (left) and transverse load (right) resulting from Model calculation

Chapter 5

Global buckling of stiffened panels

Global buckling of a stiffened panel is now considered. A computational model is developed by considering the panel as an unstiffened plate with anisotropic stiffness coefficients. The anisotropy is structural, meaning that it is caused by the plate stiffening. The material is still considered as isotropic. The local deformation of plating and stiffeners is accounted for by applying a set of reduced stiffness coefficients. These are derived from the local buckling model presented in chapter 4, as illustrated in Fig. 5.1. Due to the local buckling effects, the stiffness properties are reduced compared to the initial stiffness. However, the coupling between local and global deformation is not exactly accounted for with this approach, since the global deformation is assumed to not influence the local deformation. The model therefore considers a kind of one-way interaction between local and global buckling.

In section 5.1 the stiffness coefficients used on the global level are defined in terms of average stress and strain. In section 5.2, it is described how the coefficients can be derived using the local buckling model presented in section 4.1. Finally, derivation of the global buckling model is given in section 5.3.

5.1 Definition of global stiffness coefficients

The definitions used in this section follow (Det Norske Veritas 2002a). The stiffness coefficients C_{ij} are defined as the change in load N_i resulting from a change in displacement ε_j,

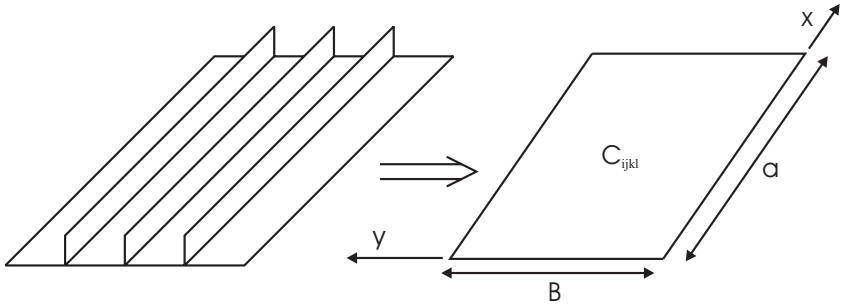

Figure 5.1: Illustration of global buckling model

provided that all other displacements are kept fixed. The loads considered on the global level are defined as, see Fig. 5.2:

N_1 = Axial force per unit breadth in x-direction
N_2 = Axial force per unit length in y-direction
N_3 = Shear flow
M_1 = Resulting moment about the plate plane due to N_1
M_2 = Resulting moment about the plate plane due to N_2
M_3 = Torsional moment

The corresponding displacements are:

ε_1 = Average strain in x-direction
ε_2 = Average strain in y-direction
ε_3 = Shear strain
κ_1 = Curvature about the y-axis
κ_2 = Curvature about the x-axis
κ_3 = Torsion

It should be noted that these definitions are somewhat unusual, since N_3 is shear flow rather than force in z-direction, and M_3 is torsional moment rather than moment about the z-axis. The displacement parameters used are all average values.Hence, the stiffness coefficients may also be considered as averaged over the panel.

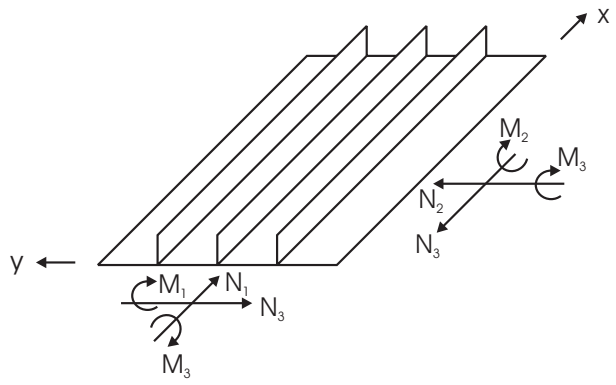

Figure 5.2: Definition of global forces and moments

The incremental force-displacement relation for the stiffened panel is:

$$\begin{bmatrix} \Delta N_1 \\ \Delta N_2 \\ \Delta N_3 \\ \Delta M_1 \\ \Delta M_2 \\ \Delta M_3 \end{bmatrix} = \begin{bmatrix} C_{11} & C_{12} & C_{13} & Q_{11} & Q_{12} & Q_{13} \\ C_{21} & C_{22} & C_{23} & Q_{21} & Q_{22} & Q_{23} \\ C_{31} & C_{32} & C_{33} & Q_{31} & Q_{32} & Q_{33} \\ Q_{11} & Q_{21} & Q_{31} & D_{11} & D_{12} & D_{13} \\ Q_{12} & Q_{22} & Q_{32} & D_{21} & D_{22} & D_{23} \\ Q_{13} & Q_{23} & Q_{33} & D_{31} & D_{32} & D_{33} \end{bmatrix} \begin{bmatrix} \Delta\varepsilon_1 \\ \Delta\varepsilon_2 \\ \Delta\varepsilon_3 \\ \Delta\kappa_1 \\ \Delta\kappa_2 \\ \Delta\kappa_3 \end{bmatrix} \tag{5.1}$$

The stiffness matrix is symmetric, so that $C_{ij} = C_{ji}$ and $D_{ij} = D_{ji}$. The stiffness coefficients may be divided into a linear and a nonlinear part:

$$C_{ij} = C_{ij}^L + C_{ij}^{NL} \tag{5.2}$$
$$D_{ij} = D_{ij}^L + D_{ij}^{NL} \tag{5.3}$$
$$Q_{ij} = Q_{ij}^L + Q_{ij}^{NL} \tag{5.4}$$

The linear parts are the ones corresponding to classical orthotropic stiffness coefficients, and these are independent of load and displacement. The nonlinear parts are calculated using the local buckling model, and will be functions of load and displacement. For compressive loads they will be negative, resulting in a stiffness reduction.

5.2 Derivation of reduced stiffness

5.2.1 General

For calculation of the stiffness coefficients, the forces are written as follows:

$$\begin{bmatrix} \mathbf{N} \\ \mathbf{M} \end{bmatrix} = \begin{bmatrix} \mathbf{C} & \mathbf{Q} \\ \mathbf{Q}^T & \mathbf{D} \end{bmatrix}^L \begin{bmatrix} \varepsilon \\ \kappa \end{bmatrix} + \begin{bmatrix} \mathbf{g}_N(A_{mn}) \\ \mathbf{g}_M(A_{mn}) \end{bmatrix} \tag{5.5}$$

The stiffness coefficients are then defined as:

$$C_{ij} = \frac{\partial N_i}{\partial \varepsilon_j} = C_{ij}^L + \frac{\partial g_{N_i}}{\partial \varepsilon_j} \tag{5.6}$$

$$Q_{ij} = \frac{\partial N_i}{\partial \kappa_j} = Q_{ij}^L + \frac{\partial g_{N_i}}{\partial \kappa_j} \tag{5.7}$$

$$= \frac{\partial M_j}{\partial \varepsilon_i} = Q_{ij}^L + \frac{\partial g_{M_j}}{\partial \varepsilon_i} \tag{5.8}$$

$$D_{ij} = \frac{\partial M_i}{\partial \kappa_j} = M_{ij}^L + \frac{\partial g_{M_i}}{\partial \kappa_j} \tag{5.9}$$

5.2.2 Linear coefficients

The reduced stiffness coefficients are derived for the local buckling model presented for open profiles in section 4.1. First, the resultan tforces and moments are calculated by integration of the membrane stress:

$$N_i = \int_h \sigma_{ii} dz \tag{5.10}$$

$$M_i = \int_h z\sigma_{ii} dz \tag{5.11}$$

The neutral axis of the stiffener is not known, since it is continuously changing during buckling. The bending moment is therefore calculated about the middle plate plane. The neutral axis and the neutral bending stiffness coefficients can be calculated once the in-plane and bending stiffness are determined, as explained in section 5.3.

By manipulating the expressions derived using the requirement of longitudinal continuity in section 4.1.4, and introducing the axial curvature κ_1, the internal axial and transverse

force can be written:

$$N_1 = E\frac{A_T}{b}\left[1+\frac{\nu^2 bt}{A_T(1-\nu^2)}\right]\varepsilon_1 + \frac{\nu tE}{1-\nu^2}\varepsilon_2 + \frac{EA_s z_{gs}}{b}\kappa_1 \tag{5.12}$$
$$- \frac{tE}{2a}\Delta u^{p,a} - \frac{\nu tE}{2b(1-\nu^2)}\Delta v^{p,a} + \frac{E}{8ab}\int_{V_s} v_{,x}^2 dV_s$$
$$N_2 = \frac{\nu tE}{1-\nu^2}\varepsilon_1 + \frac{tE}{1-\nu^2}\varepsilon_2 - \frac{\nu tE}{2a(1-\nu^2)}\Delta u^{p,a} - \frac{tE}{2b(1-\nu^2)}\Delta v^{p,a} \tag{5.13}$$

where A_T is the total cross-sectional area, A_s is the stiffener area, and z_{gs} is the distance from the plate plane to the centroid of the stiffener. The curvature κ_1 is due to global deflection. It is set to zero in the local analysis, but is included in the formulations for deriv ation of the stiffness coefficients. The shear force and bending moment is:

$$N_3 = Gt\varepsilon_3 + \frac{Gt}{4ab}D\gamma^{p,a} \tag{5.14}$$
$$M_1 = \frac{EA_s}{b}\varepsilon_1 + \frac{EI}{b}\kappa_1 + \frac{E}{8ab}\int_{V_s} z v_{,x}^2 dV_s \tag{5.15}$$

where I is the moment of inertia of the whole cross-section. The stiffness coefficients are found by differentiation of the above expressions. The linear parts are given directly as:

$$C_{11}^L = E\frac{A_T}{b}(1+\frac{\nu^2 bt}{A_T(1-\nu^2)}) \tag{5.16}$$
$$C_{12}^L = C_{21}^L = \frac{\nu tE}{1-\nu^2} \tag{5.17}$$
$$C_{22}^L = \frac{tE}{1-\nu^2}\varepsilon_2 \tag{5.18}$$
$$C_{33}^L = Gt \tag{5.19}$$
$$Q_{11}^L = \frac{EA_s z_{gs}}{b} \tag{5.20}$$
$$D_{11}^L = \frac{EI}{b} \tag{5.21}$$

All other linear coefficients are zero for the open profile stiffeners.

5.2.3 Nonlinear coefficients

The nonlinear parts of the stiffness coefficients are calculated as:

$$C_{ij}^{NL} = \frac{\partial g_{N_i}}{\partial A_{mn}} \frac{\partial A_{mn}}{\partial \varepsilon_j} \tag{5.22}$$

$$Q_{ij}^{NL} = \frac{\partial g_{N_i}}{\partial A_{mn}} \frac{\partial A_{mn}}{\partial \kappa_j} \tag{5.23}$$

$$D_{ij}^{NL} = \frac{\partial g_{M_i}}{\partial A_{mn}} \frac{\partial A_{mn}}{\partial \kappa_j} \tag{5.24}$$

The first part may be found directly by differentiation once $\mathbf{g}_N$ and $\mathbf{g}_M$ are known. They are given from the expressions for N_i and M_1 presen ted in the previous subsection, Eq. (5.12) through Eq. (5.15)

The second part is calculated using the equilibrium equations. F rom the previous hapter, the local equilibrium equations resulting from the rate of minimum potential energy were written:

$$\mathbf{K}\dot{\mathbf{A}} + \mathbf{G}\dot{\Lambda} = \mathbf{0} \tag{5.25}$$

where

$$\mathbf{K} = \frac{\partial^2 \Pi}{\partial \mathbf{A}^2} \tag{5.26}$$

$$\mathbf{G} = \frac{\partial^2 \Pi}{\partial \mathbf{A} \partial \Lambda} \tag{5.27}$$

In the local analysis the curv ature κ_1 is defined as zero, but for calculation of stiffness coefficients it must be included in the equilibrium equations. The additional stiffness con tribution is due to the membrane strain resulting from the curvature:

$$\varepsilon_{\kappa_1} = z\kappa_1 \tag{5.28}$$

Adding this strain to the potential energy, the modified equilibrium equations become:

$$\mathbf{K}\dot{\mathbf{A}} + \mathbf{G}\dot{\Lambda} + \mathbf{G}_{\kappa_1}\dot{\kappa}_1 = \mathbf{0} \tag{5.29}$$

The load vector $\mathbf{G}$ may be split in toseparate contributions from the different loads, so that:

$$\mathbf{K}\dot{\mathbf{A}} + \mathbf{G}_{N_i}\dot{N}_i + \mathbf{G}_{\kappa_1}\dot{\kappa}_1 = \mathbf{0} \tag{5.30}$$

where

$$\mathbf{G}_{N_i} = \frac{\partial^2 \Pi}{\partial \mathbf{A} \partial N_i} \tag{5.31}$$

This equation contains both load and displacement parameters. F or calculation of stiffness coefficients, the load parameters must be replaced by displacement parameters. The in-plane loads are replaced using Eq. (5.5):

$$\mathbf{K}\dot{\mathbf{A}} + \mathbf{G}_{N_i}(\mathbf{C}^L_{ij}\dot{\varepsilon} + \mathbf{Q}^L_{ij}\dot{\kappa} + \dot{\mathbf{g}}_{N_i}) + \mathbf{G}_{\kappa_1}\dot{\kappa}_1 = \mathbf{0} \tag{5.32}$$

Introducing

$$\dot{\mathbf{g}}_{N_i} = \frac{\partial \mathbf{g}}{\partial \mathbf{A}}\dot{\mathbf{A}} \tag{5.33}$$

the modified equilibrium equation is:

$$\mathbf{K}^{'}\dot{\mathbf{A}} + \mathbf{G}^{'}_{\varepsilon_i}\dot{\varepsilon}_i + \mathbf{G}^{'}_{\kappa_1}\dot{\kappa}_1 = \mathbf{0} \tag{5.34}$$

The modified stiffness matrix and load vectors are

$$\mathbf{K}^{'} = \mathbf{K} + \mathbf{G}_{N_1}\frac{\partial g_{N_1}}{\partial A_{mn}} + \mathbf{G}_{N_2}\frac{\partial g_{N_2}}{\partial A_{mn}} + \mathbf{G}_{N_3}\frac{\partial g_{N_3}}{\partial A_{mn}} \tag{5.35}$$

$$\mathbf{G}^{'}_{\varepsilon_1} = \mathbf{G}_{N_1}C^L_{11} + \mathbf{G}_{N_2}C^L_{21} \tag{5.36}$$

$$\mathbf{G}^{'}_{\varepsilon_2} = \mathbf{G}_{N_1}C^L_{12} + \mathbf{G}_{N_2}C^L_{22} \tag{5.37}$$

$$\mathbf{G}^{'}_{\varepsilon_3} = \mathbf{G}_{N_3}C^L_{33} \tag{5.38}$$

$$\mathbf{G}^{'}_{\kappa_1} = \mathbf{G}_{N_1}Q^L_{11} + \mathbf{G}_{\kappa_1} \tag{5.39}$$

By applying partial differentiation on the minimum potential energy we get:

$$\frac{\partial(\frac{\partial \Pi}{\partial A_{mn}})}{\partial \varepsilon_i} = \frac{\partial^2 \Pi}{\partial A^2_{mn}}\frac{\partial A_{mn}}{\partial \varepsilon_i} + \frac{\partial^2 \Pi}{\partial A_{mn}\partial \varepsilon_i} = \mathbf{0} \tag{5.40}$$

$$\frac{\partial(\frac{\partial \Pi}{\partial A_{mn}})}{\partial \kappa_1} = \frac{\partial^2 \Pi}{\partial A^2_{mn}}\frac{\partial A_{mn}}{\partial \kappa_1} + \frac{\partial^2 \Pi}{\partial A_{mn}\partial \kappa_1} = \mathbf{0} \tag{5.41}$$

By defining

$$\mathbf{K}' = \frac{\partial^2 \Pi}{\partial A_{mn}^2} \tag{5.42}$$

$$\mathbf{G}'_{\varepsilon_i} = \frac{\partial^2 \Pi}{\partial A_{mn} \partial \varepsilon_i} \tag{5.43}$$

$$\mathbf{G}'_{\kappa_1} = \frac{\partial^2 \Pi}{\partial A_{mn} \partial \kappa_1} \tag{5.44}$$

we get:

$$\mathbf{K}' \frac{\partial A_{mn}}{\partial \varepsilon_i} + \mathbf{G}'_{\varepsilon_i} = \mathbf{0} \tag{5.45}$$

$$\mathbf{K}' \frac{\partial A_{mn}}{\partial \kappa_1} + \mathbf{G}'_{\kappa_1} = \mathbf{0} \tag{5.46}$$

This means that

$$\frac{\partial A_{mn}}{\partial \varepsilon_i} = -(\mathbf{K}')^{-1} \mathbf{G}'_{\varepsilon_i} \tag{5.47}$$

and

$$\frac{\partial A_{mn}}{\partial \kappa_1} = -(\mathbf{K}')^{-1} \mathbf{G}'_{\kappa_1} \tag{5.48}$$

5.2.4 Results

An example of how the stiffness coefficients may change during local deformation is given in Fig. 5.3. The calculations are for the steel angle bar from chapter 4, Table 4.1. The load is axial, and the imperfection is 1mm in the local eigenmode.

The values plotted are the ratio between the non-linear stiffness coefficients and the corresponding linear values. Q_{12} is divided by Q_{11} since Q_{12}^L is zero. The stiffness ratios are slightly smaller than 1.0 at the start of the analysis due to the imperfection. If the imperfection was larger, the stiffness ratios would also have smaller initial values.

It is seen that the stiffness reduction is significant for C_{11} and C_{22}, but the most drastic change is for C_{12} which even changes sign. The reason is that C_{12} is positive for a flat plate

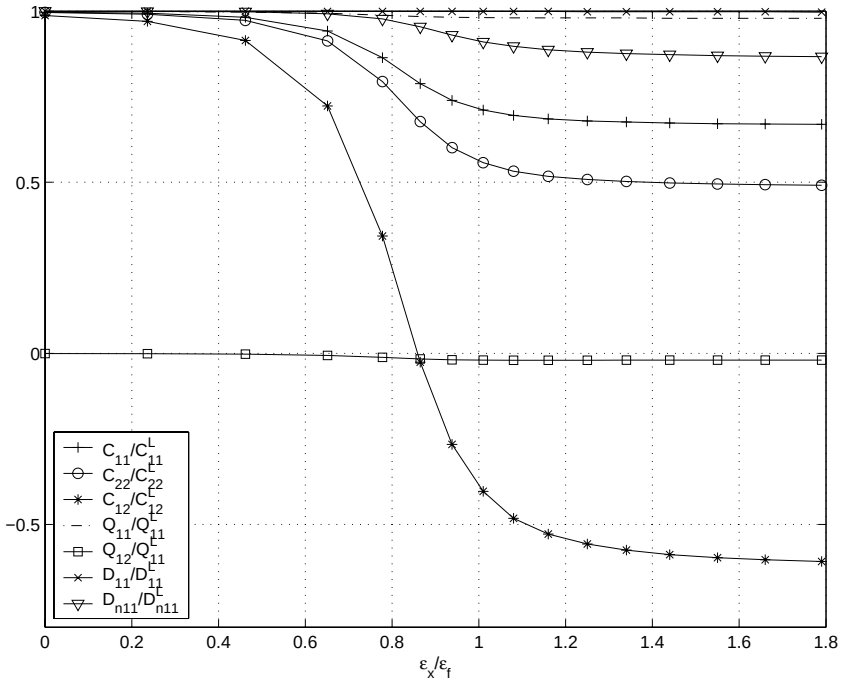

Figure 5.3: Change in stiffness properties during local buckling due to axial load for steel angle bar

due to the Poisson-effect, while it becomes negative for large deflection due to membrane stretching. The change in Q_{11}, Q_{12} and D_{11} is small. There is some reduction in D_{n11}, which is the neutral bending stiffness. This coefficient is defined in the next section.

It is seen that the stiffness reduction is quite localized around the buckling strain, and the stiffness is almost constant after this. This is a general trend found for all the stiffeners investigated here. For smaller imperfections the stiffness reduction will be even more sudden, while for larger imperfections there will be a more gradual transition. The plateau on the stiffness curves after buckling is a useful property, because it means that the global buckling response may be estimated using a single set of stiffness coefficients. Instead of continuously updating the coefficients, conservative results could be obtained by using the coefficients calculated at the end of the local analysis.

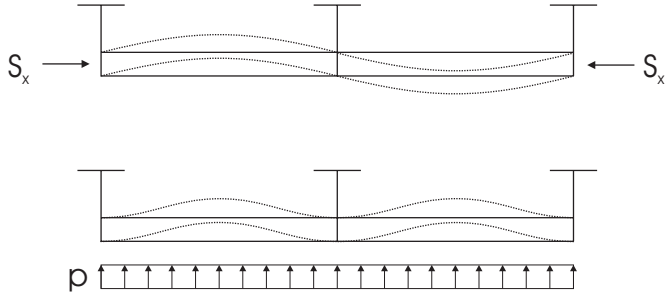

Figure 5.4: Global deflection of stiffener in simply supported mode and clamped mode

5.3 Global buckling model

In order to develop the global buckling model, the stiffened panel is considered as an elastic plate with general anisotropic stiffness coefficients. The anisotropy is structural, and the anisotropic stiffness coefficients represent the effect of plate stiffening. For analysis of global buckling alone, orthotropic plate theory is sufficient, but when nonlinear stiffness properties due to local buckling are calculated, general anisotropy must be assumed.

5.3.1 Assumptions

A rectangular plate field with stiffeners running in one direction is considered. For the following derivations the stiffeners are assumed to be in the longitudinal direction, Fig. 5.1, but transverse stiffening can be analysed simply by switching panel length and breadth. The stiffened panel is supported at all edges by transverse and longitudinal girders. The length of the panel is a, while the width is B. The loads considered are in-plane compression or tension, shear force and lateral pressure. The edge loads are assumed to be constant in magnitude. If the edge loads were to vary along the edges, the structural stiffness of the panel could no longer be assumed to be constant. The stiffness would then have to be calculated as a function of the position in the panel, and a numerical procedure would be needed for integration of the energy equations.

Two stiffener spans and panel widths are included in the model. The intention is to account properly for the effect of lateral pressure on the panel. The pressure must be carried by the stiffeners, and the deflection of the stiffeners may therefore be a combination of the simply supported mode and the clamped mode, Fig. 5.4. This is equivalent to the stiffened plate model considered in chapter 4, where it is assumed that the boundary condition for a plate between two stiffeners is somewhere in between simply supported and clamped.

The deflection shape is therefore taken as a combination of sine-terms and cosine-terms:

$$w = w^s + w^c \tag{5.49}$$
$$w_0 = w_0^s + w_0^c \tag{5.50}$$

where s and c denotes sine and cosine mode deflection, respectively:

$$w^s = \sum_{m=1}^{M_s}\sum_{n=1}^{N_s} A_{mn}^s \sin(\frac{m\pi x}{a}) \sin(\frac{n\pi y}{B}) \tag{5.51}$$
$$w^c = \sum_{m=1}^{M_c}\sum_{n=1}^{N_c} \frac{A_{mn}^c}{2}[1-\cos(\frac{2m\pi x}{a})] \sin(\frac{n\pi y}{B}) \tag{5.52}$$
$$w_0^s = \sum_{m=1}^{M_s}\sum_{n=1}^{N_s} B_{mn}^s \sin(\frac{m\pi x}{a}) \sin(\frac{n\pi y}{B}) \tag{5.53}$$
$$w_0^c = \sum_{m=1}^{M_c}\sum_{n=1}^{N_c} \frac{B_{mn}^c}{2}[1-\cos(\frac{2m\pi x}{a})] \sin(\frac{n\pi y}{B}) \tag{5.54}$$

5.3.2 Anisotropic material law

Some introductory remarks regarding the anisotropic material law are given first. The material law for plane stress is:

$$\begin{bmatrix} \sigma_{11} \\ \sigma_{22} \\ \sigma_{12} \\ \sigma_{21} \end{bmatrix} = \begin{bmatrix} C_{1111}^{**} & C_{1122}^{**} & C_{1112}^{**} & C_{1121}^{**} \\ C_{2211}^{**} & C_{2222}^{**} & C_{2212}^{**} & C_{2221}^{**} \\ C_{1211}^{**} & C_{1222}^{**} & C_{1212}^{**} & C_{1221}^{**} \\ C_{2111}^{**} & C_{2122}^{**} & C_{2112}^{**} & C_{2121}^{**} \end{bmatrix} \begin{bmatrix} \varepsilon_{11} \\ \varepsilon_{22} \\ \varepsilon_{12} \\ \varepsilon_{21} \end{bmatrix} \tag{5.55}$$

Using that $\sigma_{12} = \sigma_{21}$ and $\varepsilon_{12} = \varepsilon_{21}$, the material law for an isotropic material can be simplified to:

$$\begin{bmatrix} \sigma_{11} \\ \sigma_{22} \\ \sigma_{12} \end{bmatrix} = \begin{bmatrix} C_{1111}^{*} & C_{1122}^{*} & C_{1112}^{*} \\ C_{2211}^{*} & C_{2222}^{*} & C_{2212}^{*} \\ C_{1211}^{*} & C_{1222}^{*} & C_{1212}^{*} \end{bmatrix} \begin{bmatrix} \varepsilon_{11} \\ \varepsilon_{22} \\ \varepsilon_{12} \end{bmatrix} \tag{5.56}$$

The superscripts ** and * are used to indicate that the matrix elements are not the same in the two expressions. For an isotropic material the coefficients $C_{1112} = C_{2212} = C_{1211} = C_{1222} = 0$, while for an anisotropic material they are generally different from zero. If the

stiffness matrix is reduced by the procedure used for isotropic material, symmetry of the stiffness matrix is no longer maintained, so that $C_{1112} \neq C_{1211}$ and $C_{2212} \neq C_{1222}$. In order to maintain symmetry, it is necessary to define the stiffness matrix using the shear strain $\gamma_{12} = 2\varepsilon_{12}$:

$$\begin{bmatrix} \sigma_{11} \\ \sigma_{22} \\ \sigma_{12} \end{bmatrix} = \begin{bmatrix} C_{1111} & C_{1122} & C_{1112} \\ C_{2211} & C_{2222} & C_{2212} \\ C_{1211} & C_{1222} & C_{1212} \end{bmatrix} \begin{bmatrix} \varepsilon_{11} \\ \varepsilon_{22} \\ \gamma_{12} \end{bmatrix} \tag{5.57}$$

This last definition is used in the following derivations for the anisotropic plate. The definition of the stiffness coefficients influences the compatibility equations and the energy expressions.

5.3.3 Material law for structural anisotropic plate

For a stiffened panel, it is more convenient to express the stiffness relations in terms of stress resultants instead of stress. For the resultant forces N_1, N_2, and N_3, the material law is:

$$\begin{bmatrix} N_1 \\ N_2 \\ N_3 \end{bmatrix} = \begin{bmatrix} C_{11} & C_{12} & C_{13} \\ C_{21} & C_{22} & C_{23} \\ C_{31} & C_{32} & C_{33} \end{bmatrix} \begin{bmatrix} \varepsilon_1 \\ \varepsilon_2 \\ \gamma_3 \end{bmatrix} \tag{5.58}$$

The corresponding flexibility relation is needed for derivation of the stress function. It is written:

$$\begin{bmatrix} \varepsilon_1 \\ \varepsilon_2 \\ \gamma_3 \end{bmatrix} = \begin{bmatrix} M_{11} & M_{12} & M_{13} \\ M_{21} & M_{22} & M_{23} \\ M_{31} & M_{32} & M_{33} \end{bmatrix} \begin{bmatrix} N_1 \\ N_2 \\ N_3 \end{bmatrix} \tag{5.59}$$

The stiffness relation for the resultant bending moments is:

$$\begin{bmatrix} M_1 \\ M_2 \\ M_3 \end{bmatrix} = \begin{bmatrix} D_{11} & D_{12} & D_{13} \\ D_{21} & D_{22} & D_{23} \\ D_{31} & D_{32} & D_{33} \end{bmatrix} \begin{bmatrix} \kappa_1 \\ \kappa_2 \\ \kappa_3 \end{bmatrix} \tag{5.60}$$

It is assumed that there is no coupling between resultant forces and moments, i.e. all Q_{ij}-terms are zero. This can be done by performing a neutralization of the stiffness coefficients, as explained in (Det Norske Veritas 2002b). This means that the bending stiffness coefficients are redefined so that no coupling occurs. The neutral bending stiffness matrix $\tilde{\mathbf{D}}$ is calculated from the original stiffness as $\tilde{\mathbf{D}} = \mathbf{D} - \mathbf{Q}^{\mathbf{T}}\mathbf{C}^{-1}\mathbf{Q}$.

For simplicity, the symbol $\mathbf{D}$ is used in the following to denote the neutral bending stiffness matrix.

5.3.4 Stress function for stiffened panel

The general requirement for strain compatibility is:

$$\varepsilon_{x,yy} + \varepsilon_{y,xx} - \gamma_{xy,xy} = w_{,xy}^2 - w_{,xx}w_{,yy} + 2w_{0,xy}w_{,xy} - w_{0,yy}w_{,xx} - w_{,yy}w_{0,xx} \tag{5.61}$$

A stress function F is now defined in terms of the stress resultants N_i in the stiffened plate, so that:

$$N_1 = F_{,yy} \tag{5.62}$$
$$N_2 = F_{,xx} \tag{5.63}$$
$$N_3 = -F_{,xy} \tag{5.64}$$

Using the material law as defined above, and introducing the stress function F, the compatibility equation for the anisotropic plate can be written:

$$\begin{aligned} & M_{1111}F_{,yyyy} + M_{2222}F_{,xxxx} + (2M_{1122} + M_{1212})F_{,xxyy} - 2M_{1112}F_{,xyyy} - 2M_{2221}F_{,yxxx} \\ = \; & w_{,xy}^2 + 2w_{0,xy}w_{,xy} - w_{,xx}w_{,yy} - w_{0,yy}w_{,xx} - w_{,yy}w_{0,xx} \end{aligned} \tag{5.65}$$

The solution to this equation is more complex than for the isotropic plate, due to the nonzero coefficients M_{1112} and M_{2221}. A solution is found by assuming the stress function to consist of the following terms:

$$F = F_0 + F_{s1} + F_{s2} + F_{c1} + F_{c2} + F_{sc1} + F_{sc2} \tag{5.66}$$

where

$$F_0 = -\frac{S_x y^2 t}{2} - \frac{S_y x^2 t}{2} - S_{xy} xyt \tag{5.67}$$

$$F_{s1} = \sum_{0}^{2M_s}\sum_{0}^{2N_s} f_{mn}^{s1} \cos(\frac{m\pi x}{a}) \cos(\frac{n\pi y}{B}) \tag{5.68}$$

$$F_{s2} = \sum_{0}^{2M_s}\sum_{0}^{2N_s} f_{mn}^{s2} \sin(\frac{m\pi x}{a}) \sin(\frac{n\pi y}{B}) \tag{5.69}$$

$$F_{c1} = \sum_{0}^{2M_c}\sum_{0}^{2N_c} f_{mn}^{c1} \cos(\frac{2m\pi x}{a}) \cos(\frac{n\pi y}{B}) \tag{5.70}$$

$$F_{c2} = \sum_{0}^{2M_c}\sum_{0}^{2N_c} f_{mn}^{c2} \sin(\frac{2m\pi x}{a}) \sin(\frac{n\pi y}{B}) \tag{5.71}$$

$$F_{sc1} = \sum_{0}^{M_s+M_c}\sum_{0}^{N_s+2N_c} f_{mn}^{sc1} \sin(\frac{m\pi x}{a}) \cos(\frac{n\pi y}{B}) \tag{5.72}$$

$$F_{sc2} = \sum_{0}^{M_s+M_c}\sum_{0}^{N_s+2N_c} f_{mn}^{s2} \cos(\frac{m\pi x}{a}) \sin(\frac{n\pi y}{B}) \tag{5.73}$$

By substitution of the assumed stress function into the compatibility equation, it is found that the coefficients f_{mn}^1 and f_{mn}^2 must be:

$$f_{mn}^{s1} = \frac{1}{4a^2B^2(K1s - \frac{K2s^2}{K1s})} \sum_{rspq} b_{rspq}^s (A_{rs}^s A_{pq}^s + A_{rs}^s B_{pq}^s + A_{pq}^s B_{rs}^s) \tag{5.74}$$

$$f_{mn}^{s2} = -\frac{K2s}{K1s} f_{mn}^{s1} \tag{5.75}$$

$$f_{mn}^{c1} = \frac{1}{4a^2B^2(K1c - \frac{K2c^2}{K1c})} \sum_{rspq} b_{rspq}^c (A_{rs}^c A_{pq}^c + A_{rs}^c B_{pq}^c + A_{pq}^c B_{rs}^c) \tag{5.76}$$

$$f_{mn}^{c2} = -\frac{K2c}{K1c} f_{mn}^{c1} \tag{5.77}$$

$$f_{mn}^{sc1} = \frac{1}{4a^2B^2(K1sc - \frac{K2sc^2}{K1sc})} \sum_{rspq} b_{rspq}^{sc} (A_{rs}^s A_{pq}^c + A_{rs}^s B_{pq}^c + A_{pq}^c B_{rs}^s) \tag{5.78}$$

$$f_{mn}^{sc2} = -\frac{K2sc}{K1sc} f_{mn}^{sc1} \tag{5.79}$$

where

$$K1s = \frac{m^4}{a^4}M_{2222} + \frac{m^2n^2}{a^2B^2}(2M_{1122} + M_{1212}) + \frac{n^4}{B^4}M_{1111} \quad (5.80)$$

$$K2s = 2\frac{m^3n}{a^3B}M_{2221} + 2\frac{mn^3}{aB^3}M_{1112} \quad (5.81)$$

$$K1c = 16\frac{m^4}{a^4}M_{2222} + 4\frac{m^2n^2}{a^2B^2}(2M_{1122} + M_{1212}) + \frac{n^4}{B^4}M_{1111} \quad (5.82)$$

$$K2c = 16\frac{m^3n}{a^3B}M_{2221} + 4\frac{mn^3}{aB^3}M_{1112} \quad (5.83)$$

$$K1sc = \frac{m^4}{a^4}M_{2222} + \frac{m^2n^2}{a^2B^2}(2M_{1122} + M_{1212}) + \frac{n^4}{B^4}M_{1111} \quad (5.84)$$

$$K2sc = -2\frac{m^3n}{a^3B}M_{2221} - 2\frac{mn^3}{aB^3}M_{1112} \quad (5.85)$$

and $f_{0,0}$ is defined as zero. The coefficients b^s_{rspq}, b^c_{rspq}, and b^{sc}_{rspq} are the same integer numbers as defined previously in Eq. (3.9), Eq. (3.35), and Eq. (4.10).

5.3.5 Internal potential energy

The potential of in ternal energy is generally written as

$$U = \frac{1}{2}\int_V \sigma\varepsilon dV \quad (5.86)$$

The strain is first divided into a constant membrane part ε^m and a linearly varying bending part $\varepsilon^b = z\kappa$. Integration is then performed over the thic kness in order to express the potential energy as a function of stress resultants:

$$U = \frac{1}{2}\int_V \sigma(\varepsilon^m + \varepsilon^b)dV \quad (5.87)$$

$$= \frac{1}{2}\int_V \sigma\varepsilon^m dV + \frac{1}{2}\int_V z\sigma\kappa dV \quad (5.88)$$

$$= \frac{1}{2}\int_A N\varepsilon^m dV + \frac{1}{2}\int_V M\kappa dV \quad (5.89)$$

$$= U_m + U_b \quad (5.90)$$

By substitution of the material law, the membrane energy is written:

$$\begin{aligned} U_m &= \frac{1}{2}\left(M_{11}\int_A N_1^2 dA + M_{22}\int_A N_2^2 dA + M_{33}\int_A N_3^2 dA \right. \\ &+ \left. 2M_{12}\int_A N_1 N_2 dA + 2M_{13}\int_A N_1 N_3 dA + 2M_{23}\int_A N_2 N_3 dA\right) \end{aligned} \tag{5.91}$$

The membrane energy is calculated by substitution of the stress function and integrating over the plate area. The final expression is given in appendix C.

The bending energy is:

$$\begin{aligned} U_b &= \frac{1}{2}\left(D_{11}\int_A \kappa_1^2 dA + D_{22}\int_A \kappa_2^2 dA + D_{33}\int_A \kappa_3^2 dA \right. \\ &+ \left. 2D_{12}\int_A \kappa_1\kappa_2 dA + 2D_{13}\int_A \kappa_1\kappa_3 dA + 2D_{23}\int_A \kappa_2\kappa_3 dA\right) \end{aligned} \tag{5.92}$$

The resulting expression is found by substituting $\kappa_1 = w_{,xx}$, $\kappa_2 = w_{,yy}$, $\kappa_3 = 2w_{,xy}$, and performing the integration. The result is given in appendix C.

5.3.6 Potential of external loads

The displacements are partly due the membrane effect of the external load (subscript F), and partly due to the deflection of the plate (subscript D):

$$\Delta u = \Delta u^F + \Delta u^D \tag{5.93}$$
$$\Delta v = \Delta v^F + \Delta v^D \tag{5.94}$$
$$\gamma_{xy} = \gamma_{xy}^F + \gamma_{xy}^D \tag{5.95}$$

The part due to the deflection is independent of the material properties, and is therefore the same as for an isotropic plate. The part due to external load is:

$$\Delta u^F = 2a(M_{11}N_1 + M_{12}N_2 + M_{13}N_3) \tag{5.96}$$
$$\Delta v^F = 2b(M_{21}N_1 + M_{22}N_2 + M_{23}N_3) \tag{5.97}$$
$$\gamma_{xy}^F = M_{21}N_1 + M_{22}N_2 + M_{23}N_3) \tag{5.98}$$

This part is relevant for calculation of the actual load-elongation response of the plate, but has no effect on the potential energy since it disappears when differentiating with respect to the deflection. The potential of external energy is therefore the same as for an isotropic plate.

The external energy consists of a part due to sine-deflection, a part due to cosine-deflection, and a coupling part. The sine- and cosine-part are calculated as for the unstiffened plate in chapter 3, except for different areas of integration.

The energy due to in-plane tension or compression load is:

$$T_c = N_1 \Delta u + N_2 \Delta v \tag{5.99}$$

The shear energy is:

$$T_\tau = N_3 \int_0^{2a} \int_0^{2B} (u_{,y} + v_{,x}) dy dx \tag{5.100}$$

The energy due to lateral pressure is:

$$T_{lp} = -\int_0^{2a} \int_0^{2B} pw dy dx \tag{5.101}$$

It is seen that contribution from the sine deflection to the lateral pressure energy vanishes upon integration. This is due to the anti-symmetry of the sine-deflection. Physically, this means that lateral pressure will only give rise to deflection in the cosine mode. For combined loads, the deflection will be a combination of the two.

All final potential energy expressions are given in appendix C.

5.4 Results

Analyses of anisotropic plates may be performed with ABAQUS using the anisotropic material option for the case of an unstiffened plate. Results from such analyses are compared with results obtained using the presented model. Only in-plane anisotropic stiffness coefficients can be specified with this option. The material is assumed to be uniform over the thickness. This means that the bending stiffness is given directly from the in-plane stiffness, in contrast to the current model where the bending stiffness may be specified independently of the in-plane stiffness.

The case shown in Fig. 5.5 is for a 840x980x11mm aluminium plate with E=70000MPa and σ_f=240MPa. A combination of lateral pressure p=0.2MPa, corresponding to 20m water

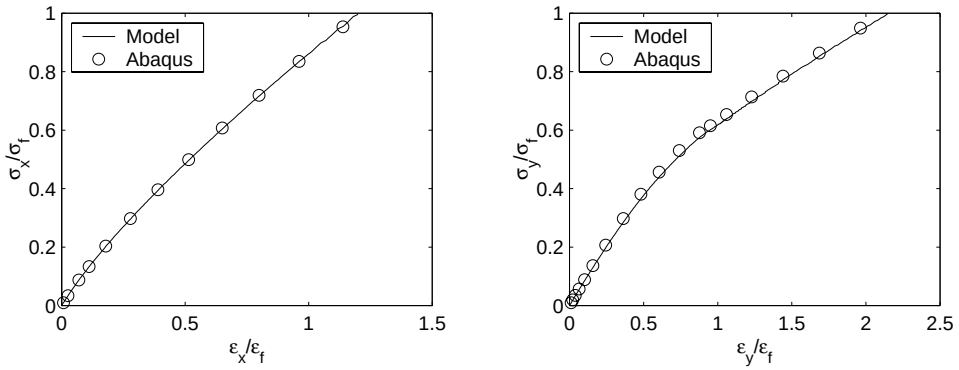

Figure 5.5: Load-average strain response for anisotropic plate subjected to combined axial load and lateral pressure (left) and transverse load and lateral pressure (right)

column, and axial or transverse compression, S_x=240MPa or S_y=240MPa, is applied. This gives a deflection mode in between simply supported and clamped. For this specific case, a stiffness coefficient $C_{1111} = 2C^{iso}_{1111}$ is used. The imperfection is 10mm in the eigenmode. It is seen that the agreement is good, which indicates that the effect of anisotropic stiffness is well handled by the model. Also, the lateral pressure effect, which gives a resulting deflection mode in between simply supported and clamped, is well taken care of.

In order to check the bending stiffness formulations, analyses are performed using a stiffened panel in ABAQUS. It is desirable to compare the model with a stiffened panel deflecting in a pure global mode, i.e. without local buckling of plate and stiffeners. One way to achieve this is to model a panel with very large plate thickness compared to the panel dimensions. Such a panel is likely to deflect globally without local deformations. Another way to achieve the same type of response is to model the panel using the shell general section option.

A stiffened panel consisting of three of the aluminium profiles analysed in section 4.1, Table 4.2, is modelled in ABAQUS. The thickness of the plate, the web and the flange is increased to 50mm. This geometry is so stocky that the resulting deformation is purely in the global mode. Analyses are performed on the stiffened panel in ABAQUS for axial and transverse loading, with an imperfection in the global mode equal to 3.6mm. Analyses are then performed with the global buckling model using linear anisotropic stiffness coefficients according to the stiffener dimensions, as explained previously. The results are shown in Fig. 5.6. It is seen that the agreement is very good.

In Fig. 5.7 the response of this panel under axial loading, calculated using linear stiffness coefficients, is compared with the response calculated using reduced stiffness obtained from

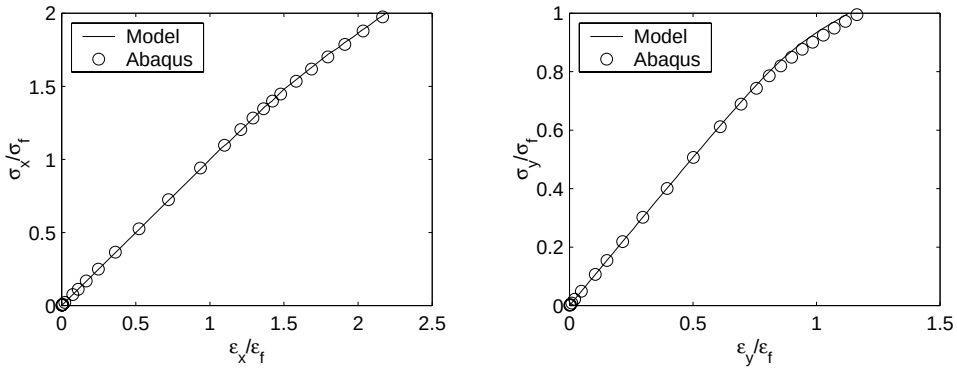

Figure 5.6: Load-average strainresponse due to pure global buckling for stiffened panel subjected to axial compression (left) and transverse compression (right)

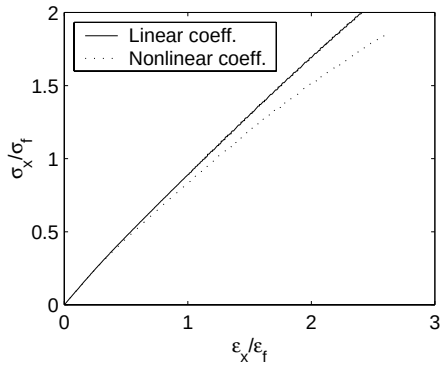

Figure 5.7: Load-average strain response during axial load calculated from global buckling model using linear and nonlinear stiffness coefficients

the local model from chapter 4. The imperfection is 3.2mm in the local mode and 3.6mm in the global mode. It is seen that the global deflection is larger when the reduced stiffness is applied, as expected. In this analysis, the stiffness coefficients input to the global model are gradually reduced, corresponding to the current load factor.

In chapter 7, capacit yestimates calculated using reduced stiffness coefficients obtained from the present approach are presented.

Chapter 6

Coupled local and global buckling

For panels with heavy stiffeners, local buckling effects are the most important. Global deflection must also be accounted for, but the interaction with local buckling is likely to be small. It can therefore be included by using a separate model like the one described in chapter 5. For panels with small stiffeners, however, the global eigenvalue may be close to the local eigenvalue. The interaction between local and global buckling effects could then be significant. The global model presented in chapter 5 can be used to predict the reduction in global buckling strength due to local effects, but the two-way interaction between local and global deformation is not exactly accounted for with this approach.

In this chapter, methods for analysis of the coupled response due to local and global buckling is presented. In the first section, a simplified model for a single stiffened plate is described. In the second section, a model for a complete stiffened panel is presented.

6.1 Coupled local and global buckling for a stiffened plate

Combined local and global buckling of a single stiffened plate is considered first. This means that only one stiffener is included, and global buckling is assumed to be in the column mode. The stiffened plate is assumed to be simply supported at each end by

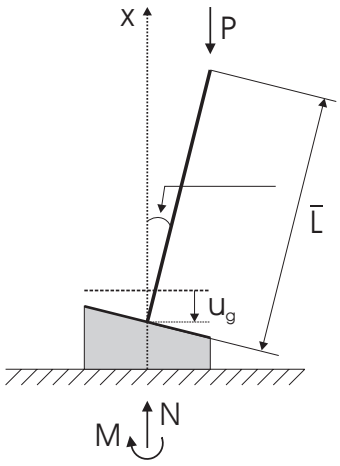

Figure 6.1: Shanley model (reproduced from (Steen 2001))

transverse girders, but the effect of longitudinal girders is not included. Only axial load has been considered here.

The model is derived using the local model presented in chapter 4.1 for open profiles, and combining it with a Shanley method. This approach was used by Steen in (Steen 2001). The Shanley model was originally developed as a method for analysing nonlinear material behavior, (Shanley 1947). It was used by Steen for handling geometrical nonlinearities in a column due to local buckling effects. Here, the model developed by Steen is extended to an indefinite number of plate degrees of freedom, and a more refined web deflection shape.

The Shanley model developed by Steen is a column buckling formulation in which the local cross-sectional behavior follows a two-dimensional spring via Fig. 6.1. It consists of a rigid beam attached to a spring at the lower end, where the spring characteristics represent an integrated effect of local buckling and imperfection effects of the whole cross-section. In the limit of compact cross-sections, the spring characteristic represents the uni-axial linear elastic material stress-strain law.

The global equilibrium equations for the Shanley model are:

$$P - N = 0 \tag{6.1}$$

$$PL\overline{L}(\kappa + \kappa_0) - M = 0 \tag{6.2}$$

where $\kappa = \theta/L$ and $\kappa_0 = \theta_0/L$ are average curvatures, and L is the total length of the

stiffened plate. P is the external load, and N and M are the resultan taxial force and moment acting at the column midspan. They are defined as:

$$N = \int_A \sigma_x dA \tag{6.3}$$

$$M = \int_A z\sigma_x dA \tag{6.4}$$

The length of the rigid beam, $\overline{L}$, is defined as the length giving the same linear buckling load for the Shanley model as for the Euler column. For the simply supported column, it means that

$$\overline{L} = \frac{L}{\pi^2} \tag{6.5}$$

The equation system resulting from the local model is modified by introducing κ as an unknown parameter . The additional strain in a material point due to the global curvature κ is, assuming the Bernoulli-Euler hypothesis,

$$\varepsilon_g = z\kappa \tag{6.6}$$

The unknown κ enters the local equation system through the potential energy. The system of equations with one additional degree of freedom is solved by introducing the moment equilibrium equation above. The local displacements and the global curvature are then solved instantaneously.

6.1.1 Local equilibrium equations

The local buckling model derived in chapter 4 is used. The axial stress and strain in a material point is modified to account for κ. For the membrane stress and strain in the plate we now have:

$$\sigma_x = \sigma^D + \sigma^F - Ez_g\kappa \tag{6.7}$$

$$\varepsilon_x = \varepsilon^D + \varepsilon^F - z_g\kappa \tag{6.8}$$

where z_g is the distance from the plate plane to the plane about which the stiffened plate is bending.

The plate membrane energy is:

$$U_m^p = \frac{E}{2(1-\nu^2)}\int_{V_p}(\varepsilon_x^2+\varepsilon_y^2+2\nu\varepsilon_x\varepsilon_y+\frac{1-\nu}{2}\gamma_{xy}^2)dV_p \quad (6.9)$$

$$= U^D + U^F + U^\kappa \quad (6.10)$$

The new term here compared to earlier is the part involving κ which becomes:

$$U_\kappa^s = 2Ez_g^2\kappa^2bta - 4Ez_g\kappa\varepsilon^{F,p}bta \quad (6.11)$$

For the stiffener, the modified membrane strain in position z is:

$$\varepsilon_x = \varepsilon^{D,s} + \varepsilon^{F,s} + (z-z_g)\kappa \quad (6.12)$$

The stiffener membrane energy is

$$U_m^s = \frac{E}{2}\int_{V_s}\varepsilon_x^2 dV_s \quad (6.13)$$

$$= U^A + U^F + U^\kappa \quad (6.14)$$

where the new contribution due to κ is

$$U_\kappa^s = \frac{E}{2}(z-z_g)^2\kappa^2V_s + \kappa E\int_{V_s}\varepsilon^D(z-z_g)dV_s + \kappa E\varepsilon^F\int_{V_s}(z-z_g)dV_s \quad (6.15)$$

The contribution from external energy is the same as before, since the κ-terms disappear upon differentiation with respect to A_{fg}.

6.1.2 Bending moment

The plate bending moment when the global curvature is included is:

$$M^p = z_g t\int_b \sigma_x dy \quad (6.16)$$

$$= -2z_g bt\sigma^F + 2Ez_g^2bt\kappa \quad (6.17)$$

The contribution due to σ^D is zero when integrated over the plate area. The stiffener bending moment is:

$$M^s = 2t_w E\int_h (z-z_g)\sigma_x(z)dz + b_f t_f E(h-z_g)\sigma_x(z=h) \tag{6.18}$$

$$= 2t_w\kappa E(\frac{h^3}{3} - z_g h^2 + z_g^2 h) + 2b_f t_f \kappa E(h-z_g)^2 \tag{6.19}$$

$$+ 2t_w\sigma^f(\frac{h^2}{2} - z_g h) + 2b_f t_f \sigma^f(h-z_g) \tag{6.20}$$

The contribution from $\sigma^{D,s}$ is zero at the midspan.

6.1.3 Solving the equation system

Including κ in the local equilibrium equations lead to a system of equations on the form:

$$\mathbf{K}_{11}\dot{\mathbf{A}} + \mathbf{K}_{12}\dot{\kappa} + \mathbf{G}_1\dot{\Lambda} = \mathbf{0} \tag{6.21}$$

The moment equilibrium equation can be written

$$\mathbf{K}_{21}\dot{\mathbf{A}} + \mathbf{K}_{22}\dot{\kappa} + \mathbf{G}_2\dot{\Lambda} = \mathbf{0} \tag{6.22}$$

Assembling the above equations, an equation system with equal number of equations and unknowns is obtained, and the rates $\dot{A}_{mn}$ and $\dot{\kappa}$ are solved for simultaneously.

6.1.4 Results

One case is presented as an example of how local and global buckling may interact for a slender panel, Fig. 6.2. This is the aluminium stiffener used for comparison in chapter 4, which is quite weak with respect to global buckling. It is seen that the overall capacity is smaller than the pure global strength, due to the effect of local deformations.

This example show that interaction effects may be important for panels with weak stiffeners. However, the model presented here is not very well suited for analysis of stiffened panels. One reason is that lateral support provided by longitudinal girders at the edges of the stiffened panel are not accounted for. This may have a significant stiffening effect in the postbuckling region. Another reason is that the single stiffened plate model is not well suited for analysis of transverse in-plane compression. Therefore, a more appropriate stiffened panel model is developed in the next section.

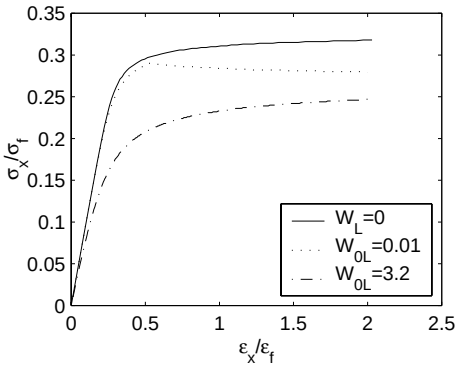

Figure 6.2: Load-average strain response due to pure global buckling ($w_L = 0$) and combined local and global buckling for stiffened aluminium plate subjected to axial compression

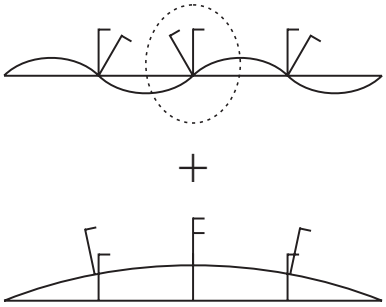

Figure 6.3: Combined local and global buckling model

6.2 Coupled local and global buckling for a stiffened panel

The local buckling model presented in section 4.1 for open profiles is used as the basis also for the model of a stiffened panel including several stiffeners. The model developed in the following is also presented in (Byklum and Amdahl 2002a).

The local deflection is assumed to be the same for all stiffeners in the panel, Fig. 6.3. That means that potential energy for one stiffened plate may be multiplied to represent the whole panel. If different deflection shapes were to be included for each stiffener, the total number of degrees of freedom would be too large for efficient solution of the problem.

Global deflection is added to the local. The global deformation is represented by a Fourier series, but in order to limit the number of unknowns in the model it is assumed that one global degree of freedom is sufficient to represen tthe global deflection. The number of degrees of freedom can be reduced to one by determining the deflection shape beforehand using linear theory, and let only the amplitude of the deflection be the unknown in the nonlinear analysis. This approach is justified by the design-philosophy that local buckling is acceptable, but large lateral deflection of the stiffeners should not occur. For moderate global deflection, the linear global eigenmode of the panel is a good approximation of the actual deformation shape also in the nonlinear region. The global deflection shape used is therefore

$$w^g = A_g \sum_{m=1}^{M_g} \sum_{n=1}^{N_g} k_{mn} \sin(\frac{m\pi x}{a}) \sin(\frac{n\pi y}{B}) \tag{6.23}$$

$$w_0^g = B_g \sum_{m=1}^{M_g} \sum_{n=1}^{N_g} k_{mn} \sin(\frac{m\pi x}{a}) \sin(\frac{n\pi y}{B}) \tag{6.24}$$

B is the breadth of the whole panel, in contrast to b which is the stiffener spacing. The deflection amplitude A_g is the global degree of freedom, while the coefficients k_{mn} defines the deflection shape. They are determined at the start of the analysis by calculation of the linear eigenmode. For this purpose, the stiffened panel is treated as a geometrically orthotropic plate. This is similar to the model presented in chapter 5, but for the eigenmode calculation, initial stiffness coefficients are used. This is because the global deflection shape is assumed to be constant.

The additional potential energy due to the global deflection causes an interaction between the local and the global deflection, which gives coupling terms in the stiffness matrix. This effect cannot be correctly included for a continuous stiffener, because the interaction will be different for stiffener-induced buckling and for plate-induced buckling. For global buckling, stiffener-induced means deflection towards the plate, while plate-induced means deflection towards the stiffener. If the deflection is stiffener-induced in one span, it is usually plate-induced in the next span. The interaction with the local deflection is therefore different in two consecutive spans, and this cannot be properly represented by a single set of continuous deflection functions.

The problem is simplified by using the same coupling effect for the span (0 to a) as for (a to $2a$). This is a conservative assumption, since it gives larger interaction and therefore larger resulting deflection. For moderate amounts of global deflection, it is believed that this approximation will not introduce large errors.

6.2.1 Global bending

Global deflection leads to additional membrane strain in the plate and stiffeners. This effect is referred to as global bending, although the strain is of the membrane type. This is to distinguish it from the effect of membrane stretching of the panel due to global deformation, which is considered in the next section.

The membrane strain due to global bending is

$$\varepsilon_b^g = (z - z_g) w^g_{,xx} \tag{6.25}$$

The bending energy due to global deflection is calculated for the stiffeners and the plating separately . This is more correct than to multiply the energy for one stiffened plate with the total number of stiffeners. The reason is that the total panel breadth is usually larger than the sum of plating associated to each stiffener: $B = (n_s+1)b$, where n_s is the n unber of stiffeners in the panel.

The bending energy for a stiffener located at $y = y_s$ is

$$U_b^{s,g}(y_s) = \frac{1}{2} E I_s \int_0^{2a} w^g_{,xx}(y_s) dx \tag{6.26}$$

where I_s is the moment of inertia of the stiffener without plating, and the integration is over the length of the stiffener. The total global energy is calculated by performing the integration and summing over all stiffeners. The result is given in appendix D.

The bending energy for the plating due to global deflection is calculated as:

$$U_b^{p,g} = \frac{D}{2} \int_0^{2a} \int_0^{2B} \left[(w^g_{,xx} + w^g_{,yy})^2 - 2(1-\nu)(w^g_{,xx} w^g_{,yy} - (w^g_{,xy})^2) \right] dy dx \tag{6.27}$$

The result is given in appendix D.

6.2.2 Global membrane stretching

For calculation of the global membrane effect in the stiffeners and plating, an average strain approach is used. The exact strain distribution is difficult to calculate for the plate and stiffeners in combination, but average strains can be calculated by requiring overall equilibrium for the stiffener and the plate.

The membrane strain $\varepsilon_x(x,y)$ averaged over the length of the plate is:

$$\begin{aligned}\varepsilon_x^{av}(y) &= \frac{1}{a}\int_a \varepsilon_x dx && (6.28)\\ &= \frac{1}{a}\int_a (u_x + \frac{1}{2}w_{,x}^2 + w_{,x}w_{0,x})dx && (6.29)\\ &= \frac{\Delta u}{a} + \frac{1}{a}\int_a (\frac{1}{2}w_{,x}^2 + w_{,x}w_{0,x})dx && (6.30)\end{aligned}$$

Similarly, the membrane strain $\varepsilon_y(x,y)$ averaged over the width of the plate is:

$$\begin{aligned}\varepsilon_y^{av}(x) &= \frac{1}{B}\int_B \varepsilon_y dy && (6.31)\\ &= \frac{1}{B}\int_B (v_y + \frac{1}{2}w_{,y}^2 + w_{,y}w_{0,y})dy && (6.32)\\ &= \frac{\Delta v}{B} + \frac{1}{B}\int_B (\frac{1}{2}w_{,y}^2 + w_{,y}w_{0,y})dy && (6.33)\end{aligned}$$

The elongations Δu and Δv are calculated by requiring that the membrane strain integrated over the whole stiffened panel must be zero, in order to fulfill static equilibrium:

$$\int_V \varepsilon_x dV = 0 \quad (6.34)$$

$$\int_V \varepsilon_y dV = 0 \quad (6.35)$$

For the axial strain, this gives:

$$t\int_0^B \varepsilon_x^{av}(y)dy + A_s\sum_{N_s}\varepsilon_x^{av}(y_s) = 0 \quad (6.36)$$

Rearranging, the axial elongation becomes

$$\Delta u = \frac{-\pi^2(A_g^2 + 2A_gB_g)(tI_3 + A_s\sum_{N_s} I_1(y_s))}{2a^2(Bt + N_sA_s)} \quad (6.37)$$

while the average axial strain becomes:

$$\varepsilon_x^{av}(y) = \frac{\Delta u}{a} + \frac{1}{2a}(\frac{\Pi}{a})^2(A_g^2 + 2A_gB_g)I_1(y) \quad (6.38)$$

The integration constants I_1 and I_3 are given in appendix D.

For the transverse strain, we have:

$$t\int_0^a \varepsilon_x^{av}(y)dx = 0 \tag{6.39}$$

The transverse elongation is

$$\Delta v = -\frac{1}{2a}(\frac{\pi}{B})^2 I_7(A_g^2 + 2A_gB_g)2a^2(Bt + N_sA_s) \tag{6.40}$$

while the average transverse strain becomes:

$$\varepsilon_y^{av}(x) = \frac{\Delta v}{B} + \frac{1}{2B}(\frac{\pi}{B})^2(A_g^2 + 2A_gB_g)I_5(x) \tag{6.41}$$

The global membrane energy for the plate is:

$$U_m^p = \frac{Et}{2}\int_0^{2a}\int_0^{2B}(\varepsilon_x^2 + \varepsilon_y^2)dxdy \tag{6.42}$$

The coupling term between the axial and transverse membrane strain vanishes when integrating over the plate area.

The global membrane energy for the stiffener is:

$$U_m^s = 2aEA_s\sum_{N_s}\varepsilon_x^2 \tag{6.43}$$

The final expressions are given in appendix D.

6.2.3 Coupling between local and global buckling

There are two possible coupling effects between the local and the global deflection. The first one is between the local membrane strain and the global membrane strain. The importance of this coupling is investigated by considering that the plate usually deflects locally with a short wavelength compared to the global deflection. By looking at the membrane stiffness matrix for the unstiffened plate, it is found that the coupling stiffness between short-wave deflection and long-wave deflection is small. Considering also that the global membrane strain effect is usually moderate compared to the global bending effect, it is decided to neglected this stiffness contribution.

The coupling effect between the global bending strain and the local membrane strain is believed to be more significant, and is therefore included in the model.

The potential energy due to this coupling is:

$$U^{cp} = E\varepsilon^{p,F}\int_{V_p}\varepsilon^g dV + E\sum_{N_s}\varepsilon^{s,F}\int_{V_s}\varepsilon^g dV + E\sum_{N_s}\int_{V_s}\varepsilon^{s,D}\varepsilon^g dV \tag{6.44}$$

The contribution from $\varepsilon^{p,D}$ vanishes upon integration. The resulting expressions are given in appendix D.

6.2.4 Global potential of external loads

The global external energy due to in-plane compression is calculated using the elongations derived in previous sections:

$$T_c = 2S_x(Bt + N_sA_s)\Delta u + 2S_y at\Delta v \tag{6.45}$$

The global external energy due to shear force and lateral pressure is calculated as for an unstiffened plate, only using the global displacement function instead of the plate displacement functions. Resulting expressions are given in appendix D.

6.2.5 Results

Analyses are performed with the proposed model for two quite different stiffened panels, and comparisons are made with ABAQUS for verification. The panels are full-width versions of the local stiffened plates considered in chapter 4. The first one is the typical steel panel with angle profiles, Table 4.1, and the second one is the slender aluminium panel with quite small tee profiles, Table 4.2. For both panels three stiffeners are included. Imperfections are taken according to the DNV Classification Note (Det Norske Veritas 1995), so that the local plate tolerance is $0.05b$, the local stiffener tilt is $0.0015a$, and the global initial deflection is $0.0015a$.

For the ABAQUS analyses, one panel width is modelled in the transverse direction, while (1/2+1+1/2) stiffener spans are modelled in the longitudinal direction, Fig. 6.4. Simply supported boundary conditions are applied on the longitudinal edges, while symmetry conditions are applied on the transverse edges. All edges are free to move in-plane, but forced to remain straight.

Load-elongation curves are presented for both panels for axial load and transverse load, Fig. 6.5 and Fig. 6.6. It is seen that the agreement is good.

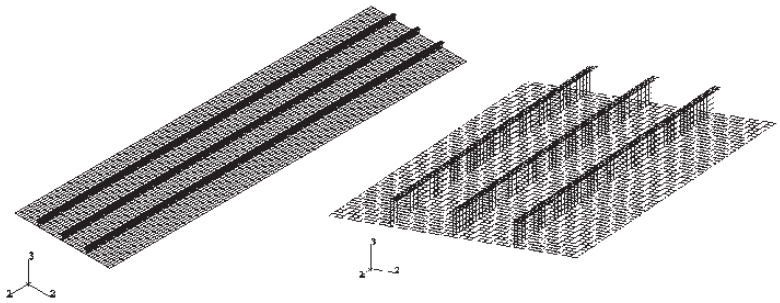

Figure 6.4: ABAQUS models of aluminium panel (left) and steel panel (right)

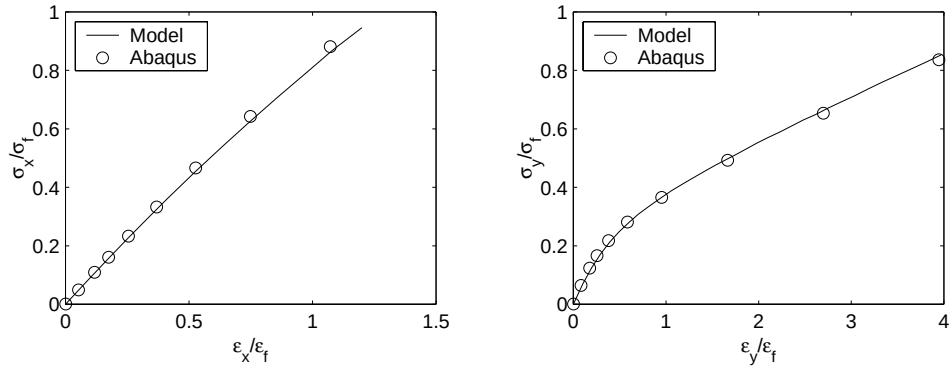

Figure 6.5: Steel angle bar under axial loading (left) and transverse loading (right)

The resulting deflection shapes for the two panels are quite different. The steel stiffeners are heavy, and the deformations are almost purely local. The aluminium stiffeners are weak, and global deformation is significant. For axial load it is dominating, as seen in Fig. 6.7. This indicates that the proposed model works well both for panels with heavy and with weak stiffeners.

The model developed here is now compared with the models presented in the previous chapters. The response calculated from the coupled model is compared with the results calculated using the local model from section 4.1 alone, and the local model combined with the global model from chapter 5. To the left in Fig. 6.8 it is seen that the pure local response coincides with the coupled response for the steel panel under axial loading. The global response is negligible. To the right, it is seen that the pure local response is lower than the total response for the aluminium panel under axial loading. The response found

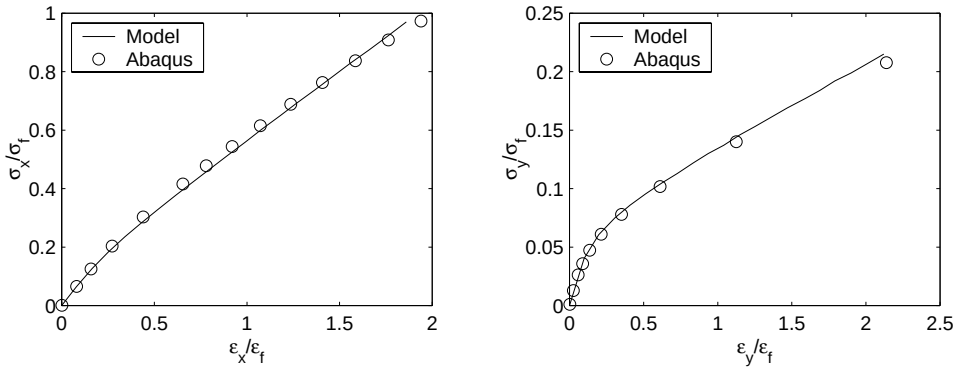

Figure 6.6: Aluminium tee bar under axial loading (left) and transverse loading (right)

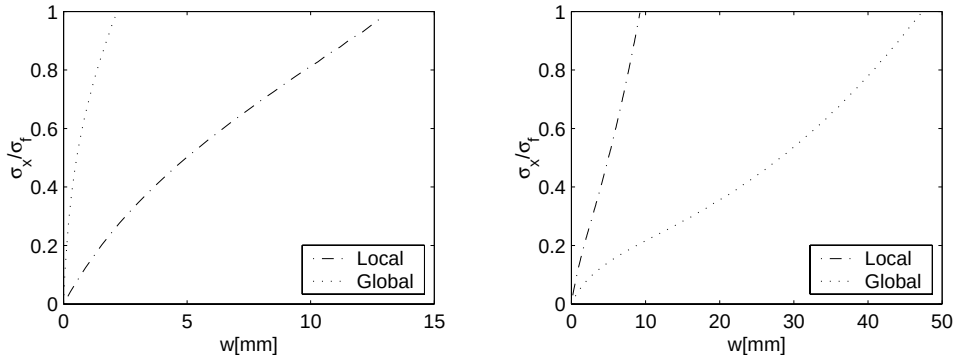

Figure 6.7: Comparison between lateral deflection in the local mode and the global mode for steel angle bar panel (left) and aluminium tee bar panel (right) under axial loading

by adding the local response and the global response is quite close to the response from the coupled model, and both agree well with ABAQUS.

It is interesting to see that the response is well predicted by performing separate local and global analyses, even for the aluminium panel in axial loading where both deflection modes are important. The interaction between the two modes may be further investigated by setting the coupling terms in the stiffness matrix in the coupled model equal to zero. For the steel panel, where the global deflection is small, the interaction is also small as expected. The aluminium panel is a more interesting case, since the eigenvalues for local and global buckling are closer to each other. Comparison of the deflection using the presented formulations and a formulation without coupling is shown in Fig. 6.9. It is seen

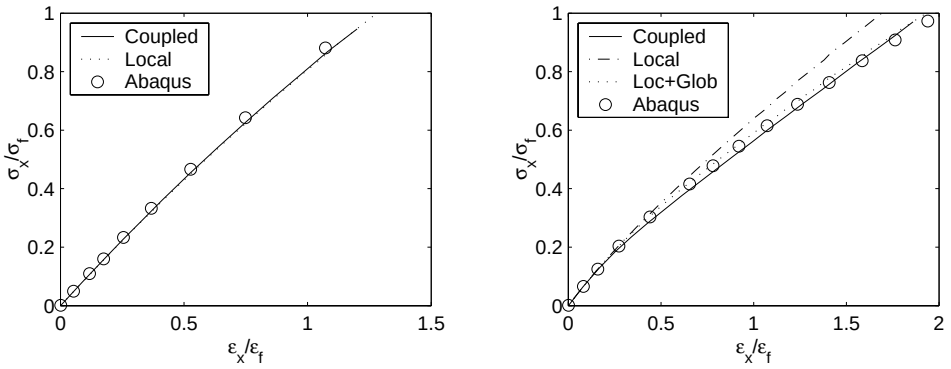

Figure 6.8: Comparison between pure local response and coupled local and global response for the steel angle bar panel (left) and the aluminium tee bar panel (right) under axial loading

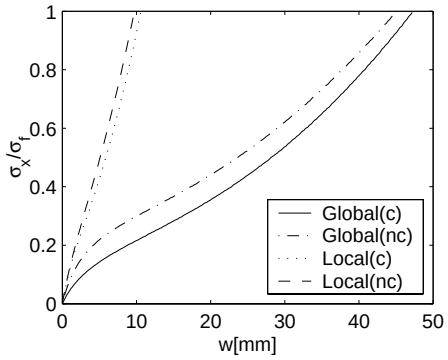

Figure 6.9: Comparison between lateral deflection in the local mode and the global mode for aluminium tee bar using the coupled formulation (c) and the uncoupled formulation (nc)

that both the local and the global deflection are smaller when the coupling is not accounted for, as expected. However, the effect is much larger for the global deflection than for the local. This suggests that even for this panel it may be sufficient to use a kind of one-way interaction, as presented in chapter 4 and 5, i.e. the effect of local deflection on the global deflection is accounted for, but not the opposite.

Although the coupled model presented in this chapter is more consistent than treating global and local deflection separately, the latter approach has several advantages. First, it

is possible to use more degrees of freedom also in the global analysis. This may sometimes be necessary when the applied load condition is such that the deflection shape may change significantly during the analysis, e.g. when lateral pressure is applied. Second, it is easier to refine the model to handle linearly varying edge loads. Finally, it is possible to have different types of local models, e.g. one for open profiles and one for closed profiles, but to use the same global model.

Chapter 7

Estimation of ultimate limit state

There are several possible applications of the computational models presented in the previous chapters. One field of application is deflection analyses of plates or stiffened panels for servicability limit state checks. Another application could be to use the derived stiffness coefficients for each panel as input to a larger structural analysis, e.g. a ship hull girder cross section. This would be very useful for determining how the forces redistribute over the cross section due to buckling of individual panels.

In the current work the aim is to develop a design tool that can estimate the ultimate limit state for individual stiffened panels. This is done by combining the elastic models with appropriate limit state criteria. Here, first yield due to membrane stress is taken as the design capacity, as described in the following. Several of the models developed in the current work have been implemented in the Det Norske Veritas computer code PULS, and some examples produced by this computer code are therefore presented.

7.1 PULS

7.1.1 Description

PULS (Panel Ultimate Limit State), (Det Norske Veritas 2002b), is a new buckling code which is currently being implemented at DNV. It is based on a direct calculation approach,

and will form a new standard for buckling strength assessment in DNV. PULS consists partly of formulations and computer code developed in the current work, and some results obtained using PULS will therefore be presented as examples of application of the proposed methods. The examples are produced using version 1.3 of the program, released May 2002. The program is going through a continuous development, and some of the results may therefore deviate somewhat from results from the later versions.

Among the unstiffened plate models presented in chapter 3, the simply supported, isotropic elastic model has been implemented in PULS. In addition, the local stiffener model presented in chapter 4 for open profiles has been implemented. The hat profile model is considered for implementation at a later time, while the nonlinear global model presented in chapter 5 is being implemented at the time of writing. The coupled models presented in chapter 6 has not been considered for PULS implementation, since the simpler approach of using reduced stiffness coefficients from the local analysis as input to the global analysis gives satisfactory results.

The graphical user interface implemented in PULS makes it an intuitive and easy to use calculation tool, Fig. 7.1. The input is much easier, and the pitfalls are fewer, than what is the case when using a nonlinear FEM code. The output from PULS is much more instructive than ordinary buckling codes, because of the possibility to display stress patterns and displacement shapes, in addition to the usual ultimate limit state value.

7.1.2 Imperfections

An important decision to make when performing nonlinear analyses, whether it is by NFEM or analytical methods, is the choice of imperfections. Both the shape and the amplitude of the initial deflection may have a large effect on the resulting response. This is a considerable complication compared to standard code formulations, where imperfection effects are implicitly accounted for by empirical factors.

If the actual imperfection for a plate is known, it can be included directly by calculating the Fourier coefficients and using these as input to the analysis. In design, however, the imperfections are not known. A common strategy has been to calculate the first linear eigenmode for the actual load case, and use this as the imperfection shape. The amplitude can be taken according to tolerance limits defined in rules and regulations. This approach has been assumed to give a lower bound for the collapse strength.

Investigations have shown, however, that the first eigenmode does not always give the lowest ultimate limit state, (Featherston 2000). For thin plates, where the eigenvalue is low compared to the collapse load, the postbuckling range becomes more important relative to the prebuckling range. For such cases, the preferred deflection mode in the postbukling range may be different from the eigenmode, and the use of the eigenmode as imperfection

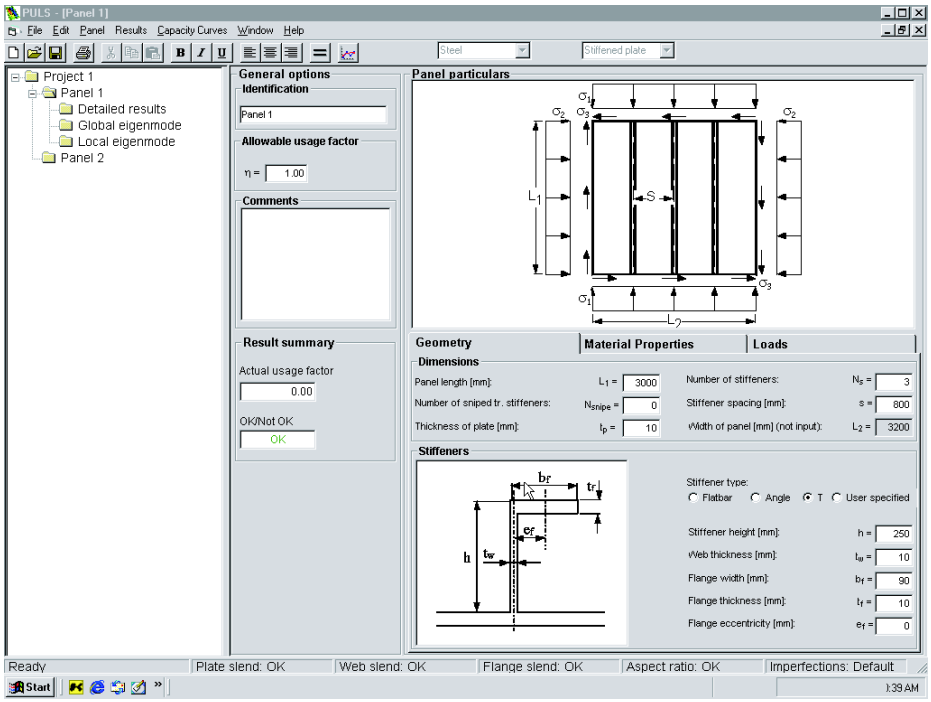

Figure 7.1: PULS user interface

shape can be unconservative. For axial load, it is typical that the plate prefers to deflect in a more short-wave pattern in the postbuckling range than in the prebuckling range. For instance, if the eigenmode for axial load has three half-waves, defining the imperfection with four half-waves may give a lower collapse load.

On the other hand, applying imperfections with a large number of half-waves may underestimate the strength significantly, since this type of imperfection shape may be unrealistic compared to what is the typical shape in real structures. Even if one plate has an unfavorable imperfection shape, it is part of an integrated structure where the other plates are likely to have imperfections that are more favorable with respect to strength. Therefore, force will be redistributed from weak plates to stronger plates.

Imperfection sensitivity is a topic which needs more attention, and is not further discussed here. In PULS, the imperfection level may be adjusted by the user, but default values are suggested. These are 1/200 of the stiffener spacing for plate deflection between stiffeners, and 1/1000 of the stiffener span for stiffener tilt and global imperfection. The minimum eigenmodes are used to define the imperfection shape. The imperfections for local plate

deflection and stiffener tilt are defined by scaling the local eigenmode, while the global imperfection is defined by scaling the global eigenmode. The default levels are a little below standard shipbuilding tolerances, reflecting that the eigenmode is an unrealistic and conservative deflection shape compared to the imperfections found in real plates.

7.1.3 Limit state criteria

A first yield approach is used for estimation of the collapse load. First yield has often been applied to assess the critical load in design formulations, such as in the DNV Classification Note 30.1 for Buckling Strength Analysis, (Det Norske Veritas 1995). In the Classification Note, a column model is used together with a first yield criterion. This is commonly referred to as the Perry-Robertson approach, and has been widely used in design.

First yield is a sound design criterion, because yielding will give unwanted permanent deformations in the structure, and it is questionable to utilize the strength reserves in the plastic region at the design stage. There are different ways to define the collapse criterion. First yield in an extreme fiber is usually a quite conservative criterion, since redistribution of stress through the thickness gives additional capacity. A more appropriate criterion is to use yielding in the middle of the plate, i.e. membrane stress yielding, since this indicates that the cross-sectional capacity is exceeded, and further increase in the load must be carried by stress redistribution in the plate plane.

Comparison with ABAQUS shows that this strategy gives satisfactory results for most practical cases. For thin plates the membrane stress will redistribute in the plate plane after first membrane yield, so that some post-yield capacity exists. One way to account for some of the reserve capacity after the onset of yielding, is the approach used by for instance (Paik, Thayamballi, Lee, and Kang 2001) for unstiffened plates. The plate is then divided into a mesh, considered to consist of several fibers. When yielding starts in the outer fibers, they loose their strength, and the total stiffness is reduced accordingly. Yielding will then spread to more and more fibers, until the panel collapses. In this way, the panel may be able to sustain some additional loading after the first yield.

For thicker plates the bending stress becomes increasingly more important, and the capacity of a cross section may then be exceeded before the membrane stress reaches yield. For such cases the ULS estimates obtained using a membrane stress criterion alone may be higher than those obtained from nonlinear FEM. The membrane stress criterion can be combined with a bending moment capacity criterion, using an interaction formulae for the combined bending/membrane action. In the current version of PULS however, a pure membrane stress criterion is applied. This is considered to be safe, since the imperfection pattern used in the analyses are quite conservative compared to a more realistic imperfection pattern. The imperfection shape applied has a very regular up-down-pattern in the transverse direction, while real ship panels are much more likely to be much more random.

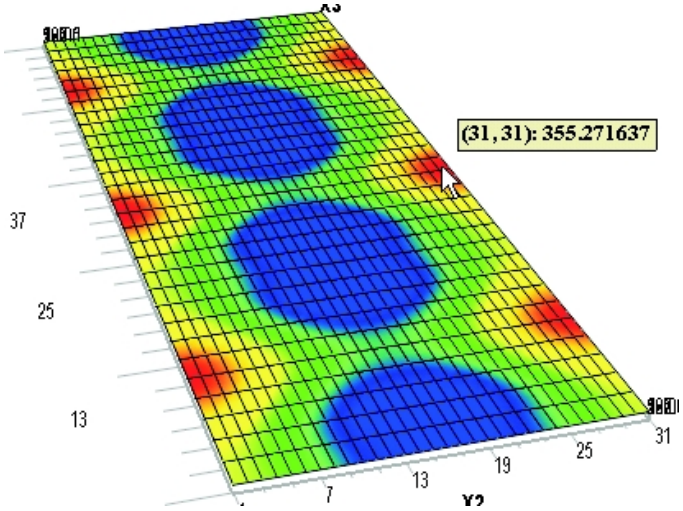

Figure 7.2: von Mises membrane stress distribution from PULS for 3.0x1.0x0.01m plate ($\beta = 4.1$) subjected to axial load

In addition, the rotational restraint from the transverse girders is neglected in the analyses, which may have a significant effect on the transverse load cases where the stresses are very localized around the transverse supports. It is therefore believed that the real strength of actual ship panels is higher than the ULS values obtained with ABAQUS.

7.2 Results

7.2.1 Unstiffened plates

An example of unstiffened plate analysis using PULS is presented. The plate analysed is 3.0x1.0x0.01m, with E=20800MPa and σ_f=355MPa. The applied load is pure axial compression. The von Mises membrane stress distribution at the defined ULS is shown in Fig. 7.2. The cursor on this plot is pointing on the point with maximum equivalent membrane stress, which has just reached the yield stress.

Fig. 7.3 shows the minimum eigenmode for the same plate under a combination of transverse compression, S_y=20MPa, and shear stress, S_{xy}=100MPa. Fig. 7.4 shows the deflection shape at the ultimate limit state. This deflection shape is quite different from the eigenmode, which shows the importance of the nonlinear membrane effect in the postbuck-

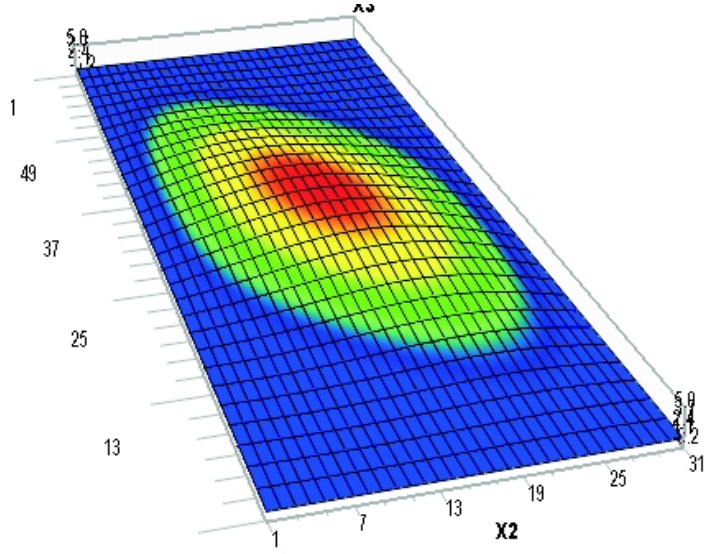

Figure 7.3: Minimum eigenmode from PULS for 3.0x1.0x0.01m plate ($\beta = 4.1$) subjected to transverse compression and shear load

ling region. The eigenmode is here clearly not the preferred deflection shape for the plate in the postbuckling region.

Some ultimate limit state analyses are carried out with ABAQUS for comparison with the PULS estimates. The ABAQUS analyses are performed with linear elastic, hardening plastic material, and the ULS values are the maximum loads attained from the load-response curves. The PULS estimates are based on a limit state definition in the form of a first yield criterion, as explained in the previous section.

Results are presented for plates with three different aspect ratios. The first is a 810x810mm plate, Fig. 7.5, the second a 2430x810mm plate, Fig. 7.6, and the third a 4050x810mm plate, Fig. 7.7. For all plates, the thicknesses 8mm and 12mm have been considered. The yield stress is taken as 315MPa and the elastic modulus as 206000MPa. For the ABAQUS analyses, a hardening parameter of 1000MPa is used. Since PULS is intended as a ship design tool, the buckling criteria in the current DNV Rules for Ships are also included for comparison.

It is seen that the PULS ULS estimates compare reasonably well with the ABAQUS results, and much better than the Ship Rules. However, for predominantly transverse loading, some of the PULS estimates are higher than the ABAQUS results. This is because PULS only considers membrane stresses in the limit state criteria, as discussed in the previous section.

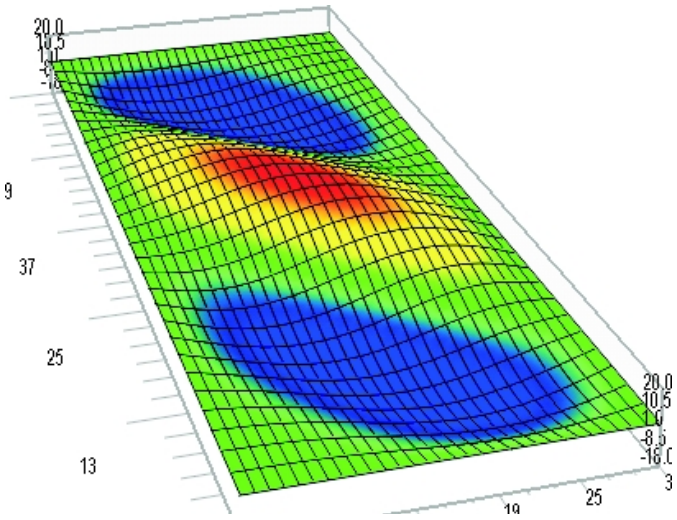

Figure 7.4: Final deflection shape from PULS for 3.0x1.0x0.01m plate ($\beta = 4.1$) subjected to transverse compression and shear load

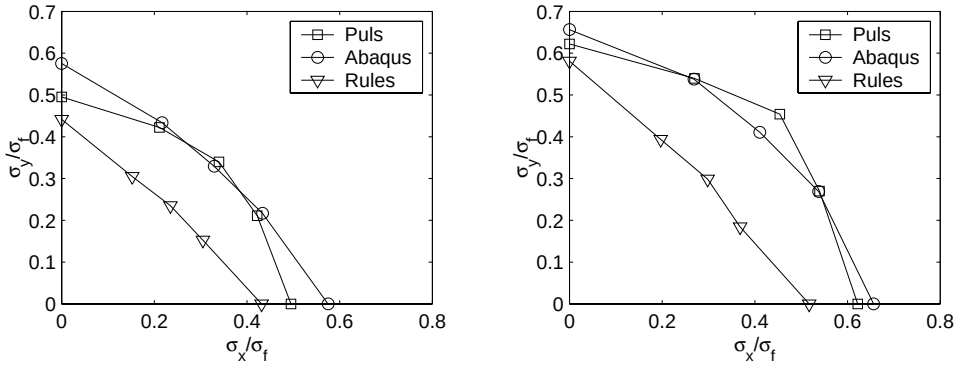

Figure 7.5: Biaxial interaction curves from PULS, ABAQUS, and the Ship Rules for 810x810mm plate with t=8mm, $\beta = 3.9$ (left), and t=12mm, $\beta = 2.6$ (righ t)

F or transverse loading, large bending stresses develop in the plate, and collapse may occur before yield due to membrane stress is reached.

For the 4050x810mm plate there is another source of discrepancy. V ersion 1.3of PULS applies 7x7 terms in the displacement shape. F or plates with such a high aspect ratio, it is

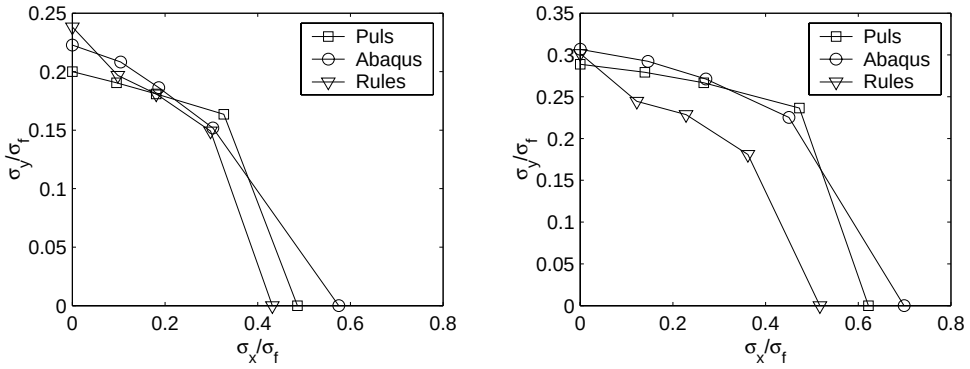

Figure 7.6: Biaxial interaction curves from PULS, ABAQUS, and the Ship Rules for 2430x810mm plate with t=8mm, $\beta = 3.9$ (left), and t=12mm, $\beta = 2.6$ (right)

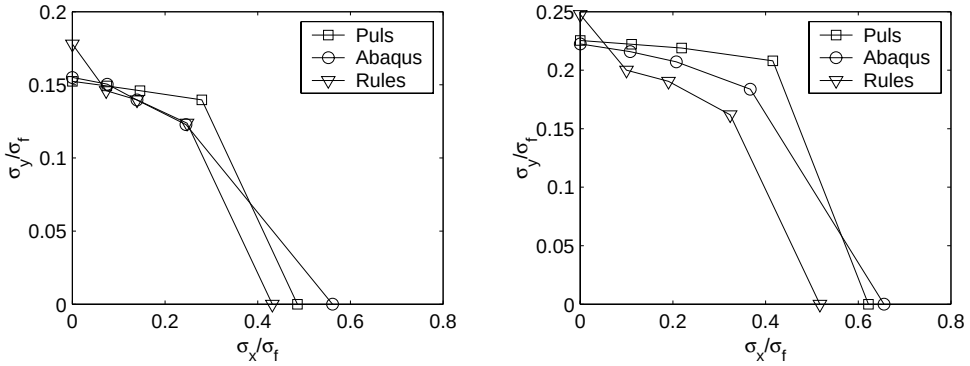

Figure 7.7: Biaxial interaction curves from PULS, ABAQUS, and the Ship Rules for 4050x810mm plate with t=8mm, $\beta = 3.9$ (left), and t=12mm, $\beta = 2.6$ (right)

sometimes necessary to have more terms in the longitudinal direction in order to represent the displacement shape correctly. If the number of terms is too small, the calculated response is too stiff and the ULS estimate is too optimistic. In version 1.4 of PULS, released in September 2002, the number of displacement shape terms is increased.

7.2.2 Buckling of stiffened panels using PULS: Current version

The stiffened plate model in version 1.3 of PULS is based on the local model presented in section 4.1, combined with a linear, global eigenvalue calculation. The local analysis is performed first, and a set of reduced stiffness coefficients are calculated at the instant when yielding due to local deflection starts. The calculated reduced bending stiffness is used for the global eigen value calculation,where the stiffened panel is treated as an orthotropic plate. The eigenvalue is used to calculate the displacements due to global buckling effects as:

$$\xi_1 = \frac{\Lambda}{\Lambda_E - \Lambda}\xi_{10} \tag{7.1}$$

where Λ_E is the eigen valueload factor, Λ is the curren tload factor, ξ_1 is the curren t dimensionless global displacement amplitude, and ξ_{10} is the initial dimensionless global displacement amplitude. Knowing the global displacement shape, the maximum curvature of the panel can be calculated for eac h load lev el. The global stress is giv en from the curvature. The local membrane stress is then calculated for the same load lev el using the in-plane stiffness coefficients. The local stress is added to the global, and the sum is checked against the yield stress. The load factor is then increased until yield is reached.

Interaction curves may be produced in PULS for all load combinations of axial load, transverse load and shear force. The interaction curves are plotted together with eigenvalues for local and global buckling. As an example, an interaction curve for biaxial loading is produced for a stiffened steel panel consisting of three stiffeners, Fig. 7.8. The plate and stiffener dimensions are as for the angle bar analysed in section 4.1, see Table 4.1. It is seen that curv es areplotted for local elastic buckling and for ULS. Global elastic buckling is normally also included, but for this case the global buckling values are so high that they are outside the plotting range. The points on the ULS curve are marked with Limitstate 1-5 in order to indicate the location in the panel where yielding starts. Limitstate 1 refers to yielding in the plate corner, Limitstate 2 refers to yielding at the stiffener flange (tension), Limitstate 3 refers to yielding at the plate/stiffener connection (compression), Limitstate 4 refers to yielding at the stiffener flange (compression), and Limitstate 5 refers to yielding at the plate/stiffener connection (tension).

Some ULS analyses have been performed with ABAQUS for comparison. The first case is a panel with three of the steel angle bar stiffeners analysed in section 4.1, see Table 4.1. The results for this case is shown in Fig. 7.9. It is seen that the correspondence between the PULS results and the ABAQUS results is good. The PULS results are conservative for pure axial load and for pure transv erse load, while they are a little higher than the ABAQUS results for the biaxial load cases. The DNV Ship Rules are also plotted for comparison. It should be noted that the Ship Rules does only have buc kling formulations for stiffeners in the case of pure axial load. The other points on the interaction curve are therefore based on the formulations for unstiffened plates.

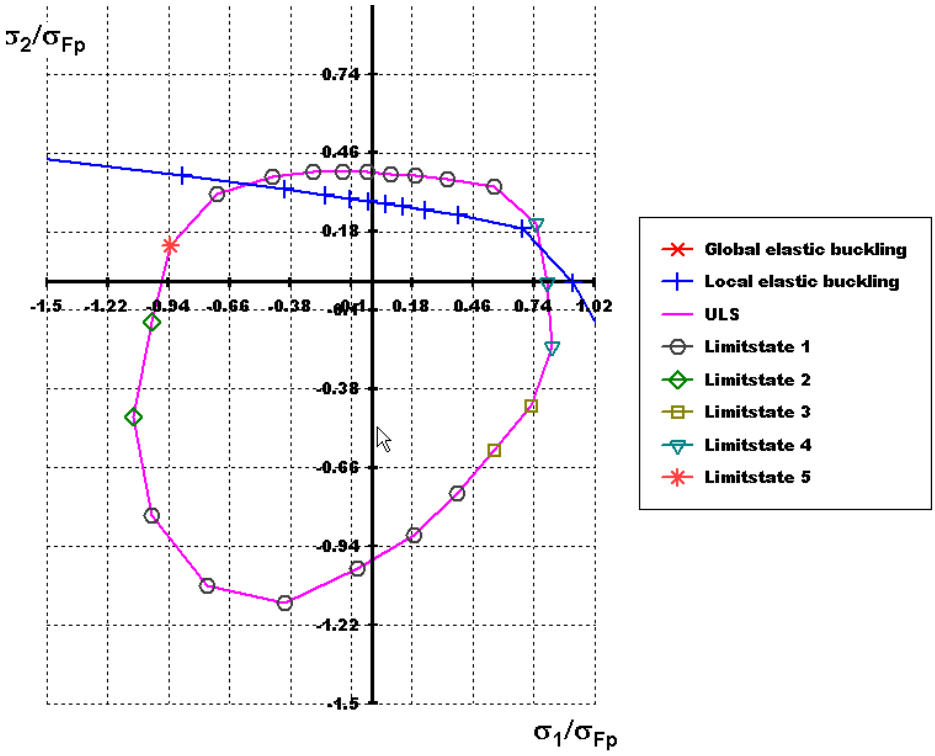

Figure 7.8: Interaction curve for biaxial loading for flatbar steel panel

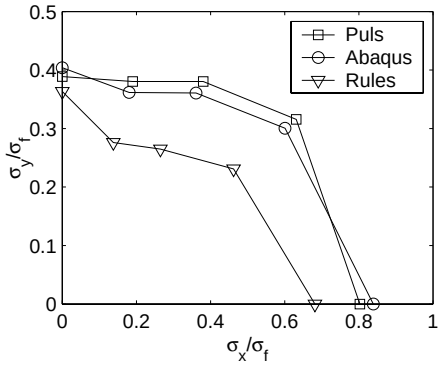

Figure 7.9: Biaxial interaction curves from PULS, ABAQUS, and the Ship Rules for steel angle bar panel

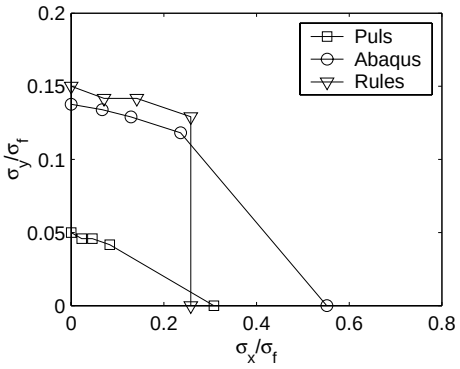

Figure 7.10: Biaxial interaction curves from PULS, ABAQUS, and the Ship Rules for aluminium panel

The second case is a panel with three of the aluminium tee bar stiffeners analysed in section 4.1, Table 4.2. The results for this case is shown in Fig. 7.10. This panel has weak stiffeners, and global deflection is important. It is seen that PULS significantly underestimates the ultimate strength of the panel. This is due to the linear global model, which neglects second order effects on the global level. Results using the nonlinear global model presented in chapter 5 are given in the next subsection.

Some analyses performed at DNV for three different tankers are also included. These cases are selected from three actual ships that are considered to be representative for stiffened panels in the bottom of tankers, and are therefore of particular interest. The geometry and the material parameters for the three panels are given in Table 7.1. For all cases, the elastic modulus is taken as E=206000MPa. For case 3 and 4, the two yield stresses given in the table are for the plate and the stiffener, respectively. The number of stiffeners in these two panels is 16, but this number is reduced to 9 in the ABAQUS analyses in order to limit the computational cost. This should not affect the results much. For case 5 and 6, the stiffener is of the Holland Profile (HP) type, which means that the flange is a bulb. These are modelled in PULS and ABAQUS as L-profiles with equivalent cross-section area and moment of inertia. For all analyses, the imperfections are defined as explained in subsection 7.1.2, both for the ABAQUS analyses and the PULS analyses.

The results for case 1 and 2 are shown in Fig. 7.11, the results for case 3 and 4 are shown in Fig. 7.12, and the results for case 5 and 6 is shown in Fig. 7.13. It is seen that the agreement is quite good for axial load, while the capacity in the biaxial range is somewhat overestimated for the thick plate cases 1-4. For case 5 and 6, where the plate thickness is moderate, the agreement is very good in the whole biaxial range. As already pointed out, the deviation in the biaxial range for the thick plates is due to the effect of large bending

T able 7.1: Dimensions for tanker cases

	a[m]	b[m]	B[m]	N_s	Bar	t[m]	h[m]	t_w[m]	b_f[m]	t_f[m]	σ_f[MPa]
1	5.12	0.91	9.1	9	L	0.020	0.5985	0.012	0.200	0.020	315
2	5.12	0.91	9.1	9	L	0.022	0.5985	0.012	0.200	0.020	315
3	3.92	0.82	8.2	16	L	0.017	0.400	0.013	0.100	0.018	235/315
4	3.92	0.82	8.2	16	L	0.019	0.400	0.013	0.100	0.018	235/315
5	2.4	0.80	5.6	6	HP	0.0135	0.240	0.011			355
6	2.4	0.80	5.6	6	HP	0.0145	0.240	0.011			355

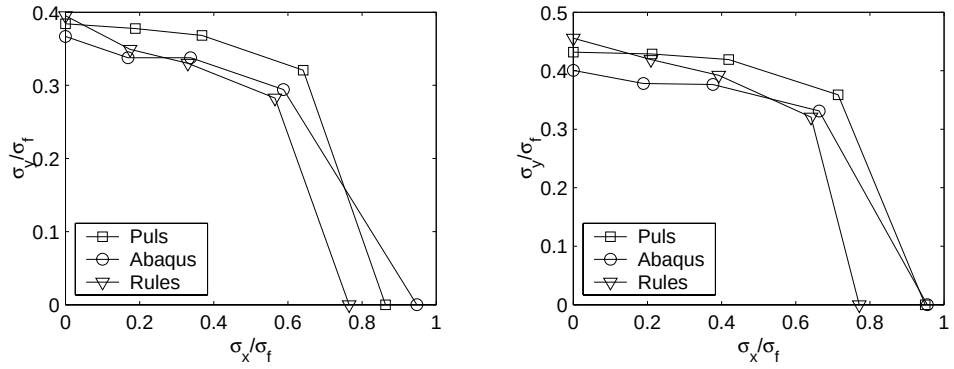

Figure 7.11: Biaxial interaction curves from PULS, ABAQUS, and the Ship Rules for tank er case 1 (left) and 2 (right)

stress when transv erse loading is dominating. This could be corrected by introducing a bending stress criterion in the limit state check.

7.2.3 Buckling of stiffened panels using PULS: Modified v ersion

The nonlinear global model developed in chapter 5 is currently being implemented in PULS, and some examples using this new version of the program is presented. Using the nonlinear global model means that more accurate results are obtained for stiffened panels with weak stiffeners, where global effects are important. The effect of lateral pressure may also be accounted for on the global level, since a t w o-span global model is used.

In order to achiev e maximum computational efficiency, a simplified version of the model presented in chapter 5 is implemented in PULS. This version performs the calculation in

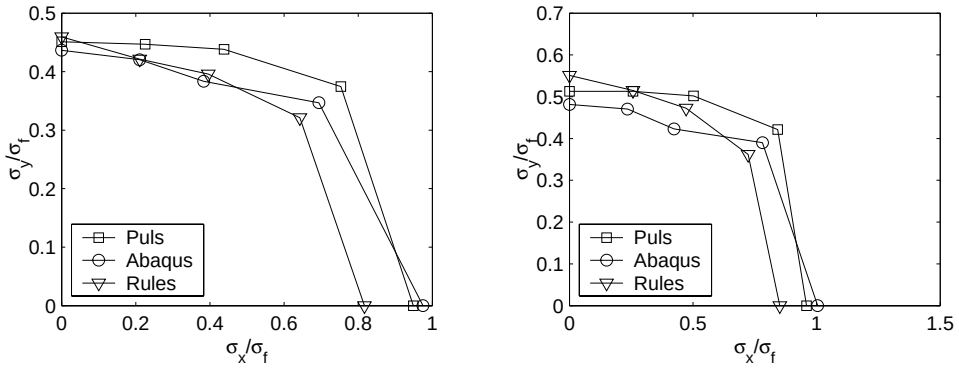

Figure 7.12: Biaxial interaction curves from PULS, ABAQUS, and the Ship Rules for tanker case 3 (left) and 4 (right)

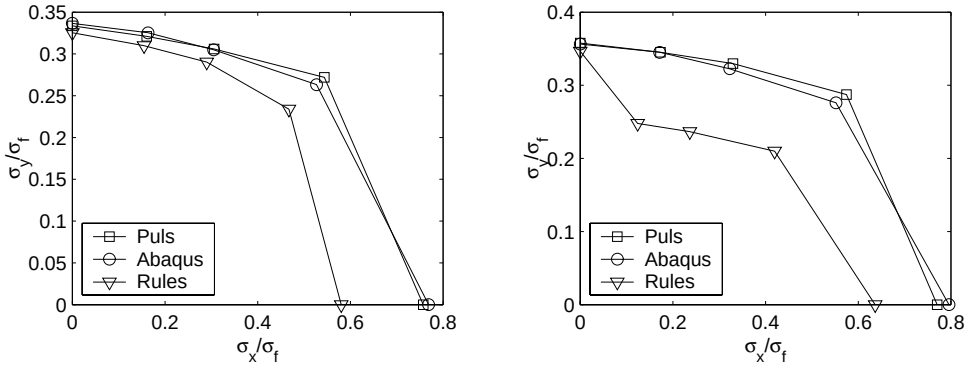

Figure 7.13: Biaxial interaction curves from PULS, ABAQUS, and the Ship Rules for tanker case 5 (left) 6 (right)

two steps. The first is a linear step, where two deflection shapes are calculated. The first is the eigenmode due to in-plane loads, while the second is the lateral deflection due to lateral pressure. In the linear step, a high number of deflection shape terms may be used. In the second step, a geometrical nonlinear calculation is carried out, using the amplitudes of these two deflection shapes as the only degrees of freedom. Comparisons with the original model show that this approach gives good results, and significantly improved computational efficiency.

Comparisons are performed between this modified PULS version and the current version.

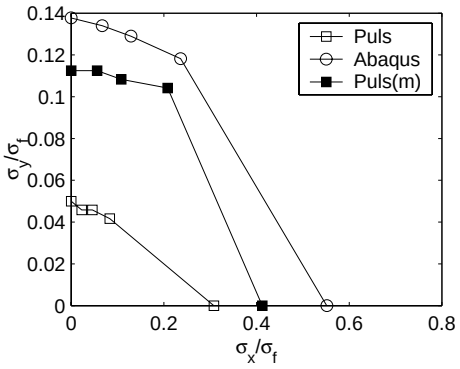

Figure 7.14: Biaxial interaction curves from PULS and ABAQUS for aluminium panel. Modified version of PULS indicated by (m)

It is found that for the steel panels considered in the previous section, there is no difference in the results. This is as expected, since the global eigenvalue is very high for all these cases. The linear global model does then perform equally well as the nonlinear. For the slender aluminium panel, however, the nonlinear global effect is significant, see Fig. 7.14. It is seen that the PULS version modified for nonlinear, global effects performs much better than the current linear version.

The effect of lateral pressure is accounted for in the global nonlinear model, but this feature has not yet been finalized in PULS. This is because lateral pressure makes it necessary to introduce new limit state criteria. Usually the global effect is most significant at mid-span, but global deflection due to lateral pressure may give rise to large global stresses at the transverse frames. This is presently not checked, but it will be included in the next version of PULS.

Some analyses have already been performed with ABAQUS in order to investigate the pressure effect. One example is shown in Fig. 7.15. A lateral pressure of p=0.2531MPa, corresponding to the design sea pressure, is applied first. The in-plane loads are then applied incrementally up to yield. It is seen that the pressure reduces the capacity in the whole biaxial range. This is because of the increased global curvature due to the pressure. It is observed that yielding first occurs at midspan for axial load, as before, while it occurs at the transverse frames for the load conditions with transverse load.

PULS can be applied with lateral pressure with the existing limit state criteria. The effect of the pressure is then to increase the global deflection and the global curvature at midspan, but the global stresses at the transverse supports are not accounted for. It is seen that the result for axial load agrees fairly well with ABAQUS, while the predictions in the biaxial

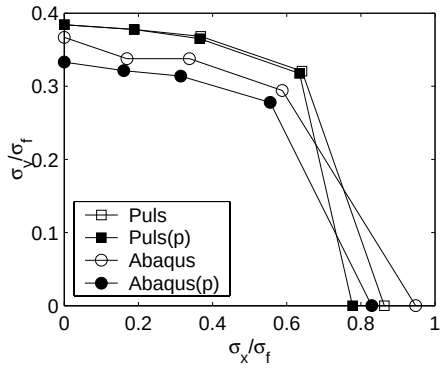

Figure 7.15: Biaxial interaction curves from ABAQUS and PULS for tanker case 1. Results with lateral pressure, p=0.2531MPa, is indicated by (p)

range does not exhibit significant strength reduction due to the pressure. This was as expected, and should be improved with modification of the limit state criteria in PULS.

Analyses have also been performed with shear loading. This is a quite difficult case to analyse using finite element methods, since the boundary conditions must be carefully chosen. The edges should be kept straight, but free to rotate and translate in-plane, as well as to contract or stretch. The load should be evenly distributed along the edges. The best approach is to use a large model, so that the deflection in the interior of the panel is not significantly affected by the boundary conditions at the edges. The tanker cases 1 and 2 discussed previously are considered to be well suited, since three stiffener spans and ten stiffener spacings are modelled. It is found that collapse due to pure shear loading does not occur until the external shear stress reaches shear yielding, i.e. $\tau = \sigma_f/\sqrt{3} \approx 0.77\sigma_f$. The same result is obtained with PULS. This indicates that shear is not a critical load for the tanker panels considered here. For more slender panels, the effect of shear load may be more significant.

7.3 Special considerations

7.3.1 Intermediate stiffening

A common way to increase the local buckling strength of stiffened panels is to add intermediate stiffening such as tripping brackets, transverse sniped stiffeners, or transverse connected stiffeners. A tripping bracket will provide both lateral support for the plate

and sideways support for the stiffener, and this can be accounted for by reducing the panel length in the model to the length between the tripping brackets. A sniped stiffener, however, provides lateral support for the plate, but does not provide any support for the stiffener. For most cases the stiffener deflection is governed by the plate deflection, and the effect of a sniped stiffener is then approximately the same as the effect of a tripping bracket. If the stiffener height is very large, however, the stiffener may deflect independently of the plate.

This case is handled in PULS by treating the sniped stiffener as a very stiff lateral spring. The stiffness contribution of this spring ensures that the plate deflection at the sniped stiffener location is zero, but leaves the web free to deflect sideways. One example where this is important, is the tanker case 2 studied above. This panel has very high webs, and for axial load the local deformation is in the form of a single half-wave. The plate has a high aspect ratio and would therefore prefer a more short-waved deflection, but the high web forces the plate into a one-wave deflection. When a sniped stiffener is applied at midspan, the plate is forced down at the middle, while the web keeps the one-wave deflection shape.

7.3.2 Freeedges

All the models presented are based on the assumption that the edges are supported in-plane by the surrounding structure, so that they will remain straight. This is not entirely correct for all parts of a ship structure. One example is web girders, which are continuous in the longitudinal direction, but not in the vertical direction. It may be too optimistic to assume that the long edges of such girders remain straight, and the membrane stiffness in the vertical direction may be over-predicted.

A simplified way to account for this effect, is to neglect the membrane strains in the vertical direction completely. This reduces the membrane stiffness compared to the straight edge case. There will always be some membrane effect in the vertical direction even if the edge is free to deform, and this method will therefore give results that are on the safe side. Modified versions of the unstiffened plate model and the local stiffener model have been developed to account for this and will be implemented in PULS in the future.

7.3.3 Residual stress

Residual stress is an effect of welding that is present in both steel and aluminium structures. When the material contracts due to cool-down after the welding, tension stress develops close to the weld. These are balanced by compressive stress further out in the plate.

If the residual stress pattern is known, it can be accounted for by simply adding the residual

stress to the stress calculated in the analysis. The effect of the residual stress may be that first yield occurs in a different position than if the initial condition is stress-free. Usually the maximum compressive stress occurs at the edges, but when residual tension stress is present first yield may occur further inside the plate. The critical points which are to be checked for yielding must therefore be chosen with care if residual stress is to be accounted for.

The effect of residual stress is a topic for further discussion. Since the plates and stiffeners in a ship are subjected to dynamically varying loads, the residual stress will gradually be relieved. It is therefore a question whether it is correct to include them in the analysis, and, if so, which magnitude to use. The effect of residual stress is currently not included in PULS, but will be considered for implementation later.

7.3.4 Heat affected zones

Heat affected zones (HAZ) is a problem for welded structures that are produced by heat treatable aluminium alloys. The effect of HAZ on unstiffened plates was investigated by (Kristensen 2001). In heat treatable alloys the yield strength is increased by heat treating, followed by artificial aging. When plates are welded, the heat from the welding process will reduce the yield strength of the material close to the weld. It is common to assume a loss in yield strength of 50%, (British Standards Institution 1996).

For aluminium applications, the limit state criteria in PULS are modified according to basic principles used in DNV Rules for High Speed Light Crafts (HSLC) and Eurocode 9. The minimum of the following three criteria is used:

1. First yield in the base material just outside of the HAZ.
2. Local material failure in the most highly stressed area of the HAZ, based on the ultimate tensile strength of the material in the HAZ.
3. Gross yielding in the HAZ, disregarding all non-linear geometrical buckling effects.

There are many uncertainties with respect to the effects of HAZ in aluminium structures, and it is a topic that will be given further attention in the continuous development of PULS.

Chapter 8

Concluding remarks

8.1 Conclusions

Computational models for analysis of buckling and postbuckling of plates and stiffened panels have been derived. The motivation was to develop a design tool that is more accurate than existing code formulations, and more efficient than nonlinear finite element methods. The models are formulated using large deflection plate theory and energy principles. Biaxial in-plane compression or tension, shear, and lateral pressure are considered, and any combination of these may be analysed with the models developed. The procedure is semi-analytical in the sense that all energy formulations are derived analytically, while a numerical method is used for solving the resulting set of equations, and for incrementation of the solution.

For the unstiffened plate, a model was developed both for the simply supported case and for the clamped case. For the simply supported case the material types considered was isotropic elastic, orthotropic elastic, and elastic-plastic. Load-deflection curves produced by the proposed models was compared with results from nonlinear FEM. For the elastic models, good correspondence and very high efficiency were achieved. For the elastic-plastic model, the accuracy and efficiency were less satisfactory. Based on these findings, it was decided to apply first yield as the collapse criterion for the subsequent models, and thereby eliminate the need for plasticity calculation. This ensures efficient computation of the response in the elastic region, and conservative estimates of the ultimate limit strength.

Two models have been developed for analysis of local buckling, one for open profiles and one for closed profiles. Geometrical nonlinearities were accounted for both in the plates and stiffeners, and rotational and longitudinal continuity between the members were ensured. A local buckling model is sufficient for analysis of panels with stocky stiffeners, since global deflection is of little significance. For more slender stiffeners, the local model is used to calculate the reduction in in-plane and bending stiffness due to local buckling. The reduced stiffness can then be used as input to a global buckling model.

A global buckling model was developed by considering the stiffened panel as a plate with general anisotropic stiffness. The stiffness coefficients are input from the local analysis. The global model is geometrically nonlinear, and is modelled with two spans to account for lateral pressure effects. Two combined models were developed in order to account for interaction between local and global buckling. The first is for a single stiffened plate, and uses a column approach. Only axial load is considered. The second is for a stiffened panel with several stiffeners. Biaxial compression, shear and lateral pressure was considered.

Computations have been performed on a variety of plate and stiffener geometries for verification of the proposed model, and comparisons were made with nonlinear finite element methods. Some examples have been presented. For all models, the response in the elastic region is well predicted compared with results from ABAQUS. The efficiency of the calculations is also very high. The deviation from the ABAQUS results is larger for the strength estimates than for the elastic response calculations. This is because redistribution of stress due to plasticity is not accounted for in the models. In most cases, this leads to conservative results. It is considered a sound principle to not utilize post-yield strength reserves in design calculations, and the deviation in the strength estimates is therefore acceptable. For thick plates in transverse compression, the results may be on the nonconservative side if a pure membrane stress criterion is used, and it should be considered to account for the bending stresses in the collapse criterion.

The most important advantage of the present models compared to nonlinear finite element methods is the large gain in computational efficiency. In addition, no geometric modelling is necessary, and no element mesh has to be created. Finally, the input of imperfections is very easy, since the user can specify any initial deflection. Compared to conventional design formulas, the major advantage of the method is a more direct calculation strategy which gives increased accuracy. This is especially important for non-conventional geometries, for which the explicit design formulas were not originally created. More information is also obtained in form of displacement shapes and amplitudes. Analyses may be performed with different imperfections, by contrast to the design formulas, where a fixed imperfection is implicit in the expressions.

The unstiffened plate model and the local model for open profiles have been implemented in the DNV buckling code PULS. The local model is there combined with a linear global buckling calculation. In addition to calculating the ultimate strength, the program pro-

duces interaction curves, stress plots and displacement plots. These are very useful for improved understanding of buckling effects, which is essential in the design process.

8.2 Recommendations

The elastic response is well predicted with the models developed, and the ULS estimates obtained using a first yield criterion show promising results. However, improvements may be made in the definitions of the limit state criteria. Some of the reserve capacity after first yield may be accounted for by simplified methods, but care should be taken before this additional strength is utilized in design. It is also observed cases where nonconservative results are obtained, and these should be investigated further. For thick plates, it may be necessary to add limit state checks that include the bending stress. For aluminium, more research is needed in order to determine how the strength reduction in the heat affected zones should be treated.

The effects of residual stress should also be further investigated. It is a question how much the residual stress is relieved after some time in service, and how much it will influence the strength. It can be included in the model by adding it to the calculated stress, if the distribution and magnitude is known.

Choosing imperfections remain a difficult task. Using the eigenmode together with tolerances set in standards, may give results that are too conservative compared with real plates and panels. On the other hand, using an imperfection shape that is more representative for real panels may be nonconservative for plates that have a more unfavorable imperfection shape. In addition, there is the complicating factor that the eigenmode is sometimes not the imperfection shape that gives the lowest collapse loadMore knowledge is needed about the shapes and amplitudes of the imperfections in real ships, and more research should be carried out in order to define appropriate imperfections for nonlinear analyses.

When it comes to application to ship structures, several additions to the current models are desirable. First of all, linearly varying edge loads should be implemented in the stiffened panel models. For large panels, the change in in-plane load can be quite large from one end to another. This is a complication, since the stiffness reduction will be different for each stiffener unit in the panel. Hence, the stiffness of the panel is no longer uniform, which means that numerical integration is necessary on the global level.

In addition, a more refined way to handle panels with unconstrained edges could be useful. This can be done with the current models by neglecting the membrane strain normal to the unconstrained edges, but this is probably too conservative. A model for curved panels should also be developed, for application in the bilge region. Considering the bilge panels as flat gives results that are overly conservative.

References

A yr ton, W. and JPerry (1886). On struts. *The Engineer 62*, 464–465,513–515.

Bleich, F. (1952). *Buckling Strength of Metal Structures*. New York: McGraw-Hill Book Company.

British St andards Institution (1996). British standard 8118, structural use of aluminium, part 1, code of practice for design.

Brush, D. and B. Almroth (1975). *Buckling of Bars, Plates and Shells*. New York: McGraw-Hill Book Company.

Bulson, P. (1970). *The Stability of Flat Plates*. London: Chatto & Windus.

Byklum, E. and J. Amdahl (2002a, 21-23 August). Nonlinear buckling analysis and ultimate strength prediction of stiffened steel and aluminium panels. In *The Second International Conference on Advances in Structural Engineering and Mechanics*, Pusan.

Byklum, E. and J. Amdahl (2002b). A simplified method for elastic large deflection analysis of plates and stiffened panels due to local buc kling. *Thin-Walled Structures 40*(11), 923–951.

Caldwell, J. (1965). Ultimate longitudinal strength. In *Trans. RINA*, V olume 107, pp. 411.

Carlsen, C. (1980). A parametric study of collapse of stiffened plates in compression. *The structural engineer 58b*, 33–40.

Chen, W. and D. Han (1988). *Plasticity for Structural Engineers*. New York: Springer-Verlag.

Cui, W. and A. Mansour (1998). Effects of welding distortions and residual stresses on the ultimate strength of long rectangular plates under uniaxial compression. *Marine Structures 11*, 251–269.

Det Norske Veritas (1995). Dnv classification note 30.1, buckling strength analysis.

Det Norske Veritas (2001). Dnv rules for classification of ships.

Det Norske Veritas (2002a). *PULS 1.3 Theory Manual*.

Det Norske Veritas (2002b). *PULS 1.3 User's Manual*.

Dym, C. and I. Shames (1973). *Solid mechanics: A Variational Approach*. New York: McGraw-Hill Book Company.

Euler, L. (1759). Sur la force de colonnes. *Mém. acad. Berlin*.

Faulkner,D. (1975). A review of effective plating for use in the analysis of stiffened plating in bending and compression. *Journal of Ship Research 19*(1), 1–17.

Featherston, C. (2000). Imperfection sensitivity of flat plates under combined compression and shear. *Non-linear Mechanics 36*, 249–259.

Fujikubo, M., P. Keading, and T. Yao (2000). Isum rectangular plate element with new lateral shape functions (1st report). *Journal of The Society of Naval Architects of Japan 187*, 209–219.

Fujikubo, M. and T. Yao (1999). Elastic local buckling strength of stiffened plate considering plate/stiffener interaction and welding residual stress. *Marine Structures 12*, 543–564.

Fujikubo, M., T. Yao, and M. Khedmati (2000). Estimation of ultimate strength of ship bottom plating under combined transverse thrust and lateral pressure. *Journal of The Society of Naval Architects of Japan 186*, 621–630.

Gerard, G. (1962). *Introduction to Structural Stability Theory*. New York: McGraw-Hill Book Company.

Hibbitt, Karlsson, and Sorensen (1994). *ABAQUS, User's Manuals, Version 5_8*.

Hughes, O. (1988). *Ship Structural Design. A Rationally-Based, Computer-Aided Optimization Approach* (2nd ed.). New Jersey: The Society of Naval Architects and Marine Engineers.

Hughes, O. and M. Ma (1996). Elastic tripping analysis of asymmetrical stiffeners. *Computers & Structures 60*(3), 369–389.

ISSC (2000). Ultimate strength. Report, ISSC.

Kirchoff, G. (1850). Über das gleichgewicht und die bewegung einer elastichen scheibe. *J. Reine und Angewandte Mathematic 40*, 51–88.

Kristensen, O. (2001). *Ultimate Capacity of Aluminium Plates under Multiple Loads, Considering HAZ Properties* Ph. D. thesis, Norwegian University of Science and Technology.

Lanczos, C. (1986). *The Variational Principles of Mechanics* (4th ed.). New York: Dover Publications.

Langseth, M. and O. Hopperstad (1996). Static and dynamic axial crushing of square thin-walled aluminium extrusions. *International Journal of Impact Engineering 18*(7-8), 949–968.

Lemaitre, J. and J. Chaboche (1994). *Mechanics of solid materials*. Cambridge: Cambridge University Press.

Levy, S. (1942). Bending of rectangular plates with large deflection. Report 737, NACA.

Marguerre, K. (1937). Die mittragende breite der gedruckten platte. *Luftfahrtsforschung 14*(3), 121–128.

Masaoka, K. and H. Okada (1996, 26-31 May). Estimating method of buckling strength of rectangular plates using selected eigenfunction. In *Proceedings of the Sixth International Offshore and Polar Engineering Conference*, Los Angeles, pp. 341–346.

Masaoka, K., H. Okada, and Y. Ueda (1998). A rectangular plate element for ultimate strength analysis. In *2nd International Conference on Thin-Walled Structures*, Singapore, pp. 469–476.

Mazzolani, F. (1995). *Aluminium Alloy Structures*. London: E&FN SPON.

Murray, N. (1984). *Introduction to the Theory of Thin-Walled Structures*. Oxford: Clarendon Press.

Paik, J. (1987). *Ultimate Strength Analysis of Ship Structures by Idealized Structural Unit Method*. Ph. D. thesis, Osaka University, Japan.

Paik, J. and B. Kim (2002). Ultimate strength formulations for stiffened panels under combined axial load, in-plane bending and lateral pressure: a benchmark study. *Thin-Walled Structures 40*, 45–83.

Paik, J. and P. Pedersen (1995). Ultimate and crushing strength of plated structures. *Journal of Ship Research 39*(3), 250–261.

Paik, J., A. Thayamballi, S. Lee, and S. Kang (2001). A semi-analytical method for the elastic-plastic large deflection analysis of welded steel or aluminium plating under combined in-plane and lateral pressure loads. *Thin-Walled Structures 39*, 125–152.

Paik, J., A. Thayamballi, and Y. Park (1998). Local buckling of stiffeners in ship plating. *Journal of Ship Research 42*(1), 56–67.

Paik, J., A. Thayamballi, G. Wang, and B. Kim (2000). On advanced buckling and ultimate strength of ship plating. *Trans., SNAME 108*.

Robertson, A. (1925). *Institution of Civil Engineers, Selected Engineering Papers 28*.

Shames, I. and C. Dym (1985). *Energy and Finite Element Methods in Structural Mechanics*. New York: Hemisphere Publishing Corporation.

Shanley, F. (1947). Inelastic column theory. *J. Aeronautical Sci. 14*, 261–267.

Soares, C. (1988). Design equation for the compressive strength ofunstiffened plate elements with initial imperfections. *Journal of Constructional Steel R esearch 9*, 287–310.

Soares, C. and J. Gordo (1996a). Collapse strength of rectangular plates under transv erse compression.*Journal of Constructional Steel R esearch 36*(3), 215–234.

Soares, C. and J. Gordo (1996b). Compressive strength of rectangular plates under biaxial load and lateral pressure. *Thin-Walled Structures 24*, 231–259.

Steen, E. (1989). Elastic buckling and postbuckling of eccen trically stiffened plates. *International Journal of Solids and Structures 25*(7), 751–768.

Steen, E. (1998). Application of the perturbation method to plate buckling problems. Research report in mechanics 98-1, University of Oslo.

Steen, E. (2001). *Buckling and Postbuckling of Stiffened Plates*. Ph. D. thesis, University of Oslo.

Steen, E. and T. Østvold (2000). Basis for a new buc kling model for strength assessment of stiffened panels. In *DNV Seminar: Buckling and Ultimate Strength of Ship Structures*, Høvik, Norway.

Szilard, R. (1974). *Theory and Analysis of Plates*. New Jersey: Prentice-Hall, Inc.

Timoshenko, S. and J. Gere (1959). *Theory of Plates and Shells* (2nd ed.). New York: McGraw-Hill Book Company.

Timoshenko, S. and J. Gere (1961). *Theory of Elastic Stability* (2nd ed.). New York: McGraw-Hill Book Company.

Troitsky, M. (1976). *Stiffened Plates. Bending, Stability and Vibrations*. Amsterdam: Elsevier Scientific Publishing Company.

Turner, M., R. Clough, G. Martin, and L. Topp (1956). Stiffness and deflection analysis of complex structures. *Journal of Aeron. Sci. 23*, 805–823.

Ueda, Y. and M. Fujikubo (1992). Plastic node method considering strain-hardening effects. *Computer Methods in Applied Mechanics and Engineering 94*, 317–337.

Ueda, Y. and S. Rashed (1984). The idealized structural unit method and its application on deep girder structures. *Computers and Structures 18*(2), 277–293.

Ueda, Y., S. Rashed, and Y. Abdel-Nasser (1993). An improved isum rectangular plate element taking account of post-ultimate strength behavior. *Marine Structures 6*, 139–172.

Ueda, Y., S. Rashed, and J. Paik (1987). An incremental galerkin method for plates and stiffened plates. *Computers and Structures 27*(1), 147–156.

Ueda, Y., S. Rashed, and J. Paik (1995). Buckling and ultimate strength interaction in plates and stiffened panels under combined inplane biaxial and shearing forces. *Marine Structures 8*, 1–36.

Valsgard, S. (1980). Numerical design prediction of the capacity of plates in biaxial in-plane compression. *Computers and Structures 12*, 729–739.

von Karman, T. (1910). Festigkeitsproblemeim maschinenbau. *Encycl. der math. Wiss. 4*, 348–351.

Washizu, K. (1975). *Variational Methods in Elasticity and Plasticity* (2nd ed.). Oxford: Pergamon Press.

Yao, T., M. Fujikubo, and D. Yanagihara (1997, 25-30 May). Buckling/plastic collapse behaviour and strength of stiffened plates under thrust. In *Proceedings of the Seventh International Offshore and Polar Engineering Conference*, Honolulu, pp. 353–360.

Appendix A

Buckling of unstiffened plates

A.1 Simply supported plate

For all derivations in the following, the superscript s, indicating deflection in the sine-mode, is omitted for increased readability.

A.1.1 Solution of the compatibility equation

For an initially flat plate, the compatibility equation is:

$$\nabla^4 F = E(w_{,xy}^2 - w_{,xx}w_{,yy}) \tag{A.1}$$

The solution of this equation was proposed written in the following form by Levy:

$$F = -\frac{P_x y^2}{2bt} - \frac{P_y x^2}{2at} + \sum_0^{2M}\sum_0^{2N} f_{mn}\cos(\frac{m\pi x}{a})\cos(\frac{n\pi y}{b}) \tag{A.2}$$

The coefficients f_{mn} are found by substitution of the above expression into the compatibility equation. The approach proposed by Levy is also used her, but for some reason the

coefficients derived here are not equal to those presented in the work by Levy. For the initially flat plate the following equation results:

$$\begin{aligned}
&\pi^4 \sum_{0}^{2M}\sum_{0}^{2N} f_{mn}\cos(\frac{m\pi x}{a})\cos(\frac{n\pi y}{b})\left[(\frac{m}{a})^2+(\frac{n}{b})^2\right]^2 \\
&= \frac{E\pi^4}{a^2b^2}\sum_{rspq}\Big[rspqA_{rs}A_{pq}\cos(\frac{r\pi x}{a})\cos(\frac{s\pi y}{b})\cos(\frac{p\pi x}{a})\cos(\frac{q\pi y}{b}) \\
&-r^2q^2A_{rs}A_{pq}\sin(\frac{r\pi x}{a})\sin(\frac{s\pi y}{b})\sin(\frac{p\pi x}{a})\sin(\frac{q\pi y}{b})\Big]
\end{aligned} \tag{A.3}$$

By manipulation of the trigonometric functions, the right hand side can be written as:

$$\begin{aligned}
&\frac{E\pi^4}{4a^2b^2}\sum_{rspq} rspqA_{rs}A_{pq}\left[\cos\left(\frac{(r-p)\pi x}{a}\right)\cos\left(\frac{(s-q)\pi y}{b}\right)+\cos\left(\frac{(r-p)\pi x}{a}\right)\cos\left(\frac{(s+q)\pi y}{b}\right)\right. \\
&\left.+\cos\left(\frac{(r+p)\pi x}{a}\right)\cos\left(\frac{(s-q)\pi y}{b}\right)+\cos\left(\frac{(r+p)\pi x}{a}\right)\cos\left(\frac{(s+q)\pi y}{b}\right)\right] \\
&-r^2q^2A_{rs}A_{pq}\left[\cos\left(\frac{(r-p)\pi x}{a}\right)\cos\left(\frac{(s-q)\pi y}{b}\right)-\cos\left(\frac{(r-p)\pi x}{a}\right)\cos\left(\frac{(s+q)\pi y}{b}\right)\right. \\
&\left.-\cos\left(\frac{(r+p)\pi x}{a}\right)\cos\left(\frac{(s-q)\pi y}{b}\right)+\cos\left(\frac{(r+p)\pi x}{a}\right)\cos\left(\frac{(s+q)\pi y}{b}\right)\right]
\end{aligned} \tag{A.4}$$

It is then found that for Eq. (A.3) to be true, the coefficients f_{mn} must be:

$$f_{mn} = \frac{E}{4(m^2\frac{b}{a}+n^2\frac{a}{b})^2}\sum_{rspq} b_{rspq}A_{rs}A_{pq} \tag{A.5}$$

where $f_{0,0}$ is defined to be zero, and the coefficients b_{rspq} are:

$$b^s_{rspq} = rspq + r^2q^2 \quad \text{if} \quad \begin{cases} \pm(r-p)=m, s+q=n \\ r+p=m, \pm(s-q)=n \end{cases} \tag{A.6}$$

$$b^s_{rspq} = rspq - r^2q^2 \quad \text{if} \quad \begin{cases} r+p=m, s+q=n \\ \pm(r-p)=m, \pm(s-q)=n \end{cases} \tag{A.7}$$

For the plate with initial deflection, the compatibility equation can be rewritten in the

follo wing manner:

$$\begin{aligned}\nabla^4 F &= E(w_{,xy}^2 - w_{,xx}w_{,yy} + 2w_{0,xy}w_{,xy} - w_{0,xx}w_{,yy} - w_{0,yy}w_{,xx}) \\ &= E\left[(w_{,xy} + w_{0,xy})^2 - (w_{,xx} + w_{0,xx})(w_{,yy} + w_{0,yy})\right] \\ &- E\left[w_{0,xy}^2 - w_{0,xx}w_{0,yy}\right] \end{aligned} \tag{A.8}$$

This shows that the solution of the stress function F can be written as the difference betw een the t w o solutions

$$F = F(w + w_0) - F(w_0) \tag{A.9}$$

Hence, the coefficients f_{mn} for a plate with initial deflection must be:

$$\begin{aligned} f_{mn} &= \frac{E}{4(m^2\frac{b}{a} + n^2\frac{a}{b})^2}\sum_{rspq}[b_{rspq}(A_{rs} + B_{rs})(A_{pq} + B_{pq}) - b_{rspq}B_{rs}B_{pq}] \\ &= \frac{E}{4(m^2\frac{b}{a} + n^2\frac{a}{b})^2}\sum_{rspq} b_{rspq}(A_{rs}A_{pq} + A_{rs}B_{pq} + A_{pq}B_{rs}) \end{aligned} \tag{A.10}$$

A.1.2 Derivatives and rates of the stress function

By differentiation, the derivativ es and rates of the coefficients f_{mn} involv ed in calculation of the stiffness matrix is:

$$\frac{\partial f_{mn}}{\partial A_{fg}} = \frac{E}{4(m^2\frac{b}{a} + n^2\frac{a}{b})^2}\sum_{rs}(b_{fgrs} + b_{rsfg})(A_{rs} + B_{rs}) \tag{A.11}$$

$$\dot{f}_{mn} = \frac{E}{4(m^2\frac{b}{a} + n^2\frac{a}{b})^2}\sum_{rspq}(b_{rspq} + b_{pqrs})(A_{rs} + B_{rs})\dot{A}_{pq} \tag{A.12}$$

$$(\frac{\partial \dot{f}_{mn}}{\partial A_{fg}}) = \frac{E}{4(m^2\frac{b}{a} + n^2\frac{a}{b})^2}\sum_{pq}(b_{fgpq} + b_{pqfg})\dot{A}_{pq} \tag{A.13}$$

where all the b-coefficients are calculated by the same rule as b_{rspq}.

A.1.3 Membrane energy

The potential energy due to membrane stretching is:

$$U_m = \frac{t}{2E}\int_0^a\int_0^b \left[(\sigma_x+\sigma_y)^2 - 2(1+\nu)(\sigma_x\sigma_y-\sigma_{xy}^2)\right] dydx \tag{A.14}$$

Substituting the stress function, and rewriting the trigonometric functions, the integrations can be carried out analytically. The resulting expression is:

$$\begin{aligned} U_m &= \frac{t}{2E}\left[F(S_x,S_y,S_{xy}) + \frac{ab}{4}\pi^4\sum_0^{2M}\sum_0^{2N} f_{mn}^2(\frac{m^2}{a^2}+\frac{n^2}{b^2})^2\right. \\ &+ \left.\frac{ab}{2}\pi^4\sum_0^{2M} f_{m0}^2(\frac{m}{a})^4 + \frac{ab}{2}\pi^4\sum_0^{2N} f_{0n}^2(\frac{n}{b})^4\right] \end{aligned} \tag{A.15}$$

By differentiation, the rate of minimum membrane energy is:

$$\begin{aligned} (\frac{\partial\dot{U}_m}{\partial A_{fg}}) &= \frac{abt}{4E}\pi^4\sum_0^{2M}\sum_0^{2N}\left[\frac{\partial f_{mn}}{\partial A_{fg}}\dot{f}_{mn} + (\frac{\partial\dot{f}_{mn}}{\partial A_{fg}})f_{mn}\right](\frac{m^2}{a^2}+\frac{n^2}{b^2})^2 \\ &+ \frac{abt}{2E}\pi^4\sum_0^{2M}\left[\frac{\partial f_{m0}}{\partial A_{fg}}\dot{f}_{m0} + (\frac{\partial\dot{f}_{m0}}{\partial A_{fg}})f_{m0}\right](\frac{m}{a})^4 \\ &+ \frac{abt}{2E}\pi^4\sum_0^{2N}\left[\frac{\partial f_{0n}}{\partial A_{fg}}\dot{f}_{0n} + (\frac{\partial\dot{f}_{0n}}{\partial A_{fg}})f_{0n}\right](\frac{n}{b})^4 \end{aligned} \tag{A.16}$$

A.1.4 Bending energy

The potential energy due to bending is

$$U_b = \frac{D}{2}\int_0^a\int_0^b \left[(w_{,xx}+w_{,yy})^2 - 2(1-\nu)(w_{,xx}w_{,yy}-w_{,xy}^2)\right] dydx \tag{A.17}$$

By substitution of the assumed displacement functions, the integration can be carried out:

$$U_b = \frac{abD}{8}\pi^4\sum_{m=1}^{M}\sum_{n=1}^{N} A_{mn}^2(\frac{m^2}{a^2}+\frac{n^2}{b^2})^2 \tag{A.18}$$

By differentiation rate of minimum bending energy is:

$$(\frac{\partial \dot{U}_b}{\partial A_{fg}}) = D\pi^4 \frac{ab}{4} \left(\frac{f^2}{a^2} + \frac{g^2}{b^2}\right)^2 \dot{A}_{fg} \tag{A.19}$$

A.1.5 External energy

For constant edge-loads, the potential of external in-plane forces is:

$$T_c = S_x bt\Delta u + S_y at\Delta v \tag{A.20}$$

where the elongations are:

$$\begin{aligned} \Delta u &= \int_0^a u_{,x} dx \qquad (A.21)\\ &= \int_0^a (\varepsilon_x - \frac{1}{2} w_{,x}^2 - w_{0,x} w_{,x}) dx \\ \Delta v &= \int_0^b v_{,y} dy \qquad (A.22)\\ &= \int_0^b (\varepsilon_y - \frac{1}{2} w_{,y}^2 - w_{0,y} w_{,y}) dy \end{aligned}$$

The membrane strain is calculated from Hook's law, using the assumed stress function:

$$\begin{aligned} \varepsilon_x &= \frac{1}{E}(\sigma_x - \nu\sigma_y) \qquad (A.23)\\ &= \frac{1}{E}\left[-S_x + \nu S_y - \sum_{-2M}^{2M}\sum_{-2N}^{2N} f_{mn} \cos(\frac{m\pi x}{a}) \cos(\frac{n\pi y}{b}) \pi^2 (\frac{n^2}{b^2} - \nu\frac{m^2}{a^2})\right] \\ \varepsilon_y &= \frac{1}{E}(\sigma_y - \nu\sigma_x) \qquad (A.24)\\ &= \frac{1}{E}\left[-S_y + \nu S_x - \sum_{-2M}^{2M}\sum_{-2N}^{2N} f_{mn} \cos(\frac{m\pi x}{a}) \cos(\frac{n\pi y}{b}) \pi^2 (\frac{m^2}{a^2} - \nu\frac{n^2}{b^2})\right] \end{aligned}$$

Substituting the above relations into the elongation expressions, the integrations can be

carried out:

$$\Delta u = -\frac{S_x a}{E} + \nu\frac{S_y a}{E} - \frac{\pi^2}{8a}\sum_{m=1}^{M}\sum_{n=1}^{N} m^2(A_{mn}^2 + 2A_{mn}B_{mn}) \tag{A.25}$$

$$\Delta v = -\frac{S_y b}{E} + \nu\frac{S_x b}{E} - \frac{\pi^2}{8b}\sum_{m=1}^{M}\sum_{n=1}^{N} n^2(A_{mn}^2 + 2A_{mn}B_{mn}) \tag{A.26}$$

Hence, the potential of external loads becomes:

$$\begin{aligned} T_c = & -\frac{abt}{E}S_x^2 + \frac{2\nu abt}{E}S_x S_y - \frac{abt}{E}S_y^2 \\ & -\frac{S_x bt}{8}\sum_{m=1}^{M}\sum_{n=1}^{N}\frac{m^2\pi^2}{a}(A_{mn}^2 + 2A_{mn}B_{mn}) \\ & -\frac{S_y at}{8}\sum_{m=1}^{M}\sum_{n=1}^{N}\frac{n^2\pi^2}{b}(A_{mn}^2 + 2A_{mn}B_{mn}) \end{aligned} \tag{A.27}$$

By differentiation the rate of minimum external energy is:

$$\begin{aligned} (\frac{\partial \dot{T}_c}{\partial A_{fg}}) = & -\dot{\Lambda}\left[\frac{f^2 bt}{4a}(S_x^s - S_x^{s-1}) + \frac{g^2 at}{4b}(S_y^s - S_y^{s-1})\right](A_{fg} + B_{fg})\pi^2 \\ & -\Lambda\left[\frac{f^2 bt}{4a}(S_x^s - S_x^{s-1}) + \frac{g^2 at}{4b}(S_y^s - S_y^{s-1})\right]\dot{A}_{fg}\pi^2 \end{aligned} \tag{A.28}$$

The first part contributes to the load vector $\mathbf{G}$, and is proportional to the displacement. The second part contributes to the stiffness matrix $\mathbf{K}$, and this is proportional to the external load parameter Λ.

For linearly varying edge-loads, the modified stress function is:

$$\begin{aligned} F = & -S_x^1\frac{y^2}{2} - (S_x^2 - S_x^1)\frac{y^3}{6b} - S_y^1\frac{x^2}{2} - (S_y^2 - S_y^1)\frac{x^3}{6a} - S_{xy}xy \\ & + \sum_{0}^{2M}\sum_{0}^{2N} f_{mn}\cos(\frac{m\pi x}{a})\cos(\frac{n\pi y}{b}) \end{aligned} \tag{A.29}$$

And:

$$F_{,xx} = -S_y(x) - (\frac{\pi}{a})^2 \sum_0^{2M} \sum_0^{2N} m^2 f_{mn} \cos(\frac{m\pi x}{a}) \cos(\frac{n\pi y}{b}) \quad \text{(A.30)}$$

$$F_{,yy} = -S_x(y) - (\frac{\pi}{b})^2 \sum_0^{2M} \sum_0^{2N} n^2 f_{mn} \cos(\frac{m\pi x}{a}) \cos(\frac{n\pi y}{b}) \quad \text{(A.31)}$$

The potential energy is:

$$T_c = t \int_0^a \int_0^b (S_x(y) u_{,x} + S_y(x) v_{,y}) dx dy \quad \text{(A.32)}$$

$$= t \int_0^a \int_0^b \left(S_x(y)(\varepsilon_x - \frac{1}{2} w_{,x}^2 - w_{,x} w_{0,x}) + S_y(x)(\varepsilon_y - \frac{1}{2} w_{,y}^2 - w_{,y} w_{0,y}) \right) dx dy \quad \text{(A.33)}$$

Ignoring the membrane strain the potential energy is calculated as:

$$T_c = -t \int_0^a \int_0^b \left(S_x(y)(\frac{1}{2} w_{,x}^2 + w_{,x} w_{0,x}) + S_y(x)(\frac{1}{2} w_{,y}^2 + w_{,y} w_{0,y}) \right) dx dy \quad \text{(A.34)}$$

Carrying out the integration gives:

$$\begin{aligned} T_c = & - \frac{S_x^1 b t \pi^2}{8a} \sum_{mn} m^2 (A_{mn}^2 + 2 A_{mn} B_{mn}) \quad \text{(A.35)} \\ & - (S_x^2 - S_x^1) \frac{\pi^2 t}{4ab} \sum_{mnq} m^2 (A_{mn} A_{mq} + 2 A_{mq} B_{mn}) I_{nq} \\ & - \frac{S_y^1 a t \pi^2}{8b} \sum_{mn} n^2 (A_{mn}^2 + 2 A_{mn} B_{mn}) \\ & - (S_y^2 - S_y^1) \frac{\pi^2 t}{4ab} \sum_{mnq} n^2 (A_{mn} A_{qn} + 2 A_{mn} B_{qn}) I_{mq} \end{aligned}$$

where I_{nq} and I_{mq} are the integrals:

$$I_{nq} = \int_0^b y \sin(\frac{n\pi y}{b}) \sin(\frac{q\pi y}{b}) dy = \begin{cases} 0 & n \neq q \ , \ n \pm q \text{ even} \\ \frac{b^2}{4} & n = q \\ -\frac{4b^2}{\pi^2} \frac{nq}{(n^2-q^2)^2} & \text{else} \end{cases} \quad \text{(A.36)}$$

$$I_{mq} = \int_0^a x \sin(\frac{m\pi x}{a}) \sin(\frac{q\pi x}{a}) dx = \begin{cases} 0 & m \neq q \ , \ m \pm q \text{ even} \\ \frac{a^2}{4} & m = q \\ -\frac{4a^2}{\pi^2} \frac{mq}{(m^2-q^2)^2} & \text{else} \end{cases} \quad \text{(A.37)}$$

The rate of minimum potential energy is:

$$\begin{aligned} (\frac{\partial \dot{T}_c}{\partial A_{fg}}) = & - \frac{\dot{S}_x^1 bt\pi^2}{4a} f^2 (A_{fg} + B_{fg}) - (\dot{S}_x^2 - \dot{S}_x^1) \frac{\pi^2 t}{2ab} f^2 \sum_q (A_{fq} + B_{fq}) I_{qg} \\ & - \frac{\dot{S}_y^1 at\pi^2}{4b} g^2 (A_{fg} + B_{fg}) - (\dot{S}_y^2 - \dot{S}_y^1) \frac{\pi^2 t}{2ab} g^2 \sum_q (A_{qg} + B_{qg}) I_{mq} \\ & - \frac{S_x^1 bt\pi^2}{4a} f^2 \dot{A}_{fg} - (S_x^2 - S_x^1) \frac{\pi^2 t}{2ab} f^2 \sum_q \dot{A}_{fq} I_{qg} \\ & - \frac{S_y^1 at\pi^2}{4b} g^2 \dot{A}_{fg} - (S_y^2 - S_y^1) \frac{\pi^2 t}{2ab} g^2 \sum_q \dot{A}_{qg} I_{mq} \end{aligned} \quad \text{(A.38)}$$

The external potential energy due to shear force is:

$$T_\tau = S_{xy} t \int_0^a \int_0^b (u_{,y} + v_{,x}) dy dx \quad \text{(A.39)}$$

Rearranging and integrating gives:

$$T_\tau = -S_{xy} t \int_0^a \int_0^b (w_{,x} w_{,y} + w_{0,x} w_{,y} + w_{,x} w_{0,y}) dA \quad \text{(A.40)}$$

$$= -S_{xy} t \sum_{mnpq} (A_{mn} A_{pq} + B_{mn} A_{pq} + A_{mn} B_{pq}) \frac{mq}{ab} \pi^2 I \quad \text{(A.41)}$$

where I is the in tegral:

$$
\begin{aligned}
I &= \int_0^a \int_0^b \cos(\frac{m\pi x}{a}) \sin(\frac{p\pi x}{a}) \sin(\frac{n\pi y}{b}) \cos(\frac{q\pi y}{b}) dxdy && \text{(A.42)} \\
&= \begin{cases} 0 & \text{if m=p or n=q} \\ \frac{1}{4\pi^2}\left(\frac{a}{m+p}[\cos(\pi(m+p))-1] + \frac{a}{p-m}[\cos(\pi(p-m))-1]\right) & \\ \left(\frac{b}{n+q}[\cos(\pi(n+q))-1] + \frac{b}{n-q}[\cos(\pi(n-q))-1]\right) & \text{else} \end{cases}
\end{aligned}
$$

By differentiation, the rate of minimum potential energy is:

$$
\begin{aligned}
(\frac{\partial \dot{T}_\tau}{\partial A_{fg}}) = &- \dot{\Lambda}\frac{\pi^2 t}{ab}(S_{xy}^s - S_{xy}^{s-1}) \sum_{mn}(A_{mn}+B_{mn})(mgI_{mnfg} + fnI_{fgmn}) \\
&- \frac{S_{xy}\pi^2 t}{ab}\sum_{mn}\dot{A}_{mn}(mgI_{mnfg} + fnI_{fgmn}) && \text{(A.43)}
\end{aligned}
$$

The first part is here the incremental load vector contribution, while the second part is the incremental stiffness matrix contribution.

The contribution from lateral pressure to the potential of external energy is:

$$
\begin{aligned}
T_{lp} &= -\int_0^a \int_0^b pwdxdy && \text{(A.44)} \\
&= -p\frac{ab}{\pi^2}\sum_m \sum_n \frac{1}{mn}[\cos(m\pi)-1][\cos(n\pi)-1]A_{mn} && \text{(A.45)}
\end{aligned}
$$

By differentiation we get:

$$
(\frac{\partial \dot{T}_{lp}}{\partial A_{fg}}) = -\dot{\Lambda}(p^s - p^{s-1})\frac{ab}{\pi^2}\frac{1}{fg}[\cos(f\pi)-1][\cos(g\pi)-1] \qquad \text{(A.46)}
$$

It is seen that the lateral pressure gives a con tribution to the incremental load vector, but no contribution to the incremental stiffness matrix.

A.2 Clamped plate

For all derivations in the following, the sub- and superscript c, indicating deflection in the cosine-mode, is omitted for increased readability.

A.2.1 Membrane energy

The membrane energy is calculated in the same way as for the simply supported plate. Substituting the new stress function, and carrying out the integration, we get:

$$U_m = \frac{t}{2E}\left[F(S_x,S_y,S_{xy}) + \frac{ab\pi^4}{4}\sum_{m,n} f_{mn}^2(\frac{m^2}{a^2}+4\frac{n^2}{b^2})^2 \right. \tag{A.47}$$
$$\left. +\frac{ab\pi^4}{2}\sum_m f_{m0}^2(\frac{m}{a})^4 + 8ab\pi^4\sum_n f_{0n}^2(\frac{n}{b})^4\right]$$

The rate of minimum membrane potential energy is:

$$(\frac{\partial \dot{U}_m}{\partial A_{fg}}) = \frac{t}{2E}\left[\frac{ab\pi^4}{2}\sum_{m,n}(\dot{f}_{mn}\frac{\partial f_{mn}}{\partial A_{fg}} + f_{mn}(\frac{\partial \dot{f}_{mn}}{\partial A_{fg}}))(\frac{m^2}{a^2}+4\frac{n^2}{b^2})^2 \right. \tag{A.48}$$
$$\left. +ab\pi^4\sum_m(\dot{f}_{m0}\frac{\partial f_{m0}}{\partial A_{fg}} + f_{m0}(\frac{\partial \dot{f}_{m0}}{\partial A_{fg}}))(\frac{m}{a})^4 + 16ab\pi^4\sum_n(\dot{f}_{0n}\frac{\partial f_{0n}}{\partial A_{fg}} + f_{0n}(\frac{\partial \dot{f}_{0n}}{\partial A_{fg}}))(\frac{n}{b})^4\right]$$

A.2.2 Bending energy

By substitution of the assumed displacement functions into the general bending energy expression and carrying out the integration, the bending energy becomes:

$$U_b = \frac{abD}{2}\pi^4\sum_{m=1}^{M}\sum_{n=1}^{N}\left(A_{mn}^2(\frac{m^4}{16a^4}+\frac{n^4}{b^4}+\frac{m^2n^2}{2a^2b^2}) + \sum_{q=1}^{N}A_{mn}A_{mq}\frac{m^4}{8a^4}\right) \tag{A.49}$$

The rate of minimum bending energy is:

$$(\frac{\partial \dot{U}_b}{\partial A_{fg}}) = \frac{abD}{2}\pi^4\left(\dot{A}_{fg}(\frac{f^4}{8a^4}+2\frac{g^4}{b^4}+\frac{f^2g^2}{a^2b^2}) + \frac{f^4}{4a^4}\sum_{q=1}^{N}\dot{A}_{fq}\right) \tag{A.50}$$

It is seen that the cosine shape functions leads to a non-diagonal bending stiffness matrix, in con trast to the sine shape functions used for the simply supported plate.

A.2.3 External energy

Only constant edge loads have been considered for the clamped plate, but linearly varying edge loads can be included in the same way as for the simply supported plate. The potential energy due to external in-plane forces is:

$$T_c = S_x bt\Delta u + S_y at\Delta v \tag{A.51}$$

where the elongations are calculated as for the simply supported plate. Substituting the assumed deflection shape for the clamped plate gives:

$$\begin{aligned} T_c = & - \frac{abt}{E}S_x^2 + \frac{2\nu abt}{E}S_xS_y - \frac{abt}{E}S_y^2 \\ & - \frac{S_x bt\pi^2}{32a}\sum_{m=1}^{M}\sum_{n=1}^{N} m^2\left[(A_{mn}^2 + 2A_{mn}B_{mn}) + 2\sum_{q=1}^{N}(A_{mn}A_{mq} + 2A_{mn}B_{mq})\right] \\ & - \frac{S_y at\pi^2}{8b}\sum_{m=1}^{M}\sum_{n=1}^{N} n^2(A_{mn}^2 + 2A_{mn}B_{mn}) \end{aligned} \tag{A.52}$$

The rate of minimum potential energy is:

$$\begin{aligned} (\frac{\partial \dot{T}_c}{\partial A_{fg}}) = & - \frac{S_x bt\pi^2}{16a}f^2\left[\dot{A}_{fg} + 2\sum_{q=1}^{N}\dot{A}_{fq}\right] \\ & - \frac{S_y at\pi^2}{4b}g^2\dot{A}_{fg} \\ & - \frac{\dot{\Lambda}\pi^2 bt}{16a}(S_x^s - S_x^{s-1})f^2\left[(A_{fg} + B_{fg}) + 2\sum_{q=1}^{N}(A_{fq} + B_{fq})\right] \\ & - \frac{\dot{\Lambda}\pi^2 at}{4b}(S_y^s - S_y^{s-1})g^2(A_{fg} + B_{fg}) \end{aligned} \tag{A.53}$$

F or the shear force, substitution of the assumed displacements into the energy expression

used previously for the simply supported plate gives:

$$T_\tau = P_{xy}\int_0^a\int_0^b(\gamma_{xy} - w_{,x}w_{,y} - w_{0,x}w_{,y} - w_{,x}w_{0,y})dA \quad (A.54)$$

$$= 0 \quad (A.55)$$

The potential of external energy due to lateral pressure is:

$$T_{lp} = -\int_0^a\int_0^b pwdxdy \quad (A.56)$$

$$= -p\frac{ab}{2\pi}\sum_m\sum_n\frac{1}{m}(\cos(m\pi) - 1)A_{mn} \quad (A.57)$$

By differentiation we get:

$$(\frac{\partial\dot{T}_{lp}}{\partial A_{fg}}) = -\dot{\Lambda}(p^s - p^{s-1})\frac{ab}{2\pi}\frac{1}{f}(\cos(f\pi) - 1) \quad (A.58)$$

As for the simply supported plate, the lateral pressure gives a con tribution to the incremental load vector, but no contribution to the incremental stiffness matrix.

A.3 Orthotropic plate

A.3.1 Membrane energy

The membrane energy for the orthotropic plate is:

$$U_m = \frac{abt}{8}\pi^4\sum_m\sum_n f_{mn}^2\left(M_{2222}\frac{m^4}{a^4} + M_{1111}\frac{n^4}{b^4} + 2(M_{1122} + 2M_{1212})\frac{m^2n^2}{a^2b^2}\right) \quad (A.59)$$

The rate of minimum membrane energy is

$$(\frac{\partial\dot{U}_m}{\partial A_{fg}}) = \frac{abt}{4}\pi^4\sum_m\sum_n(\dot{f}_{mn}\frac{\partial f_{mn}}{\partial A_{fg}} + f_{mn}(\frac{\partial\dot{f}_{mn}}{\partial A_{fg}})) \quad (A.60)$$

$$\cdot \left(M_{2222}\frac{m^4}{a^4} + M_{1111}\frac{n^4}{b^4} + 2(M_{1122} + 2M_{1212})\frac{m^2n^2}{a^2b^2}\right)$$

A.3.2 Bending energy

The bending energy for the orthotropic plate is:

$$U_b = \frac{abt^3}{96}\pi^4 \sum_m \sum_n A_{mn}^2 \left(C_{1111}\frac{m^4}{a^4} + C_{2222}\frac{n^4}{b^4} + 2(C_{1122} + 2C_{1212})\frac{m^2 n^2}{a^2 b^2} \right) \tag{A.61}$$

The of minimum potential bending energy is

$$(\frac{\partial \dot{U}_b}{\partial A_{fg}}) = \frac{abt^3}{48}\pi^4 \left(C_{1111}\frac{f^4}{a^4} + C_{2222}\frac{g^4}{b^4} + 2(C_{1122} + 2C_{1212})\frac{f^2 g^2}{a^2 b^2} \right) \dot{A}_{fg} \tag{A.62}$$

Appendix B

Local buckling of stiffened plates

B.1 Open profiles

B.1.1 Plate bending energy

The plate bending energy is due to the combined effect of the sine-deflection and the cosine-deflection. Writing the total deflection w as the sum $w = w_s + w_c$ the bending energy becomes:

$$U_b^p = \frac{D}{2}\int_{-a/2}^{a_u}\int_{-b/2}^{b_u}\left[(w_{,xx}+w_{,yy})^2 - 2(1-\nu)(w_{,xx}w_{,yy}-w_{,xy}^2)\right]dydx \quad \text{(B.1)}$$

$$= U_b^s + U_b^c + U_b^{sc} \quad \text{(B.2)}$$

where a_u and b_u are the upper integration limits. The first con tribution, due to sine-deflection, becomes:

$$U_b^s = \frac{D}{2}\pi^4\sum_{r,p}\sum_{s,q}A_{rs}^s A_{pq}^s\left[(\frac{r^2p^2}{a^4}+\frac{s^2q^2}{b^4}+2\nu\frac{r^2q^2}{a^2b^2})I_1I_2 + 2(1-\nu)\frac{rspq}{a^2b^2}I_3I_4\right] \quad \text{(B.3)}$$

When the area of integration is taken as $(-a/2, a/2)$ and $(-b/2, b/2)$ the in tegration constan ts are:

$$
\begin{aligned}
I_1 &= a/2 \ \text{r=p} && \text{(B.4)}\\
&= \frac{-2a(r\cos\frac{\pi r}{2}\sin\frac{\pi p}{2} - p\sin\frac{\pi r}{2}\cos\frac{\pi p}{2})}{\pi(r-p)(r+p)} \ \text{(r+p) odd}\\
&= 0 \ \text{else}\\
I_2 &= b/2 \ \text{s=q} && \text{(B.5)}\\
&= \frac{-2b(s\cos\frac{\pi s}{2}\sin\frac{\pi q}{2} - q\sin\frac{\pi s}{2}\cos\frac{\pi q}{2})}{\pi(s-q)(s+q)} \ \text{(s+q) odd}\\
&= 0 \ \text{else}\\
I_3 &= a/2 \ \text{r=p} && \text{(B.6)}\\
&= \frac{2a(r\sin\frac{\pi r}{2}\cos\frac{\pi p}{2} - p\cos\frac{\pi r}{2}\sin\frac{\pi p}{2})}{\pi(r-p)(r+p)} \ \text{(r+p) odd}\\
&= 0 \ \text{else}\\
I_4 &= b/2 \ \text{s=q} && \text{(B.7)}\\
&= \frac{2b(s\sin\frac{\pi s}{2}\cos\frac{\pi q}{2} - q\cos\frac{\pi s}{2}\sin\frac{\pi q}{2})}{\pi(s-q)(s+q)} \ \text{(s+q) odd}\\
&= 0 \ \text{else}
\end{aligned}
$$

When the area of integration is taken as $(-a/2, 3a/2)$ and $(-b/2, 3b/2)$ the integration constants simplify to:

$$
\begin{aligned}
I_1 &= a \ \text{r=p} && \text{(B.8)}\\
&= 0 \ \text{else}\\
I_2 &= b \ \text{s=q} && \text{(B.9)}\\
&= 0 \ \text{else}\\
I_3 &= a \ \text{r=p} && \text{(B.10)}\\
&= 0 \ \text{else}\\
I_4 &= b \ \text{s=q} && \text{(B.11)}\\
&= 0 \ \text{else}
\end{aligned}
$$

It is seen that integrating to 3a/2 and 3b/2 instead of a/2 and b/2 eliminates the coupling terms betw een odd and even half wave numbers. This ensures that the continuity of the plating is accounted for. Hence, for all derivations in the following, 3a/2 and 3b/2 is used as upper integration limits.

The second contribution to the plate bending energy, due to cosine-deflection, becomes :

$$U_b^c = \frac{D}{2}\pi^4 \sum_{r,p}\sum_{s,q} A_{rs}^c A_{pq}^c \left[\frac{r^2p^2}{4a^4} I_1 I_5 + 4\frac{s^2q^2}{b^4} I_1 I_6 - 2\nu\frac{r^2q^2}{a^2b^2} I_1 I_7 + 2(1-\nu)\frac{rspq}{a^2b^2} I_3 I_8\right] \quad \text{(B.12)}$$

where, for $(-b/2, 3b/2)$-in tegration:

$$\begin{aligned} I_5 &= 3b \text{ s=q} && \text{(B.13)}\\ &= 2b \text{ else} \\ I_6 &= b \text{ s=q} && \text{(B.14)}\\ &= 0 \text{ else} \\ I_7 &= -b \text{ s=q} && \text{(B.15)}\\ &= 0 \text{ else} \\ I_8 &= b \text{ s=q} && \text{(B.16)}\\ &= 0 \text{ else} \end{aligned}$$

The last part is the contribution due to coupling betw een sine- and cosine-deflection. This term is zero when integrating over $(-a/2, 3a/2)$ and $(-b/2, 3b/2)$:

$$U_b^{sc} = 0 \quad \text{(B.17)}$$

B.1.2 Stiffener bending energy

The web bending energy is:

$$U_b^w = \frac{D_w}{2}\int_{-a/2}^{3a/2}\int_0^h \left[(v_{,xx} + v_{,zz})^2 - 2(1-\nu)(v_{,xx}v_{,zz} - v_{,xz}^2)\right] dz dx \quad \text{(B.18)}$$

Inserting the stiffener deflection function, and integrating, the result is:

$$\begin{aligned}
U_b^w &= \frac{D_w}{2}\Bigg[\frac{h\pi^4}{3a^4}\sum_{rs} r^2s^2V_{1r}V_{1s}I_1 \\
&+ (3\pi-8)\frac{h\pi^3}{2a^4}\sum_{rs} r^2s^2V_{2r}V_{2s}I_1 \\
&+ (\pi^2-4\pi+8)\frac{h\pi^2}{a^4}\sum_{rs} r^2s^2V_{1r}V_{2s}I_1 \\
&+ \frac{\pi^4}{32h^3}\sum_{rs} V_{2r}V_{2s}I_1 \\
&+ 2\nu(\pi-4)\frac{\pi^3}{8ha^2}\sum_{rs} r^2V_{2r}V_{2s}I_1 \\
&- 2\nu(\pi-2)\frac{\pi^2}{2ha^2}\sum_{rs} r^2V_{1r}V_{2s}I_1 \\
&+ 2(1-\nu)\frac{\pi^2}{ha^2}\sum_{rs} rsV_{1r}V_{1s}I_3 \\
&+ (1-\nu)\frac{\pi^4}{4ha^2}\sum_{rs} rsV_{2r}V_{2s}I_3 \\
&+ 4(1-\nu)\frac{\pi^2}{ha^2}\sum_{rs} rsV_{1r}V_{2s}I_3\Bigg]
\end{aligned} \tag{B.19}$$

The integration coefficients are $I_1 = I_3 = a$ for the current integration limits.

The bending stiffness is found by inserting the expression for V_{1m} found from the continuity condition, and differentiating with respect to the rate and displacement amplitudes. As the resulting expressions are quite lengthy, they are not given here.

The flange bending energy is:

$$U_b^f = \frac{EI_f}{2}\int_{-a/2}^{3a/2}(v_{,xx}|_{z=h})^2dx + \frac{GJ_f}{2}\int_{-a/2}^{3a/2}(v_{,xz}|_{z=h})^2dx \tag{B.20}$$

where the first part is due to in-plane bending of the flange, and the second is due to torsion of the flange. EI_f is the bending stiffness and GJ_f the torsional stiffness of the flange. Inserting the stiffener deflection function, and integrating, the flange bending energy

becomes:

$$U_b^f = \frac{EI_f}{2a^4}\pi^4 \sum_{rs} r^2 s^2 I_1 (V_{1r}V_{1s} + V_{2r}V_{2s} + 2V_{1r}V_{2s}) \tag{B.21}$$
$$+\frac{GJ_f}{2h^2a^2}\pi^2 \sum_{rs} rsI_3 (V_{1r}V_{1s} + \frac{\pi^2}{4}V_{2r}V_{2s} + \pi V_{1r}V_{2s})$$

where again $I_1 = I_3 = a$. As for the web, the bending stiffness is found by inserting the expression for V_{1m} and differentiating with respect to the rate and displacement amplitudes.

B.1.3 Plate membrane energy

The plate membrane energy is

$$\begin{aligned}
U_m^p &= \frac{E}{2(1-\nu^2)} \int_{V_p} (\varepsilon_x^2 + \varepsilon_y^2 + 2\nu\varepsilon_x\varepsilon_y + \frac{1-\nu}{2}\gamma_{xy}^2) dV_p \\
&= \frac{E}{2(1-\nu^2)} \int_{V_p} \left((\varepsilon_x^{p,F} + \varepsilon_x^{p,D})^2 + (\varepsilon_y^{p,F} + \varepsilon_y^{p,D})^2 + 2\nu(\varepsilon_x^{p,F} + \varepsilon_x^{p,D})(\varepsilon_y^{p,F} + \varepsilon_y^{p,D}) + \frac{1-\nu}{2}\gamma_{xy}^2 \right) dV_p \\
&= \frac{E}{2(1-\nu^2)} \int_{V_p} \left((\varepsilon_x^{p,F})^2 + (\varepsilon_y^{p,F})^2 + 2\nu(\varepsilon_x^{p,F})(\varepsilon_y^{p,F}) \right) dV_p \\
&+ \frac{E}{2(1-\nu^2)} \int_{V_p} \left((\varepsilon_x^{p,D})^2 + (\varepsilon_y^{p,D})^2 + 2\nu(\varepsilon_x^{p,D})(\varepsilon_y^{p,D}) + \frac{1-\nu}{2}\gamma_{xy}^2 \right) dV_p \\
&= U_m^{p,F} + U_m^{p,D}
\end{aligned} \tag{B.22}$$

The coupling betw een$\varepsilon^{p,D}$ and $\varepsilon^{p,F}$ is zero, since $\varepsilon^{p,F}$ is constant and the integral of $\varepsilon^{p,D}$ over the plate area is zero.

The deflection part, $U_m^{p,D}$, is considered first. The stress function for the plate, F, may be written $F = F^s + F^c + F^{sc}$. The membrane energy for the plate may be written

$$U_m^{p,D} = U_m^{p,s} + U_m^{p,c} + U_m^{p,sc} \tag{B.23}$$

where $U_m^{p,s}$ is the membrane energy due to sine-deflection, $U_m^{p,c}$ is that due to cosine-

deflection, and $U_m^{p,sc}$ is due to coupling terms. It is found that:

$$\begin{aligned} U_m^{p,s} &= \frac{abt}{2E}\pi^4 \sum_{m,n} (f_{mn}^s)^2 (\frac{m^2}{a^2} + \frac{n^2}{b^2})^2 \\ &+ \frac{abt}{E}\pi^4 \sum_{m} (f_{m0}^s)^2 (\frac{m}{a})^4 + \frac{abt}{E}\pi^4 \sum_{n} (f_{0n}^s)^2 (\frac{n}{b})^4 \end{aligned} \tag{B.24}$$

and

$$\begin{aligned} U_m^{p,c} &= \frac{abt}{2E}\pi^4 \sum_{m,n} (f_{mn}^c)^2 (\frac{m^2}{a^2} + 4\frac{n^2}{b^2})^2 \\ &+ \frac{abt}{E}\pi^4 \sum_{m} (f_{m0}^c)^2 (\frac{m}{a})^4 + 16\frac{abt}{E}\pi^4 \sum_{n} (f_{0n}^c)^2 (\frac{n}{b})^4 \end{aligned} \tag{B.25}$$

These are the same expressions as derived previously for the unstiffened plate, only multiplied with 4. The coupling term is in general:

$$U_m^{p,sc} = U_m^p(F^{sc}, F^{sc}) + U_m^p(F^s, F^c) + U_m^p(F^{sc}, F^s) + U_m^p(F^{sc}, F^c) \tag{B.26}$$

The latter tw o terms becomes zero for the curren t areas of integration. The resulting expressions for the other tw o terms are:

$$\begin{aligned} U_m^p(F^{sc}, F^{sc}) &= \frac{abt}{2E}\pi^4 \sum_{m,n} (f_{mn}^{sc})^2 (\frac{m^2}{a^2} + \frac{n^2}{b^2})^2 \\ &+ \frac{abt}{E}\pi^4 \sum_{n} (f_{0n}^s)^2 (\frac{n}{b})^4 \end{aligned} \tag{B.27}$$

$$\begin{aligned} U_m^p(F^s, F^c) &= \frac{abt}{E}\pi^4 \sum_{m,n} f_{m,2n}^s f_{mn}^c (\frac{m^2}{a^2} + 4\frac{n^2}{b^2})^2 \\ &+ 2\frac{abt}{E}\pi^4 \sum_{m} f_{m,0}^s f_{m,0}^c \frac{m^4}{a^4} + 32\frac{abt}{E}\pi^4 \sum_{n} f_{0,2n}^s f_{0,n}^c \frac{n^4}{b^4} \end{aligned} \tag{B.28}$$

B.1.4 External energy

The shear energy is calculated as:

$$T_\tau = 4P_{xy}\int_0^a\int_0^b(\gamma_{xy} - w_{,x}w_{,y} - w_{0,x}w_{,y} - w_{,x}w_{0,y})dA \tag{B.29}$$

$$= -4P_{xy}\int_0^a\int_0^b(w_{s,x}w_{s,y} + w_{s0,x}w_{s,y} + w_{s,x}w_{s0,y})dA \tag{B.30}$$

Only the sine-terms contribute to the shear energy. Inserting the displacement function and carrying out the integration gives:

$$T_\tau = - 2P_{xy}\frac{\pi^2}{ab}\sum_{rspq}(A^s_{rs}A^s_{pq} + A^s_{rs}B^s_{pq} + B^s_{rs}A^s_{pq})rqI \tag{B.31}$$

where the integration constant I is:

$$I = \begin{cases} 0 & \text{if r=p or s=q} \\ \frac{1}{4\pi^2}\left(\frac{a}{r+p}[\cos(\pi(r+p)) - 1] + \frac{a}{p-r}[\cos(\pi(p-r)) - 1]\right) & \\ \left(\frac{b}{s+q}[\cos(\pi(s+q)) - 1] + \frac{b}{s-q}[\cos(\pi(s-q)) - 1]\right) & \text{else} \end{cases}$$

The potential of external energy due to lateral pressure is:

$$T_{lp} = -2\int_0^a\int_{-b/2}^{3b/2} pwdxdy \tag{B.32}$$

$$= 2p\frac{ab}{\pi^2}\sum_m\sum_n\frac{1}{mn}(\pi n - \cos(n\pi)^2\sin(n\pi))(\cos(m\pi) - 1)A^c_{mn} \tag{B.33}$$

It is seen that only the cosine-terms contribute to the lateral pressure energy.

B.2 Closed profiles

B.2.1 Corner node rotational energy

The rotation energy for the intersection between plate 1 and 2 at node a is given as an example. The contributions from the other connections are similar. However, the local coordinate system for each plate must be properly chosen in order to get the rotation signs correct. The difference in rotation between plate 1 and 2 at the corner node a is:

$$\Delta\theta_{12} = \theta_{1a} - \theta_{2a} \tag{B.34}$$

The rotations are :

$$\theta_{1a} = \left.\frac{\partial w_1}{\partial y}\right|_{y=b_1} = \frac{\pi}{b_1}\sum_{mn} nA^1_{mn}\sin(\frac{m\pi x}{a})\cos(n\pi) \tag{B.35}$$

$$\theta_{2a} = \left.\frac{\partial w_2}{\partial y}\right|_{y=b_2} = \frac{\pi}{b_2}\sum_{mn} nA^2_{mn}\sin(\frac{m\pi x}{a})\cos(n\pi) \tag{B.36}$$

The potential energy due to rotation is:

$$U_\theta = \frac{1}{2}k_\theta\int_a(\Delta\theta)^2_{12}dx \tag{B.37}$$

$$= \frac{1}{4}k_\theta\pi^2 a\sum_m\sum_{nq} nq\cos(n\pi)\cos(q\pi)(\frac{A^1_{mn}}{b_1} - \frac{A^2_{mn}}{b_2})(\frac{A^1_{mq}}{b_1} - \frac{A^2_{mq}}{b_2}) \tag{B.38}$$

The rotational stiffness is found by differentiating twice with respect to the displacement amplitudes:

$$\frac{\partial^2 U_\theta}{\partial A^1_{fg}A^1_{fq}} = \frac{1}{2}k_\theta\pi^2 gq\frac{a}{b_1^2} \tag{B.39}$$

$$\frac{\partial^2 U_\theta}{\partial A^1_{fg}A^2_{fq}} = -\frac{1}{2}k_\theta\pi^2 gq\frac{a}{b_1 b_2} \tag{B.40}$$

$$\frac{\partial^2 U_\theta}{\partial A^2_{fg}A^2_{fq}} = \frac{1}{2}k_\theta\pi^2 gq\frac{a}{b_2^2} \tag{B.41}$$

Appendix C

Global buckling of stiffened panels

C.1 Membrane energy

The membrane energy can be written as a sum of sine, cosine and coupling contributions:

$$U_m = U_m^s + U_m^c + U_m^{sc1} + U_m^{sc2} \tag{C.1}$$

The sine contribution is:

$$U_m^s = \frac{aB\pi^4}{2}\sum_m\sum_n (f_{mn}^{s1})^2(K1s - \frac{K2s^2}{K1s}) \tag{C.2}$$

The cosine contribution is:

$$U_m^c = \frac{aB\pi^4}{2}\sum_m\sum_n (f_{mn}^{c1})^2(K1c - \frac{K2c^2}{K1c}) \tag{C.3}$$

The coupling contributions are:

$$U_m^{sc1} = \frac{aB\pi^4}{2}\sum_m\sum_n (f_{mn}^{sc1})^2(K1sc - \frac{K2sc^2}{K1sc}) \tag{C.4}$$

$$U_m^{sc2} = aB\pi^4\sum_m\sum_n f_{m,2n}^{s1} f_{mn}^{c1}(K1c - \frac{K2c^2}{K1c}) \tag{C.5}$$

C.2 Bending energy

The bending energy can be written as a sum of a sine and a cosine con tribution. The coupling terms vanish upon integration.

$$U_b = U_b^s + U_b^c \tag{C.6}$$

The sine contribution is:

$$U_b^s = \frac{aB\pi^4}{2}\sum_m\sum_n \left(D_{11}(\frac{m}{a})^4 + D_{22}(\frac{n}{B})^4 + 2(D_{12}+2D_{33})(\frac{mn}{aB})^2\right)(A_{mn}^s)^2 \tag{C.7}$$

The cosine contribution is:

$$U_b^c = \frac{B\pi^4}{2}\sum_{rp}\sum_s \left(4D_{11}\frac{r^2p^2}{a^4}I_5 + D_{22}\frac{s^4}{4B^4}I_6 - 2D_{12}(\frac{rs}{aB})^2 I_7 + 4D_{33}\frac{s^2rp}{a^2B^2}I_8\right)A_{rs}^c A_{ps}^c \tag{C.8}$$

where the integration constants are:

$$\begin{aligned} I_5 &= a \ \text{r=p} && \text{(C.9)}\\ &= 0 \ \text{else} \\ I_6 &= 3a \ \text{r=p} && \text{(C.10)}\\ &= 2a \ \text{else} \\ I_7 &= -a \ \text{r=p} && \text{(C.11)}\\ &= 0 \ \text{else} \\ I_8 &= a \ \text{r=p} && \text{(C.12)}\\ &= 0 \ \text{else} \end{aligned}$$

C.3 External energy

The external energy due to in-plane compression or tension is the sum of a sine and a cosine part:

$$T_c = T_c^s + T_c^c \tag{C.13}$$

The coupling terms vanishes upon integration. The sine contribution is:

$$\begin{aligned} T_c^s = & - \frac{N_1\pi^2}{2a}\sum_m\sum_n m^2((A_{mn}^s)^2 + 2A_{mn}^s B_{mn}^s) \\ & - \frac{N_2\pi^2}{2B}\sum_m\sum_n n^2((A_{mn}^s)^2 + 2A_{mn}^s B_{mn}^s) \end{aligned} \tag{C.14}$$

The cosine contribution is:

$$\begin{aligned} T_c^c = & - \frac{N_1\pi^2}{2a}\sum_m\sum_n m^2((A_{mn}^c)^2 + 2A_{mn}^c B_{mn}^c) \\ & - \frac{N_2\pi^2}{8B}\sum_m\sum_n n^2\left[((A_{mn}^c)^2 + 2A_{mn}^c B_{mn}^c) + 2\sum_r (A_{mn}^c A_{rn}^c + 2A_{mn}^c B_{rn}^c)\right] \end{aligned} \tag{C.15}$$

The energy due to shear load is only due to sine-deflection:

$$T_\tau = -N_3\int_0^{2a}\int_0^{2B}(w_{,x}w_{,y} + w_{0,x}w_{,y} + w_{,x}w_{0,y})dA \tag{C.16}$$

$$= -N_3\sum_{mnpq}(A_{mn}^s A_{pq}^s + B_{mn}^s A_{pq}^s + A_{mn}^s B_{pq}^s)\frac{mq}{aB}\pi^2 I \tag{C.17}$$

where I is the in tegral:

$$I = \begin{cases} 0 & \text{if m=p or n=q} \\ \frac{1}{\pi^2}\left(\frac{a}{m+p}[\cos(\pi(m+p)) - 1] + \frac{a}{p-m}[\cos(\pi(p-m)) - 1]\right) & \\ \left(\frac{B}{n+q}[\cos(\pi(n+q)) - 1] + \frac{B}{n-q}[\cos(\pi(n-q)) - 1]\right) & \text{else} \end{cases} \tag{C.18}$$

The energy due to lateral pressure is only due to cosine-deflection:

$$T_{lp} = -2p\frac{aB}{\pi}\sum_m\sum_n\frac{1}{m}(\cos(m\pi) - 1)A_{mn}^c \tag{C.19}$$

Appendix D

Coupled local and global buckling

D.1 Coupled local and global buckling for a stiffened panel

D.1.1 Global bending

The global bending energy for the stiffeners is:

$$U_b^{s,g} = EIa(\frac{\pi}{a})^4 A_g^2 \sum_{N_s} \sum_{m} \sum_{n,q} m^4 k_{mn} k_{mq} \sin(\frac{n\pi y_s}{B}) \sin(\frac{q\pi y_s}{B}) \tag{D.1}$$

The global bending energy for the plating is:

$$U_b^{p,g} = \frac{aBD}{2}\pi^4 A_g^2 \sum_{m=1}^{M_g} \sum_{n=1}^{N_g} k_{mn}^2 (\frac{m^2}{a^2} + \frac{n^2}{B^2})^2 \tag{D.2}$$

D.1.2 Global membrane stretching

The global membrane energy for the plate is:

$$U_m^p = \frac{Et}{2}(A_g^2 + 2A_g B_g)^2 FG5 \tag{D.3}$$

The global membrane energy for the stiffeners is:

$$U_m^s = 2EA_s a(A_g^2 + 2A_g B_g)^2 FG7 \tag{D.4}$$

The integration constants used are:

$$I_1(y) = \frac{a}{2}\sum_m \sum_{n,q} m^2 k_{mn} k_{mq} \sin(\frac{n\pi y}{B}) \sin(\frac{q\pi y}{B}) \tag{D.5}$$

$$I_3 = \frac{aB}{4}\sum_m \sum_n m^2 k_{mn}^2 \tag{D.6}$$

$$I_5(x) = \frac{B}{2}\sum_{m,p} \sum_n n^2 k_{mn} k_{pn} \sin(\frac{m\pi x}{a}) \sin(\frac{p\pi x}{a}) \tag{D.7}$$

$$I_7 = \frac{aB}{4}\sum_m \sum_n n^2 k_{mn}^2 \tag{D.8}$$

$$\begin{aligned} FG5 &= 4\frac{B}{a}FG1^2 + \frac{4}{a}(\frac{\pi}{a})^2 I_3 FG1 + \frac{1}{16}(\frac{\pi}{a})^4 FG3 && \text{(D.9)} \\ &+ 4\frac{a}{B}FG2^2 + \frac{4}{B}(\frac{\pi}{B})^2 I_7 FG2 + \frac{1}{16}(\frac{\pi}{B})^4 FG4 && \text{(D.10)} \\ FG7 &= \sum_{N_s}(\frac{FG1^2}{a^2} + \frac{FG1}{2a}(\frac{\pi}{a})^2 FG6(y_s) + \frac{1}{16}(\frac{\pi}{a})^4 FG6^2(y_s)) && \text{(D.11)} \\ FG6 &= \sum_m \sum_{nq} m^2 k_{mn} k_{mq} \sin(\frac{n\pi y_s}{B}) \sin(\frac{q\pi y_s}{B}) && \text{(D.12)} \end{aligned}$$

$$FG1 = \frac{-\pi^2(tI_3 + A_s \sum_{N_s} I_1(y_s))}{2a^2(Bt + N_s A_s)} \tag{D.13}$$

$$FG2 = -\frac{1}{2a}(\frac{\pi}{B})^2 I_7 2a^2(Bt + N_s A_s) \tag{D.14}$$

$$FG3 = 4ab\sum_{m,p} \sum_{n,q,s,t} m^2 p^2 k_{mn} k_{mq} k_{ps} k_{pt} I_{11}(n,q,s,t) \tag{D.15}$$

$$FG4 = 4ab\sum_{m,p,r,v} \sum_{n,q} n^2 q^2 k_{mn} k_{pn} k_{rq} k_{vq} I_{12}(m,p,r,v) \tag{D.16}$$

$$I_{11}(n,q,s,t) = \frac{1}{8} \quad \text{if} \quad \begin{cases} -n+q+s-t=0 \\ n+q+s+t=0 \\ n-q+s-t=0 \\ -n-q+s+t=0 \end{cases} \tag{D.17}$$

$$= -\frac{1}{8} \quad \text{if} \quad \begin{cases} -n+q+s+t=0 \\ n-q+s+t=0 \\ -n-q+s-t=0 \\ n+q+s-t=0 \end{cases} \tag{D.18}$$

$$I_{12}(m,p,r,v) = \frac{1}{8} \quad \text{if} \quad \begin{cases} -m+p+r-v=0 \\ m+p+r+v=0 \\ m-p+r-v=0 \\ -m-p+r+v=0 \end{cases} \tag{D.19}$$

$$= -\frac{1}{8} \quad \text{if} \quad \begin{cases} -m+p+r+v=0 \\ m-p+r+v=0 \\ -m-p+r-v=0 \\ m+p+r-v=0 \end{cases} \tag{D.20}$$

D.1.3 Coupling between local and global buckling

The potential energy due to coupling betw een local membrane stretching and global bending is:

$$\begin{aligned} U^c = & -4Et(\frac{\pi}{a})^2 z_g \varepsilon^{p,F} A_g I_1 + 4E(\frac{\pi}{a})^2 (b_f t_f (h-z_g) + h t_w (\frac{h}{2} - z_g) \varepsilon^{s,F} A_g I_2 \\ & + 2E(\frac{\pi}{a})^2 A_g I_2 \int_{A_s} \varepsilon^{s,D} (z - z_g) dA \end{aligned} \tag{D.21}$$

where

$$I_1 = \frac{aB}{\pi^2} \sum_m \sum_n \frac{m}{n} k_{mn} (\cos(m\pi) - 1)(\cos(n\pi) - 1)) \tag{D.22}$$

$$I_2 = -\frac{a}{\pi} \sum_{N_s} \sum_m \sum_n m k_{mn} (\cos(m\pi) - 1)) \sin(\frac{n\pi y_s}{b}) \tag{D.23}$$

D.1.4 Global external energy

The global potential energy due to shear force is:

$$T_\tau = -\frac{S_{xy}t\pi^2}{aB}(A_g + 2A_g b_g) \sum_{m,n,p,q} mqk_{mn}k_{pq}I \tag{D.24}$$

where I is the in tegral:

$$\begin{aligned} I &= \int_0^{2a}\int_0^{2B} \cos(\frac{m\pi x}{a}) \sin(\frac{p\pi x}{a}) \sin(\frac{n\pi y}{B}) \cos(\frac{q\pi y}{B}) dxdy \qquad \text{(D.25)} \\ &= \begin{cases} 0 & \text{if m=p or n=q} \\ \frac{1}{\pi^2}\left(\frac{a}{m+p}[\cos(\pi(m+p)) - 1] + \frac{a}{p-m}[\cos(\pi(p-m)) - 1]\right) & \\ \left(\frac{B}{n+q}[\cos(\pi(n+q)) - 1] + \frac{B}{n-q}[\cos(\pi(n-q)) - 1]\right) & \text{else} \end{cases} \end{aligned}$$

The global potential energy due to lateral pressure is:

$$T_{lp} = -4p\frac{aB}{\pi^2}A_g \sum_m \sum_n \frac{1}{mn}[\cos(m\pi) - 1][\cos(n\pi) - 1]k_{mn} \tag{D.26}$$